ABSTRACT

Title of Dissertation: ASSEMBLY OF QUORUM SENSING PATHWAY ENZYMES ONTO PATTERNED MICROFABRICATED DEVICES

Angela T. Lewandowski, Doctor of Philosophy, 2007

Directed By: Professor William E. Bentley, Department of Chemical and Biomolecular Engineering

I report patterned protein assembly onto microfabricated devices using our unique assembly approach. This approach is based on electrodeposition of the aminopolysaccharide chitosan onto a selected electrode pattern of the device, and covalent conjugation of a target protein to chitosan upon biochemical activation of a genetically fused C-terminal pentatyrosine "pro-tag." With this approach, assembly is "spatially selective", occurring only at selected electrode patterns, and the entire process occurs under mild experimental conditions. Additionally, assembly is reversible and the devices reusable, as the deposited chitosan can be removed by simple incubation in dilute acid. Finally, the protein is covalently and robustly linked to chitosan through the pro-tag versus the native tyrosines, and thus our approach confers "orientational control".

I have examined patterned assembly of metabolic pathway enzymes onto both flat microfabricated chips and into 3-dimensional microfluidic devices. The assembled enzymes retain reproducible catalytic activities and protein recognition capabilities for antibody binding. Additionally, catalytic activity is retained over multiple days, demonstrating enzyme stability over extended time. Finally, substrate catalytic conversion can be controlled and manipulated through the assembly patterned area, or in the case of microfluidic devices, through the substrate flow rate over the assembled enzyme.

I specifically examined the patterned assembly of Pfs and LuxS enzymes, members of the bacterial autoinducer-2 (AI-2) biosynthesis pathway. AI-2 is a small signaling molecule that mediates interspecies bacterial communication termed type II "quorum sensing", which is involved in regulating the pathogenesis of a bacterial population. Significantly, this is the first time that Pfs and LuxS have been assembled onto devices. More significantly, Pfs and LuxS have both been assembled onto the same chip; that is, the quorum sensing pathway has been assembled onto a single device. This device could be used to screen inhibitors of AI-2 biosynthesis and discover novel "anti-pathogenic" drugs.

In summary, I have demonstrated patterned enzyme assembly onto microfabricated devices. The assembled enzymes retain reproducible catalytic activities and are capable of recognizing and binding antibodies. Importantly, patterned device-assembly of multiple enzymes representing a metabolic pathway is possible. I envision many potential biosensing, bioMEMS, drug screening, and metabolic engineering applications.

ASSEMBLY OF QUORUM SENSING PATHWAY ENZYMES ONTO PATTERNED MICROFABRICATED DEVICES

By

Angela T. Lewandowski

Dissertation submitted to the Faculty of the Graduate School of the
University of Maryland, College Park, in partial fulfillment
of the requirements for the degree of
Doctor of Philosophy
2007

Advisory Committee:
Professor William E. Bentley, Chair
Professor John P. Fisher
Professor Gregory F. Payne
Professor Srinivasa R. Raghavan
Professor Gary W. Rubloff
Professor Nam Sun Wang

Acknowledgements

I would like to especially thank my advisor Professor Bill Bentley for all of his guidance and encouragement, and for giving me a great deal of latitude to try my own ideas and make my own conclusions and recommendations. I would also like to especially thank Xiaolong Luo, my partner on all of the microfluidic experiments. It was a fantastic experience working with such an intelligent, motivated, and kind person. I would like to thank Dr. Hyunmin Yi for of his guidance and support, especially when I was new to the project. I would like to thank Stephan Koev for making the chips for me, and also for the helpful discussions with him on experimental results. Of course, a big thank you to all of the current and past members of the Bentley lab for all of encouragement, friendship, and helpful and interesting discussions of results. It has truly been a great work environment. Finally, I would like to thank the other professors involved in this research project, Prof. Ghodssi, Payne, and Rubloff for all of your guidance and support.

Table of Contents

List of Schemes

List of Figures

Chapter 1: Motivation

Bacterial resistance to traditional antibiotics

The rapidly increasing resistance of bacteria to traditional antibiotics is an important health crisis. The statistics on antibiotic-resistant bacteria are prevalent and very alarming: in a study where Streptococcus pneumoniae was isolated from outpatients at U.S. medical centers between 1994 and 1995, 23 % of these bacteria did not respond to penicillin (Gold and Moellering 1996); the Centers for Disease Control found that more than 10 % of enterococci bacteria isolated from hospitals in 1995 were resistant to vancomycin, currently the most powerful antibiotic, up from 0.5 % in 1989 (Gold and Moellering 1996); more than 95 % of Staphylococcus aureus worldwide is resistant to penicillin and ampicillin (Neu 1992); more than 16 % of Streptococcus pneumoniae isolated from hospital patients between 1991 and 1992 were resistant to at least one antibiotic (Breiman et al. 1994).

Traditional antibiotics have mainly targeted bacterial cell-wall synthesis, protein synthesis, and DNA replication and repair, all of which ultimately lead to cell lysis. Thus, the bacteria are under harsh selective pressure to develop antibiotic-resistance and survive. Such resistance is conferred by gene mutations, which can be spread throughout the population via bacteriophage, via conjugation of transferable plasmid, which replicate independently of chromosomal DNA, or via conjugation of transposons, which are genes that can "jump" from one location to another (Neu 1992). Antibiotic resistance occurs via three main mechanisms: (1) bacterial membrane proteins that pump the drug out of

the cell; (2) alteration of drug structure such that it cannot bind to the cell target; and (3) alteration of the cell target so that the drug cannot bind (Gold and Moellering 1996; Neu 1992; Walsh 2000). Drug companies have developed new antibiotics that circumvent these main resistance mechanisms, and have also developed new antibiotics based on new bacterial targets (Walsh 2000). However, it is inevitable that bacteria will eventually develop resistance to these new types of traditional antibiotics as well. Therefore, it is important to discover and develop non-traditional antibiotics with entirely novel bacterial targets that place less selective pressure on the bacteria to develop resistance. One such novel target is bacterial "quorum sensing", as it is not involved in regulating essential phenotypes; that is, it is not necessary for individual cell survival.

Quorum sensing: a target for novel antibiotic design

Quorum sensing is the process by which bacterial cells communicate in response to changing environmental cues, and results in the coordinated behavior of the entire population. Quorum sensing is mediated by small chemical signaling molecules, autoinducers, that are produced, secreted, and finally taken up by the cells when a threshold extracellular concentration of autoinducer is achieved; this ultimately leads to regulation of phenotype and a change in behavior of the population as a whole (Bassler 1999; Fuqua and Greenberg 1998; Surette and Bassler 1998). There are several types of quorum sensing, however, the focus here is on interspecies quorum sensing termed type II quorum sensing (denoted here as QS) (Bassler et al. 1997; Bassler et al. 1994; Fuqua and Greenberg 1998). QS is mediated by autoinducer-2, a "universal" chemical signaling molecule (Miller and Bassler 2001) produced in many ($\geq$ 55) various Gram-positive and

Gram-negative bacterial species (Federle and Bassler 2003). QS has become a target for novel drug design due to its involvement in the pathogenesis of the population through regulation of cellular processes such as motility (Ren et al. 2004; Sperandio et al. 2001; Sperandio et al. 2002), possibly leading to increased colonization of the host, biofilm formation and architecture (Balestrino et al. 2005; Barrios et al. 2006), and other virulence factors (Sperandio et al. 2001; Zhu et al. 2002).

Biofilms are involved in the majority of microbial infections (> 80 % according to the National Institutes of Health) (Davies 2003), but are highly tolerant of the host immune response and traditional antibiotics (Davies 2003; Ehrlich et al. 2005; Rasmussen and Givskov 2006). They consist of bacterial microcolonies (containing one or more species) embedded within a protective polymeric extracellular matrix separated by microchannels (Davies 2003). Their high tolerance of antimicrobial agents is believed to be due to several characteristics: reduced metabolism and growth rates compared to planktonic cultures of the same species, the reduced transport of the antimicrobial agent into the matrix, differences in physiology compared to their planktonic counterparts resulting from unique gene expression patterns, and the expression of multiple phenotypes within the same biofilm resulting from multiple environmental niches (Davies 2003; Ehrlich et al. 2005). Significantly, biofilms can form on surfaces introduced into a host organism (e.g. artificial joints, catheters, shunts, artificial implants). Due to their high tolerance of the host immune system and traditional antibiotics, the biofilms formed on such medical devices typically can only be eradicated by surgical removal of the infected devices (Davies 2003; Ehrlich et al. 2005). For this, researchers have investigated QS inhibitors that inhibit biofilm formation (Ren et al.

2001), and such inhibitors represent potential novel therapeutics of importance to human healthcare.

Virulence factors regulated by QS include toxin production in enterohemorrhagic *Escherichia coli* O157:H7 (Sperandio et al. 2001) and cholera toxin production in *Vibrio cholerae* (Zhu et al. 2002). Researchers have demonstrated the involvement of QS in virulence by examining bacterial colonization of the host using mouse models (Stroeher et al. 2003; Zhu et al. 2002). For example, Stroeher *et al.* (Stroeher et al. 2003) demonstrated that QS led to increased spread of Streptococcus pneumoniae throughout the host and decreased survival time. It is believed that through QS, the bacterial population launches a coordinated attack on the host organism to completely overwhelm the host's immune system (Bassler 1999). Thus, QS inhibitors represent promising novel therapeutics and are termed "anti-pathogenic drugs" (Borchardt 1980; Rasmussen and Givskov 2006). Such drugs could also be used to extend the lifetime of traditional antibiotics (Federle and Bassler 2003).

Quorum sensing pathway

Inhibitors of QS could function by inhibiting biosynthesis of the QS signaling molecule, autoinducer-2 (AI-2). AI-2 is produced from *S*-adenosylmethionine (SAM) in a metabolic pathway shown in Scheme 1. SAM is used as a methyl donor in important cellular processes such as protein and DNA methylation and metabolism and polyamine biosynthesis (Borchardt 1980; Pajula and Raina 1979; Raina et al. 1982; Riscoe et al. 1984). SAM transfers a methyl group to methyl acceptors via SAM-dependent methyltransferases, producing the intermediate *S*-adenosylhomocysteine (SAH). SAH is

toxic to the cells, as it inhibits SAM-dependent methyltransferases. Pfs (*S*-adenosylhomocysteine / 5′-methylthioadenosine nucleosidase) detoxifies SAH by catalyzing its hydrolysis into adenine and *S*-ribosylhomocysteine (SRH) (Duerre 1962). SRH is then converted by LuxS (*S*-ribosylhomocysteinase), a metalloenzyme, into homocysteine and 4,5-dihydroxy-2,3-pentanedione (DPD) (Miller and Duerre 1968; Surette et al. 1999; Zhao et al. 2003), which is unstable and presumably spontaneously cyclizes and complexes with borate to form AI-2, a furanosyl borate diester (Chen et al. 2002b). However, much is still unknown about the formation of AI-2 from DPD and the chemical structure of AI-2. Miller *et al.* (Miller et al. 2004) determined that AI-2 is in equilibrium with DPD and other furanone rings not containing boron, which may mean that AI-2 is actually a mixture of compounds. Nonetheless, the products of the LuxS reaction, regardless of species, strongly induce light production in the AI-2-specific reporter strain of the bioluminescent marine bacterium *Vibrio harveyi* (Federle and Bassler 2003; Surette and Bassler 1998). Due to the variety of possible structures, AI-2 is quantified via a bioassay developed by Surette and Bassler (Surette and Bassler 1998), which uses this *V. harveyi* reporter strain.

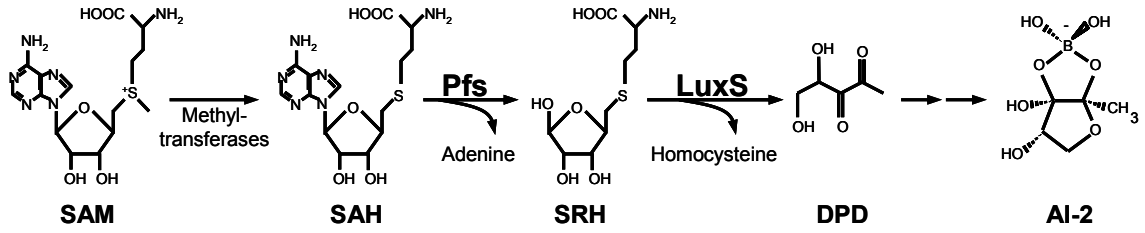

Scheme 1. Quorum sensing autoinducer-2 (AI-2) biosynthesis pathway. Abbreviations: SAM (*S*-adenosylmethionine), SAH (*S*-adenosylhomocysteine), SRH (*S*-ribosylhomocysteine), DPD (4,5-dihydroxy-2,3-pentanedione).

Importantly for drug design, Pfs and LuxS are not found in mammalian cells. For this, several researchers have designed inhibitors of Pfs catalytic activity (Cornell et al. 1996; Singh et al. 2005; Singh et al. 2006) or LuxS catalytic activity (Alfaro et al. 2004; Shen et al. 2006), and such research is ongoing. Pfs is believed to be a particularly appealing target for drug design as it is necessary for the detoxification of the SAH intermediate in bacteria. For example, Cadieux *et al.* (Cadieux et al. 2002) demonstrated that a *pfs* null-mutant strain of *Escherichia coli* was severely restricted in growth. However, due to the importance of Pfs in bacterial growth and survival, inhibitors of Pfs would place harsh selective pressure on bacteria to develop resistance. In contrast, inhibitors of LuxS would only inhibit QS, which does not regulate essential phenotypes, i.e. QS is not necessary for bacterial growth and survival. However, development of LuxS inhibitors is challenging due to the instability of LuxS in *in vitro* experiments. For example, Zhu *et al.* (Zhu et al. 2002) demonstrated improved stability of Co^{2+}-substituted LuxS compared with native LuxS (containing Fe^{2+} cofactor), however, ~ 20% loss of activity was still observed after 10 h incubation at room temperature. An additional idea is to create a pro-drug: a small molecule that is modified by Pfs (or another bacterial enzyme) to create the activated drug that inhibits LuxS. Resistance to a pro-drug would require two gene mutations compared to one, and thus, the lifetime is further extended. For example, resistant strains to penicillin developed within two years of its introduction, as only one gene mutation was required, whereas resistant strains to vancomycin developed 29 years after its introduction, as five gene mutations were required (Walsh 2000).

Bio-micro-chip for novel antibiotic screening

The overall goal of this research project is the creation of a bio-micro-chip containing assembled Pfs and LuxS enzymes, to screen for novel anti-pathogenic drugs that would inhibit AI-2 biosynthesis, and hence, QS. Bio-micro-chips, based on biofunctionalization of microfabricated devices, are advantageous for many biomedical testing applications as they enable automated and high-throughput analysis of multiple analytes in parallel, and require minimal volumes of expensive reagents. For this, bio-micro-chips are being developed for enzymatic assays (de Boer et al. 2005; Garcia et al. 2007; Hadd et al. 1997; Rusling et al. 2007), immunoassays (Choi and Cunningham 2007), ion channel profiling (Pihl et al. 2005b), and other assays for human disease markers. In particular, they hold great potential for point-of-care clinical testing, making central analysis laboratories obsolete. Additionally, bio-micro-chips are advantageous for high-throughput screening of drug candidates, where hundreds or even thousands of drug candidates are simultaneously tested (Clayton 2005; Dittrich and Manz 2006; Dove 2003; Dupuy et al. 2005). Many companies have developed and marketed chip technologies for medical diagnostics and drug screening applications (Clayton 2005; Dove 2003; Dupuy et al. 2005; Pihl et al. 2005a).

Creation of bio-micro-chip: assembly of quorum sensing pathway enzymes

To create this bio-micro-chip, it was necessary to first examine the protein assembly process. Surface-assembly of proteins onto microdevices is important but remains challenging due to their labile nature. That is, proteins can lose activity upon immobilization due to unfolding processes (Norde 1986). Surface-assembly of

catalytically active enzymes remains particularly challenging, as the overall 3-dimensional structure must be retained, and also as the active site must retain access to the substrate solution. Additionally, many assembly methods require special facilities and instrumentation, arduous multi-step procedures, and dry environments and other experimental conditions not ideal for maintaining biological activity. Several methods currently exist for protein assembly, including: physical entrapment within sol-gel films (Chen et al. 2003b; Miao and Tan 2001; Wang et al. 2006; Wang et al. 2003), affinity capture via ligand (Chang et al. 2007; Choi et al. 2002; Li and Lee 2004; Tachibana et al. 2006; Zhen et al. 2004), spotting (Angenendt et al. 2005; Caelen et al. 2002; Lee et al. 2005; Zhang et al. 2003), soft lithography (Hyun et al. 2001; Kane et al. 1999; Mayer et al. 2004; Suh et al. 2004; Wilhelm and Wittstock 2002; Xia and Whitesides 1998), photolithography (Fodor et al. 1991; Petrou et al. 2007; Sebra et al. 2006; Wilde et al. 2001), and attachment to self-assembled monolayers (Rozkiewicz et al. 2006; Su and Li 2004; Tender et al. 1996; Veiseh et al. 2002), to glutaraldehyde-activated surfaces (Diao et al. 2005; Lee et al. 2003a; Park et al. 2006; Pessela et al. 2007; Shanazarova et al. 2007; Yang et al. 2004; Yi et al. 2005c), and to other chemically modified surfaces (Williams and Blanch 1994).

Our protein assembly approach is based on two unique strategies: electrodeposition of a chitosan scaffold onto a patterned electrode surface of the device, and covalent conjugation of the target protein to the chitosan scaffold upon biochemical activation of a genetically fused "pro-tag". First, the aminopolysaccharide chitosan electrodeposits as a stable thin film onto an electrode surface due to its pH-responsive properties conferred by its abundant amine groups, as shown in Scheme 2. At low pH,

the amine groups are protonated, and chitosan is a water-soluble cationic polyelectrolyte. At pH above its pKa (> 6.3), the amine groups become deprotonated, and chitosan becomes an insoluble hydrogel network. Due to its pH-responsive properties, chitosan electrodeposits onto a negatively biased electrode surface where local high pH is created (Luo et al. 2004; Luo et al. 2005b; Pang and Zhitomirsky 2005; Tangkuaram et al. 2007; Wu et al. 2002; Wu and Payne 2004; Wu et al. 2003; Yi et al. 2004). Second, tyrosinase biochemically activates accessible tyrosine residues of the C-terminal pentatyrosine pro-tag into reactive *o*-quinones, which then covalently link to the nucleophilic amine groups of chitosan to form the protein-chitosan conjugate, as shown in Scheme 3 (Chen et al. 2002a; Chen et al. 2003a; Freddi et al. 2006; Sampaio et al. 2005; Yamada et al. 2007; Yi et al. 2005b). Chitosan confers its pH-responsive properties to the protein upon covalent conjugation.

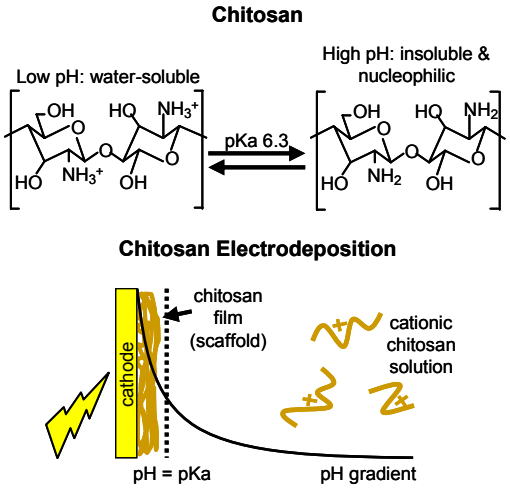

Scheme 2. The aminopolysaccharide chitosan has pH-responsive and nucleophilic properties. Chitosan electrodeposits as a stable thin film (scaffold) onto a cathode surface due to its pH-responsive properties.

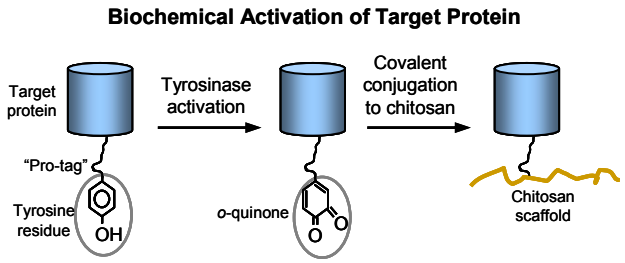

Scheme 3. Accessible tyrosine residues of the C-terminal pentatyrosine "pro-tag" are biochemically activated by tyrosinase into reactive *o*-quinones, which then covalently link to chitosan.

Summary

To summarize, the overall goal of my research project was to characterize and optimize the patterned assembly of active Pfs and LuxS enzymes onto microfabricated devices using our assembly approach. For this, I first examined the assembly of a model protein green fluorescent protein, discussed in Chapter 2. I then examined assembly of Pfs, discussed in Chapters 3 and 4, and finally, I examined assembly of LuxS, discussed in Chapter 5. I summarize my conclusions and recommendations for future work in Chapter 6.

Chapter 2: Protein Assembly onto Patterned Microfabricated Devices through Enzymatic Activation of Fusion Pro-tag

Introduction

Integrating proteins with microfabricated devices has gained significant attention for various applications such as biosensors (Chen et al. 2003b; Luo et al. 2004; Miao and Tan 2001; Wang et al. 2003; Wang et al. 1999; Yang et al. 2004), medical diagnostics (Kartalov et al. 2006; Lee et al. 2005; Sebra et al. 2006), microarrays (Caelen et al. 2002), bioMEMS (biological microelectromechanical systems) (Grayson et al. 2004; Kartalov et al. 2006; Kim et al. 2001), and metabolic engineering (Jung and Stephanopoulos 2004). Current methods for protein assembly include physical entrapment within sol-gel films (Chen et al. 2003b; Miao and Tan 2001; Wang et al. 2003), affinity capture via ligands (Choi et al. 2002; Li and Lee 2004; Zhen et al. 2004), mechanical methods such as microstamping onto polymer surfaces (Hyun et al. 2001), spotting (Caelen et al. 2002; Lee et al. 2005), and soft lithography (Kane et al. 1999; Suh et al. 2004), optical methods such as photolithography (Fodor et al. 1991; Sebra et al. 2006), and chemical methods such as attachment to self-assembled monolayers (Tender et al. 1996; Veiseh et al. 2002) and to chemically modified surfaces (Williams and Blanch 1994). Chemical methods also include cross-linking proteins through their amines to surfaces or polymer films activated by glutaraldehyde (Diao et al. 2005; Lee et al. 2003a; Park et al. 2006; Yang et al. 2004; Yi et al. 2005c). Despite these advances, protein assembly onto devices remains challenging due to the need for special facilities and instrumentation, arduous multi-step

procedures, and dry environments and other experimental conditions not ideal for maintaining biological activity.

We report an approach based on two strategies: scaffold electro-assembly onto a patterned conductive surface and covalent assembly of the target protein onto the patterned scaffold surface upon enzymatic activation of a genetically fused pro-tag. First, the scaffold is the pH-responsive aminopolysaccharide chitosan that electrodeposits as a stable thin film onto a conductive surface due to its pH-responsive properties that are conferred by its abundant primary amine groups. At low pH (< 6.3), the amine groups are protonated, and chitosan is a water-soluble cationic polyelectrolyte. At neutral to high pH, these amine groups become deprotonated, and chitosan forms an insoluble hydrogel network. Due to its pH-responsive solubility transition, chitosan electrodeposits onto a negatively biased electrode surface due to localized high pH at the cathode surface (Luo et al. 2004; Luo et al. 2005b; Pang and Zhitomirsky 2005; Wu et al. 2002; Wu and Payne 2004; Wu et al. 2003; Yi et al. 2005b). Once deposited, the chitosan film is stable and adheres to the cathode surface in the absence of an applied voltage. Second, tyrosinase enzyme activates the C-terminal pentatyrosine pro-tag that is genetically fused to the target protein. As illustrated in Scheme 4, tyrosinase converts accessible tyrosine residues of the pro-tag into reactive *o*-quinones that form covalent linkage to the nucleophilic amine groups of the chitosan scaffold (Chen et al. 2002a; Chen et al. 2003a; Freddi et al. 2006; Sampaio et al. 2005; Yi et al. 2005b). The target model protein is green fluorescent protein (GFP). GFP preferentially grafts to the chitosan scaffold through its C-terminal pro-tag versus its native tyrosines by a ratio of over 4:1 (Lewandowski et al. 2006); that is, over 80 % of GFP molecules are grafted through the

C-terminal pro-tag. Thus the GFP molecules are specifically oriented through the pro-tag with respect to the scaffold surface and are subsequently accessible in aqueous solution.

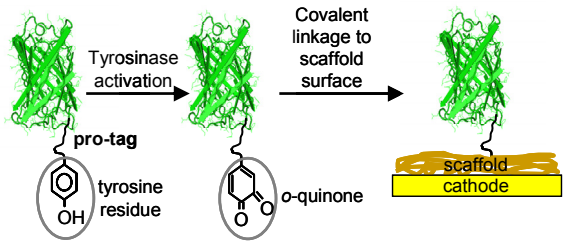

Scheme 4. Enzymatic activation and surface-assembly of target protein onto electrodeposited scaffold surface.

We report assembly of GFP fused with a pro-tag onto pre-fabricated devices using our two-step approach: electro-assembly of the scaffold onto selected electrode patterns followed by covalent assembly of GFP onto the scaffold surface upon enzymatic activation of the pro-tag. We performed assembly onto both 2-dimensional chips and within fully packaged microfluidic devices *in situ* and under flow. We also demonstrate on-site activation of the pro-tag through assembly of the activating enzyme, which allows for sequential assembly of multiple target proteins onto a single device. Our strategy covalently assembles specifically oriented proteins in a spatially selective manner onto device surfaces under mild experimental conditions, ideal for maintaining protein biological activity. We envision many potential bioMEMS and biosensing applications that require facile *in situ* "biofunctionalization" of microfabricated devices.

Materials and Methods

Materials.

Chitosan (minimum 85% deacetylated chitin; molecular weight 200,000 g/mol) from crab shells, phosphate buffered saline (PBS) (2.7 mM KCl, 137 mM NaCl, 1.5 mM KH_2PO_4, 8.1 mM Na_2HPO_4, pH 7.5), and tyrosinase from mushroom were purchased from Sigma (St. Louis, MO). Tyrosinase was reported by the manufacturer to have an activity of 1,530 Units/mg solid. Sodium hydroxide was purchased from J. T. Baker (Phillipsburg, NJ). Acetone, hydrochloric acid, sulfuric acid, and glycerol were purchased from Fisher Chemical (Fair Lawn, NJ). Bleach was purchased from James Austin Co. (Mars, PA). De-ionized water (ddH2O, 18 MΩ•cm, Milli-Q) and PBS (dissolved in de-ionized water) were autoclaved before use.

Chitosan preparation.

Chitosan solution was prepared by adding chitosan flakes in de-ionized water, with HCl added dropwise to maintain pH ~ 2, and mixing overnight. The pH was then adjusted to 3.5 by adding 1 M NaOH dropwise, and the chitosan solution was then filtered and stored at 4^oC.

Chip fabrication.

The microfabrication process for the chips was reported previously (Yi et al. 2004). Briefly, 4″ diameter silicon wafers were coated with 1 μm silicon nitride film, followed by deposition of 50 Å chromium film, and finally, deposition of 2000 Å gold film. The patterns were created by photolithography, and the photoresist removed using acetone. The chips contain two upper gold rectangular patterns (6 mm long × 3 mm wide). The left upper pattern was where the alligator clip was attached. The upper patterns are each linked by 8 mm gold lines to two lower gold rectangular patterns (8 mm

long × 1 mm wide). The left lower pattern was where assembly was performed. Chips were cleaned by incubation in ~ 1.4 M HCl for 30 minutes (to remove deposited chitosan), followed by incubation in concentrated bleach for 20 minutes (to sanitize and to ensure that organic molecules are removed), with thorough rinsing with de-ionized water after each cleaning step.

Assembly onto chips.

First, chitosan was deposited onto the left gold electrode by dipping the chip into chitosan solution (0.5 % (w/w), pH 3.7) and applying negative bias to the electrode (2 min at 16 A/m^2). This was done by connecting the cathode and anode (nickel chromium wire) using alligator clips to a DC power supply (Keithley 2400 SourceMeter). After deposition, the chip was rinsed thoroughly with de-ionized water and rinsed with PBS. The chip was then incubated in both tyrosinase (0.1 mg/mL or 166 Units/mL) and $(His)_6$-GFP-EK-$(Tyr)_5$ (0.2 mg/mL) in PBS for 16 h at 4°C. The production of $(His)_6$-GFP-EK-$(Tyr)_5$ was previously described. Briefly, the GFP was expressed in *E. coli* BL21, and IMAC-purified using a 5 mL HiTrap Chelating HP column charged with Ni^{2+} ions (Amersham Biosciences). Controls for this experiment were done by incubating a chip with deposited chitosan in GFP alone or in tyrosinase alone. For the method with two chips, the activator chip was created by incubating a chip with deposited chitosan in tyrosinase solution for 16 h at 4°C. After rinsing thoroughly with de-ionized water and washing 3 × 5 min in PBS with gentle shaking, the activator chip was then incubated face-to-face with the assembly chip (2nd chip with deposited chitosan) in GFP solution for 2 h at 30°C such that the chitosan patterns were directly opposite one another and less than 1 mm apart. This was accomplished by holding the chips in place with an alligator

clip. An additional experiment was performed where the two chips were incubated in GFP back-to-back with the chitosan patterns ≥ 5 mm apart. A control was done where the activator chip did not contain deposited chitosan. All chips were rinsed thoroughly with de-ionized water, and washed in PBS 3 × 5 min with gentle shaking before viewing under the fluorescence microscope (5 second exposure). ImageJ software (National Institutes of Health) was used to analyze the fluorescence intensity of the fluorescence micrographs.

Microfluidic device fabrication and packaging.

The fabrication process of our microfluidic device with packaging was reported previously (Park et al. 2006). Briefly, our microfluidic device features six identical microchannels evenly distributed on a 4″ pyrex wafer with two rectangular gold electrodes underneath each microchannel. A Cr adhesion layer (90 Å) and then a gold layer (2000 Å) were deposited onto a 4″ Pyrex wafer, and rectangular gold electrode patterns (1 mm × 0.5 mm) were created by photolithography. SU8-50 (MicroChem, Newton, MA) was patterned on the top of substrate and electrode surface to form structures which serve a dual function, namely (1) sidewalls for a microfluidic channel, and (2) sharp "knife-edge" structures for reliable leak-tight sealing to a PDMS layer above. The wafer was leak-tightly sealed by a 300-μm-thick top sealing PDMS layer spun on a sealing Plexiglas plate, and the SU8-50/PDMS junction was compressed by two packaging Plexiglas plates with six pressure-adjustable compression bolts (1/4″-28) hexagonally spaced on the ring and six force tunable socket screws (4-40) between every two microchannels. The microchannels thus formed were 500 μm wide by 150 μm high. Fluidic connectors (NanoportTM) and electric Pogo pins (Interconnect Devices, Inc.)

were assembled through punched holes on the sealing PDMS and drilled-holes through the top sealing and packaging Plexiglas plates, and then connected to external pressure-driven aqueous transport and electrical signal, correspondingly.

Assembly in microfluidic device.

To avoid cross contamination among different solutions, a LabView based microfluidic control system enabling selection from different solutions with separate tubing was developed to enhance control over different solutions and processes. First, the experimental microchannel and all connecting tubing (0.02" ID, Tygon®) were rinsed with de-ionized water at 50 μL/min for 30 min using a micropump (Masterflex® pump drive, Cole-Palmer). Chitosan (0.375 % (w/w), pH 5) was pumped into the microfluidic system at 5 μL/min. After the microchannel was completely filled with chitosan solution, the pump was stopped. A power supply (Keithely 2400 source meter) was then used to maintain negative bias voltage on the gold (working) electrode under constant current conditions of 3 A/m^2 for 240 seconds, while a second gold electrode served as the anode. The chitosan solution was then drained from the system, and the deposited chitosan was washed with PBS (30 min at 5 μL/min). After draining the PBS buffer, a PBS solution with $(His)_6$-GFP-EK-$(Tyr)_5$ (0.2 mg/mL) and tyrosinase (0.1 mg/mL or 166 Units/mL) was pumped at 5 μL/min over the deposited chitosan. As a control, a PBS solution with GFP but without tyrosinase was pumped at 5 μL/min over the deposited chitosan. (Between experiments the system was cleaned by rinsing with ~ 1.4 M HCl and then concentrated bleach at 5 μL/min for 10 minutes each, followed by thorough rinsing with de-ionized water at 50 μL/min for 30 min.) For real-time *in situ* fluorescence and observation, the microfluidic device was placed under a microscope (Zeiss model 310)

and a UV source (Zeiss HBO 100). Fluorescence micrographs were acquired every minute from the microscope using a digital camera (Carl Ziess AxioCam MRc5). Finally, the system was washed with PBS (30 min at 5 μL/min). ImageJ software (National Institutes of Health) was used to analyze the fluorescence intensity of the final fluorescence micrograph.

Results and Discussion

Enzymatic activation and assembly of target protein onto a patterned chip.

We demonstrate enzymatic activation of GFP for its assembly onto the patterned electro-assembled scaffold surface of a 2-dimensional chip, shown schematically in Fig. 1a. For this, we first electro-assembled chitosan scaffold onto a selected electrode pattern by dipping the chip in chitosan solution and applying negative bias to the left gold pattern (Fig. 1b). This chip with assembled scaffold was then incubated at 4^{o}C in a PBS solution containing the pro-tagged GFP (in excess of available scaffold) and the activating enzyme tyrosinase, which activates the pro-tag of GFP for its assembly onto the scaffold. Finally, the chip was thoroughly washed with PBS buffer. The fluorescence micrograph in Fig. 1c illustrates that (1) the target protein GFP assembled only onto the scaffold pattern with high spatial selectivity and uniformity, (2) the assembled GFP remained fluorescent, indicating the retention of its 3-dimensional structure, and finally, (3) non-specific binding of GFP to the other surfaces of the chip was minimal, as there is negligible fluorescence of the right gold electrode pattern or the silicon oxide. Importantly, incubating the chip with assembled scaffold in GFP alone (Fig. 1d) or tyrosinase alone (Fig. 1e) yielded significantly less fluorescence (< 3 % of the

fluorescence of Fig. 1c, based on ImageJ software analysis), indicating minimal non-specific binding of GFP to the scaffold, and that activation of the pro-tag by tyrosinase is required for GFP assembly. As GFP is covalently assembling onto the scaffold, the chip could be repeatedly washed with negligible loss in fluorescence (not shown). Additionally, the chips were reused by simply cleaning with dilute hydrochloric acid followed by concentrated bleach. Combined, these results demonstrate patterned and covalent assembly of biologically functional protein onto a 2-dimensional chip through enzymatic activation of the C-terminal pro-tag.

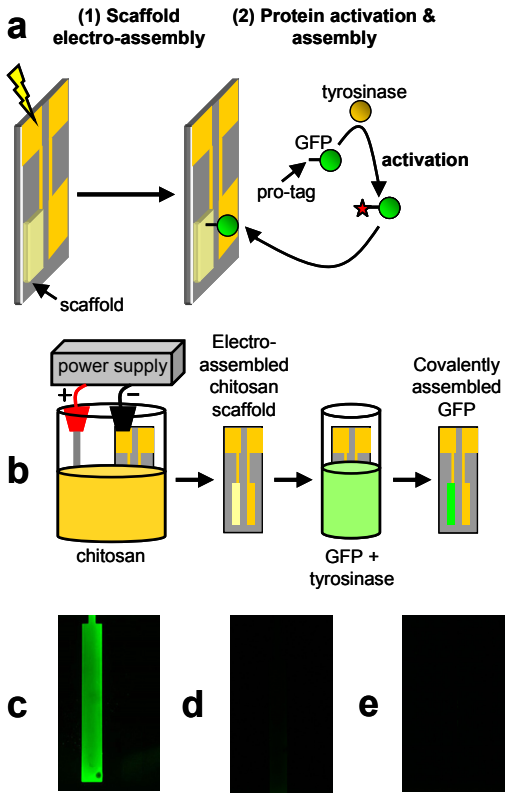

Figure 1. Enzymatic activation and assembly of target protein onto a patterned chip. **(a)** Electro-assembly of the scaffold onto a patterned electrode is followed by enzymatic activation and assembly of GFP onto the patterned scaffold surface. **(b)** The scaffold is assembled by dipping the chip into chitosan solution and applying negative bias to the selected electrode pattern. Subsequent incubation in GFP and tyrosinase solution activates and assembles GFP onto the patterned scaffold surface. **(c)** Fluorescence micrograph: chip with assembled scaffold incubated in GFP and tyrosinase. **(d)** Fluorescence micrograph: chip with assembled scaffold incubated in GFP only (control). **(e)** Fluorescence micrograph: chip with assembled scaffold incubated in tyrosinase only (control).

We have demonstrated a high degree of covalent grafting and a low degree of non-specific binding of the target protein GFP to electrodeposited chitosan scaffold. This agrees with previously reported results (Chen et al. 2003a; Lewandowski et al. 2006), which examined GFP binding to chitosan in solution. Electrodeposited chitosan may have structural and chemical properties that are distinctly different than soluble chitosan, particularly in that the chitosan experiences a high pH for a short time during the electrodeposition. In the present work, the chitosan scaffold is electrodeposited prior to target protein assembly, and thus, there is no pH-dependence for the protein assembly. Indeed, the protein assembly process takes place under mild experimental conditions ideal for maintaining protein activity and 3-dimensional structure: at low temperature, through enzymatic activation, in aqueous solution, and at neutral pH. Thus, our current assembly technique is particularly advantageous for pH- or temperature-sensitive proteins.

Due to the distinct differences between electrodeposited chitosan and soluble chitosan, the current assembly procedure was investigated as an alternative to that of previous work where the procedural order was reversed: the protein was first conjugated to chitosan in solution, and then this protein-chitosan conjugate was electrodeposited (Chen et al. 2003a; Yi et al. 2005c). Conjugation occurred at pH ~ 6 so that chitosan remained soluble, i.e. below its pKa of 6.3, and this may destabilize low pH-sensitive proteins and additionally proteins with isoelectric points at or near pH 6. Next, electrodeposition of the protein-chitosan conjugate solution occurred at pH 11 – 12, which may destabilize high pH-sensitive proteins. Additionally, the protein was embedded within the electrodeposited chitosan film and in no particular orientation. In

the current work, in contrast, the protein presumably assembles onto the scaffold surface as diffusion of proteins into the chitosan film is low. Indeed, this low diffusion allows proteins to be physically entrapped within chitosan films (Luo et al. 2005a).

Finally, we expect the vast majority of GFP molecules to be specifically oriented through the C-terminal pro-tags as they assemble onto the scaffold surface, as we previously demonstrated that GFP preferentially grafts to chitosan through the pro-tag versus native tyrosines by a ratio of over 4:1; that is, over 80 % of binding is through the pro-tag (Lewandowski et al. 2006). This enables orientational control and contrasts considerably with an additional previous approach, where the protein was covalently linked through its native amines to a glutaraldehyde-activated chitosan film surface and thus in no particular orientation (Park et al. 2006; Yi et al. 2005c). These aspects of our strategy (surface-assembly under orientational control) are especially advantageous for biosensor applications involving enzymes, which require reproducible orientation and active site accessibility.

In summary, Fig. 1 demonstrates covalent assembly of the target protein GFP onto selected patterned scaffold surfaces of 2-dimensional microfabricated chips under mild experimental conditions. Assembly occurs through the C-terminal pro-tag upon selective enzymatic activation. This assembly strategy is advantageous for pH-sensitive proteins and biosensor applications involving assembled enzymes.

On-site activation and assembly of target protein onto multiple patterned chips.

Next, we demonstrate assembly of GFP onto the patterned scaffolds of 2-dimensional chips through on-site enzymatic activation by assembled tyrosinase, shown schematically in Fig. 2a. For this, we first assembled the activating enzyme tyrosinase

(by incubation in tyrosinase solution) onto electro-assembled chitosan scaffold on one chip serving as the activator chip (Fig. 2b). After thorough rinsing, the activator chip was incubated in GFP solution directly opposite and < 1 mm from the assembly chip, which contained only electro-assembled chitosan scaffold. The fluorescence micrographs in Fig. 2c illustrate that (1) similar quantities of the target protein GFP assembled onto both activation and assembly sites, and (2) GFP assembled only onto the patterned chitosan scaffolds with high spatial selectivity and uniformity.

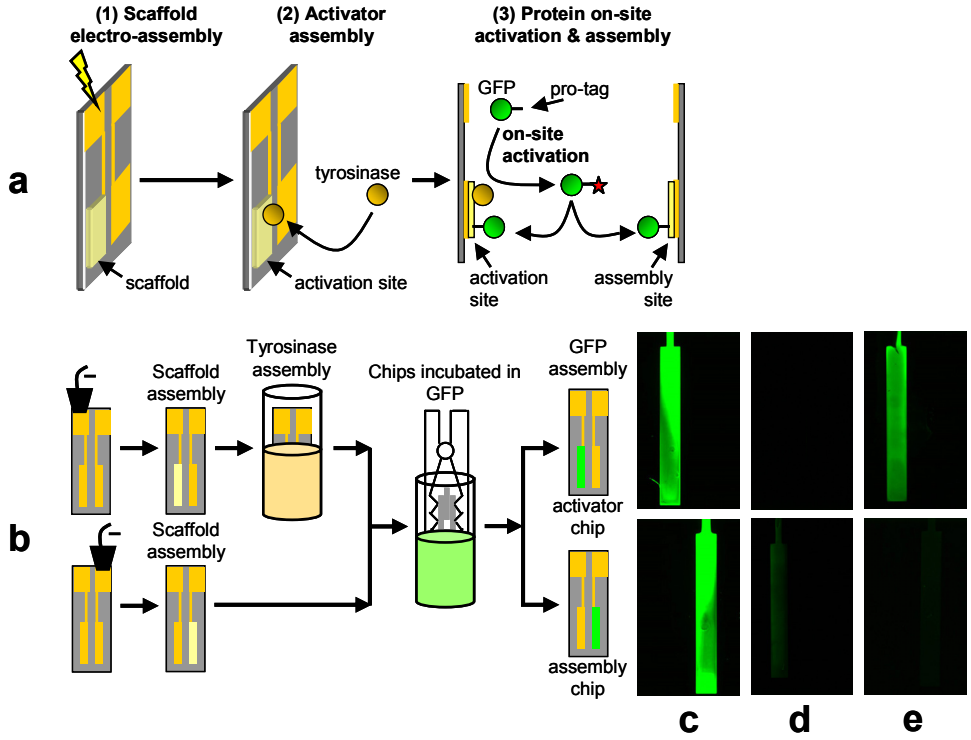

Figure 2. On-site activation and assembly of target protein onto multiple patterned chips. **(a)** Tyrosinase activator is assembled onto the patterned scaffold surface to create an activation site. GFP is activated on-site by the assembled tyrosinase for its local assembly at both the activation site and the proximal assembly site. **(b)** The activator chip is created by electro-assembly of the scaffold followed by tyrosinase incubation. The assembly chip is created by electro-assembly of the scaffold. Both chips are then incubated in GFP solution. **(c)** Fluorescence micrographs: activator and assembly chips incubated in GFP solution directly opposite each other and < 1 mm apart. **(d)** Fluorescence micrographs: minimal tyrosinase assembled onto the activator chip (control with no electro-assembled scaffold). **(e)** Fluorescence micrographs: activator and assembly chips incubated in GFP solution back-to-back with the scaffolds ≥ 5 mm apart.

These results demonstrate that (1) the tyrosinase assembled onto the activator chip, (2) the activator chip served as a heterogeneous catalyst for GFP activation, (3) the assembled tyrosinase activated GFP on-site for its assembly onto the activator chip, and finally, (4) the assembled tyrosinase activated GFP for assembly onto a second proximal chip (assembly chip). Importantly, a chip without assembled scaffold bound a minimal quantity of tyrosinase activator, and could not be used to activate and assemble GFP, as illustrated by the minimal fluorescence of both chips in Fig. 2d.

Finally, we demonstrate that the distance between activation and assembly sites is critical for target protein assembly. For this, the activator and assembly chips were incubated in GFP solution back-to-back with the scaffolds $\geq$ 5 mm apart. Here, GFP assembled only onto the activation site, as illustrated in Fig. 2e. This indicates that a minimal amount, if any, of tyrosinase was released from the scaffold and into the GFP solution, as any released tyrosinase would have activated GFP for its assembly onto the assembly site. We propose that the reactive *o*-quinones created by activation of the pro-tag each have a short half-life and can only diffuse a short distance before losing activity. The distance between activation of the target protein and available scaffold must be significantly small to result in target protein assembly onto the scaffold. In a sense, this makes our approach (pro-tag activation and assembly) a self-passivating system. This short half-life, however, also indicates that formation of multimer forms of the target protein is possible (i.e. attachment of multiple activated proteins together), if activated protein molecules encounter each other before encountering the scaffold surface; this possibility was previously noted (Chen et al. 2003a; Lewandowski et al. 2006). Nonetheless, we view the short half-life of activated protein as a strength of our assembly

strategy for the biofunctionalizaton of microfabricated devices, as it demonstrates the flexibility of our strategy, and we envision many potential applications. For example, this method can be used for the sequential assembly of multiple proteins onto separate patterned scaffold surfaces of the same device. For chip assembly, each protein would be directed to a specific scaffold pattern by placement of the scaffold proximal to the activation site during target protein incubation. This could additionally be accomplished with microfluidic devices under flow of the target protein, where each assembly site would be directly downstream of each activation site.

In summary, Fig. 2 demonstrates that tyrosinase enzyme can be assembled to form an activation site for on-site activation of the target protein, which then assembles locally onto both the activation site and onto a proximal assembly site. Local assembly of the target protein is presumably due to the short half-life of activated protein. These results demonstrate an additional flexibility to our assembly strategy, and we envision many potential applications involving sequential assembly of multiple target proteins.

In situ activation and assembly of target protein within a completely packaged microfluidic device.

Finally, we demonstrate *in situ* activation and assembly of GFP onto a selected electrode pattern within a completely packaged microfluidic device, shown in Fig. 3. For this, we fabricated a microfluidic device that features six identical microchannels evenly distributed on a 4″ pyrex wafer (Park et al. 2006); one microchannel is illustrated in Fig. 3a. The microfluidic device employs a microfabricated SU8 layer on a transparent Pyrex wafer that defines the microchannel structure, two patterned gold electrodes at the bottom of each microchannel, a top PDMS gasket that seals the microchannel by compression

bolts, and fluidic and electrical input/output ports that connect to an external micropump and electrical signals, respectively. The solution selection and pumping is controlled by LabView.

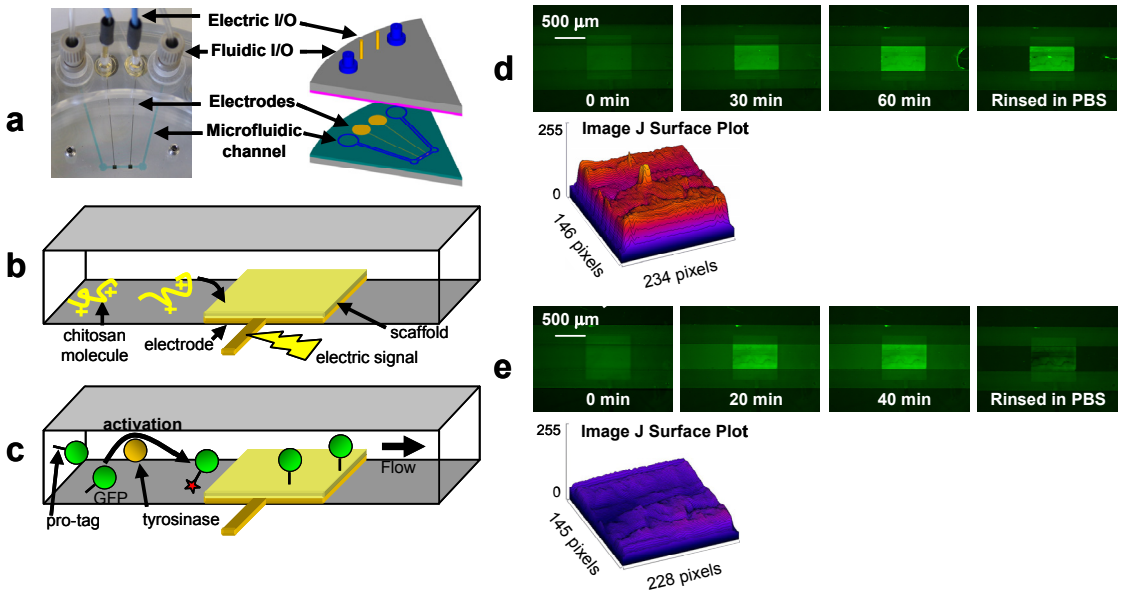

Figure 3. *In situ* activation and assembly of target protein within a completely packaged microfluidic device. **(a)** One of the six microfluidic channels of the completely packaged microfluidic device. **(b)** Chitosan scaffold is electro-assembled onto a gold electrode pattern within a microchannel (static state). **(c)** *In situ* tyrosinase activation and assembly of GFP onto the patterned scaffold surface within a microchannel under flow. **(d)** Fluorescence micrographs of the assembly site during *in situ* GFP activation and assembly, and after rinsing the assembly site with PBS buffer, with a surface plot (ImageJ) of the rinsed assembly site. **(e)** Fluorescence micrographs of the assembly site during GFP non-covalent assembly (control with no tyrosinase activation), and after rinsing the assembly site with PBS buffer, with a surface plot (ImageJ) of the rinsed assembly site.

We electro-assembled chitosan scaffold onto a selected gold electrode pattern within a microchannel by transporting chitosan solution into the channel, and then stopping the pump and applying negative bias to the electrode pattern (Fig. 3b). Next, we continually pumped through the channel a PBS solution containing the target protein GFP and the activating enzyme tyrosinase (Fig. 3c) to activate and assemble GFP onto the electro-assembled chitosan scaffold. We observed the fluorescence profile of the 1 mm ×

0.5 mm assembly site (scaffold) in real time through an on-site fluorescence microscope. As illustrated in Fig. 3d, the fluorescence intensity of the assembly site gradually increased with time until reaching a maximum constant level. Importantly, the fluorescence remained high even after thorough PBS buffer rinsing, indicating that GFP was covalently bound to the chitosan scaffold. Next, we analyzed the fluorescence intensity of the final micrograph of the assembly site using ImageJ software, which illustrates that GFP assembled relatively uniformly onto the scaffold pattern. These results demonstrate that (1) the target protein GFP assembled only onto the chitosan scaffold with high spatial selectivity and uniformity, (2) the assembled GFP remained fluorescent after thorough rinsing, and (3) non-specific binding of GFP to other channel surfaces was minimal, as there was no significant fluorescence of the microchannel floor, ceiling, or walls.

Next, we performed control experiments to examine non-specific binding of unactivated GFP to the electro-assembled scaffold. For this, we reused the same microchannel by removing the scaffold from the previous experiment with dilute hydrochloric acid. We then reassembled the chitosan scaffold onto the electrode pattern, and then continually pumped through the channel a PBS solution containing only the target protein GFP (without the activating enzyme tyrosinase). As illustrated in Fig. 3e, the fluorescence intensity of the assembly site gradually increased with time until reaching a constant level. However, the fluorescence decreased significantly upon PBS buffer rinsing, as illustrated by ImageJ software analysis of the final fluorescence micrograph. Further ImageJ analysis of the final micrograph revealed that the average fluorescence intensity was ~ 47 % compared to that of the experimental micrograph (Fig.

3d). These results indicate that the GFP here was loosely bound to the chitosan scaffold and easily rinsed off, and confirm that activation of the pro-tag by tyrosinase is required for GFP assembly.

We have demonstrated here, for the first time, *in situ* enzymatic activation and assembly of a target protein onto a patterned scaffold within a microfluidic channel under flow. The target protein GFP assembled covalently and uniformly in a spatially selective manner, and was not released upon further flow and buffer rinsing. This is significant, as we are unaware of any reports demonstrating the spatially-resolved enzymatically-activated covalent assembly of proteins in microchannels under flow. Additionally, as discussed earlier, GFP is assembling predominately through its C-terminal pro-tag, i.e. in a specific orientation onto the patterned scaffold surface. In contrast, in our previous work with microfluidic channels, the protein was covalently linked through its native amines to a glutaraldehyde-activated chitosan film surface and in no particular orientation (Park et al. 2006; Yi et al. 2005c). Finally, assembly occurs in a completely fabricated and packaged device for reusability, and as mentioned before, occurs under mild experimental conditions ideal for maintaining protein biological function: in aqueous solution, through enzymatic activation, and at neutral pH. These unique advantages of our assembly strategy combined with the well-known advantages of microfluidic devices (i.e. rapid response time and small volumes of expensive reagents) make this particularly appealing for applications that necessitate microfluidic systems.

In summary, Fig. 3 demonstrates *in situ* enzymatic activation and assembly of the target protein GFP within a pre-fabricated and fully packaged microfluidic device under flow. Assembly is covalent and robust, spatially selective (only onto selected patterned

scaffold surfaces), and occurs under mild experimental conditions. Importantly, our assembly approach is readily applicable to microfluidic systems.

Conclusions

We report a versatile approach for covalent protein assembly onto the surfaces of selected patterned scaffolds of pre-fabricated devices. Our results demonstrate assembly of the model protein GFP genetically fused with a C-terminal pentatyrosine pro-tag onto both 2-dimensional chips and within fully packaged microfluidic devices.

We believe that our assembly approach holds several unique advantages. First, the entire assembly process occurs under mild experimental conditions: in aqueous solution, through enzymatic activation, and at neutral pH, making it ideal for maintaining protein 3-dimensional structure and biological function. Second, the assembled protein is readily accessible and specifically oriented as it assembles though the C-terminal pro-tag onto the scaffold surface. This makes our approach particularly appealing for assembling enzymes, where reproducible orientation and active site accessibility are necessary for maintaining catalytic activity. Third, the activating enzyme tyrosinase can be assembled to create an activation site for on-site activation and local assembly of the target protein. This strategy can be exploited for local assembly of multiple proteins onto individual patterned scaffolds of the same device. Finally, the protein is enzymatically activated and assembled *in situ* within a microfluidic channel under flow, and thus, our approach is readily applicable to microfluidic systems, which have additional well-known advantages over batch systems. Combined, these advantages make our assembly approach appealing for a wide variety of bioMEMS and biosensing applications that require device biofunctionalization.

Chapter 3: Reproducible Assembly of Active Pfs Enzyme onto Patterned Areas of Microfabricated Chips

Introduction

Integrating biomolecules with microdevices is important but remains challenging due to the labile nature of biomolecules. For example, proteins can lose activity upon immobilization due to unfolding processes (Norde 1986). Surface-assembly of catalytically active enzymes remains particularly challenging. To enhance biocompatibility, researchers have created polymer interfaces between the enzymes and the device surfaces (Chen et al. 2003b; Cosnier et al. 2006; Miao and Tan 2001; Sung and Bae 2006; Wang et al. 2003; Wessa et al. 1999; Xu et al. 2005; Zhen et al. 2004). The next generation of "smart" biomaterials will require the intimate coupling of advances in microfabrication and biomolecular recognition. The novelty of the approach described here is the use of patterned microdevices (conductive surface patterning) for the assembly of enzymes through an activatable "pro-tag".

Our approach is based on two strategies: (1) electrodeposition of chitosan onto an electrode surface of the microfabricated device, and (2) covalent conjugation of the target enzyme to chitosan upon biochemical activation of a genetically fused pro-tag. First, the aminopolysaccharide chitosan electrodeposits as a stable thin film onto an electrode surface due to its pH-responsive properties conferred by its amine groups. At low pH, the amine groups are protonated, and chitosan is a water-soluble cationic polyelectrolyte. At pH above its pKa (> 6.3), the amine groups become deprotonated, and chitosan becomes an insoluble hydrogel network. Due to its pH-responsive properties, chitosan

electrodeposits onto a negatively biased electrode surface where local high pH is created (Luo et al. 2004; Luo et al. 2005b; Pang and Zhitomirsky 2005; Wu et al. 2002; Wu and Payne 2004; Wu et al. 2003; Yi et al. 2005b). Second, tyrosinase activates accessible tyrosine residues of the C-terminal pentatyrosine pro-tag into reactive *o*-quinones, which then covalently link to the nucleophilic amine groups of chitosan to form the protein-chitosan conjugate (Chen et al. 2003a; Chen et al. 2002b; Freddi et al. 2006; Sampaio et al. 2005; Yi et al. 2005b). Chitosan confers its pH-responsive properties to the protein upon covalent conjugation.

We report, for the first time, device-assembly of the enzyme Pfs (*S*-adenosylhomocysteine / 5′-methylthioadenosine nucleosidase) fused with a C-terminal pentatyrosine pro-tag. As shown previously in Scheme 1, Pfs is a member of the synthesis pathway for a "universal" signaling molecule in bacterial quorum sensing (autoinducer-2, AI-2) that mediates interspecies cell-cell communication. In this pathway, S-adenosylmethionine (SAM) is first converted to S-adenosylhomocysteine (SAH) by methyltransferases. Next, Pfs catalyzes the irreversible cleavage of SAH into adenine and *S*-ribosylhomocysteine (SRH) (Duerre 1962). SRH is then converted by the enzyme LuxS (*S*-ribosylhomocysteinase) into homocysteine and 4,5-dihydroxy-2,3-pentanedione, which then goes through several non-enzymatic rearrangements to become AI-2 (Miller and Duerre 1968). In addition to quorum sensing, Pfs is involved in important cellular processes, such as protein and DNA methylation and metabolism and polyamine biosynthesis (Borchardt 1980; Pajula and Raina 1979; Raina et al. 1982; Riscoe et al. 1984). The involvement of Pfs in important bacterial processes makes it an appealing target for the design of new antibiotics. Importantly for antibiotic design,

mammalian cells, in contrast, utilize the enzyme SAH hydrolase, which cleaves SAH into homocysteine and adenosine (Delahaba and Cantoni 1959). For this, several researchers have designed inhibitors of Pfs activity as possible antibiotics, and such research is ongoing (Cornell et al. 1996; Ragione et al. 1985; Singh et al. 2005; Singh et al. 2006). Thus, assembling Pfs for the controlled examination of its catalytic activity could be used to screen Pfs inhibitors with antibiotic capabilities.

As shown in Scheme 5, Pfs can be assembled by covalent conjugation to chitosan followed by electrodeposition of Pfs-chitosan conjugate onto a patterned electrode (Scheme 5a), or by electrodeposition of chitosan scaffold onto a patterned electrode followed by covalent conjugation of Pfs to the patterned scaffold (Scheme 5b). The procedural order of assembly can be chosen to suit the specific application, demonstrating the versatility of our overall assembly approach. As shown in Scheme 5, the assembled Pfs is capable of binding antibodies, and retains biocatalytic activity, converting SAH substrate into SRH and adenine. The assembly of Pfs is controlled by the electrode patterned area, resulting in reproducible rates of SAH catalytic conversion for a given area and SAH concentration. Correspondingly, using traditional enzyme reaction kinetic models (e.g., Michaelis-Menten) we can "design" specific reaction conditions based on electrode surface area. That is, this control allows us to manipulate the rate of biocatalysis and small molecule biosynthesis through modulation of the assembly area. We envision many potential biosensing and metabolic engineering applications using our versatile approach.

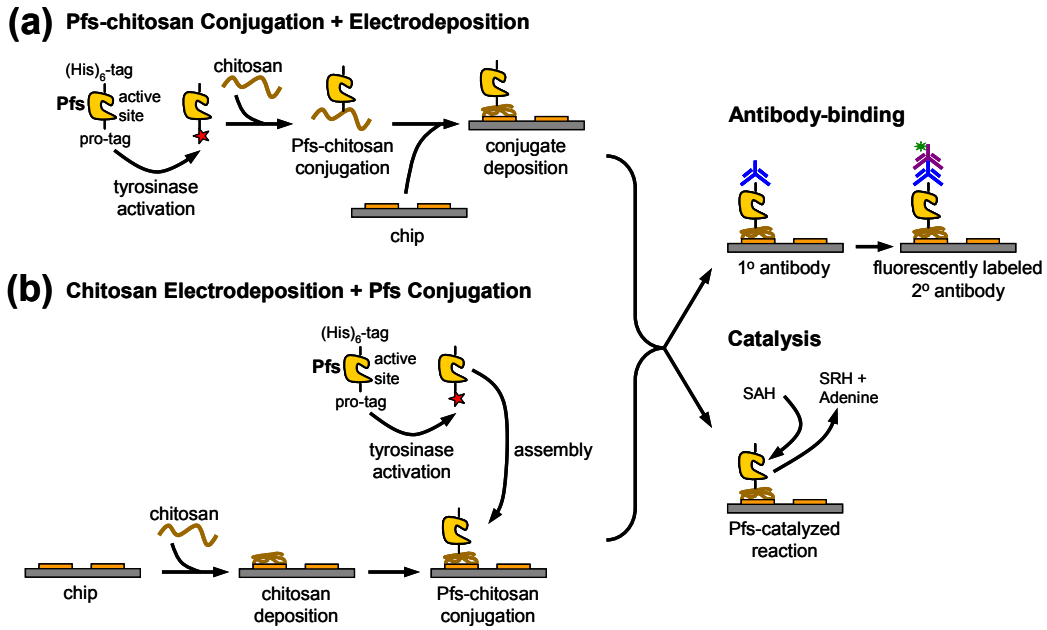

Scheme 5. (a) Pfs-chitosan conjugation followed by electrodeposition. First, Pfs conjugated to chitosan in solution upon tyrosinase activation of pro-tag. Then, Pfs-chitosan conjugate electrodeposited onto chip. **(b)** Chitosan electrodeposition followed by Pfs-chitosan conjugation. First, chitosan scaffold first electrodeposited onto chip. Then, Pfs assembled from solution onto scaffold upon tyrosinase activation of pro-tag. In both **(a)** and **(b)**, assembled Pfs bound fluorescently labeled antibody or catalyzed SAH cleavage into SRH + Adenine.

Materials and Methods

Materials.

S-adenosylhomocysteine (SAH), bovine serum albumin (BSA), chitosan (minimum 85 % deacetylated chitin; molecular weight 200,000 g/mol) from crab shells, goat anti-mouse IgG conjugated to fluorescein isothiocyanate (FITC), imidazole, isopropyl β-D-thiogalactopyranoside (IPTG), mouse anti-poly-histidine, nickel sulfate, phosphate buffered saline (PBS) (2.7 mM KCl, 137 mM NaCl, 1.5 mM KH_2PO_4, 8.1 mM Na_2HPO_4, pH 7.5), sodium cyanoborohydride, and tyrosinase from mushroom were purchased from Sigma (St. Louis, MO). Tyrosinase was reported by the manufacturer to

have an activity of 1,530 Units/mg solid. LB (Luria broth) medium was purchased from Becton Dickinson (Cockeysville, MD). Acetone, acetonitrile (HPLC grade), ampicillin sodium salt, chloroform, glycerol, sodium phosphate (monobasic), sodium phosphate (dibasic), sulfuric acid, Tris base (trishydroxymethylaminomethane), and water (HPLC grade) were purchased from Fisher Chemical (Fair Lawn, NJ). Hydrochloric acid and sodium chloride were purchased from J. T. Baker (Phillipsburg, NJ). Non-fat dry milk and Tween 20 were purchased from BioRad (Hercules, CA). Bleach was purchased from James Austin Co. (Mars, PA). De-ionized water (ddH2O, 18 MΩ·cm, Milli-Q) and PBS (dissolved in de-ionized water) were autoclaved before use.

Plasmid construction.

pTrcHis-Pfs-Tyr plasmid construction was reported previously (Fernandes et al. 2007). Briefly, the plasmid was constructed by PCR amplification of *pfs* from *E. coli* wild type strain W3110. Following digestion, the PCR products were extracted by gel purification and inserted into pTrcHisC (Invitrogen). DNA sequencing was performed to verify construct integrity. The plasmid was transformed into *E. coli* DH5α (defective *luxS* strain).

Purification of $(His)_6$-Pfs-$(Tyr)_5$.

E. coli DH5α containing pTrcHis-Pfs-Tyr was cultured at 37°C and 250 rpm in LB medium supplemented with ampicillin at 50 μg/mL. When the OD_{600nm} reached 0.5 – 0.6, IPTG was added to induce enzyme production at a final concentration of 1 mM IPTG. After an additional 5 hr, the culture was centrifuged for 10 min at 10,000 g's, and the cell pellet stored at – 20°C. The thawed pellet was resuspended in PBS + 10 mM

imidazole, pH 7.5, placed in an ice-water bath, and the cells lysed by sonication (Fisher Scientific Sonic Dismembrator 550). The lysed cells were centrifuged for 10 min 16,000 g's to remove insoluble cell debris, and the supernatant filtered though 0.22 μm PES filter. The enzyme was purified from the filtered soluble cell extract by immobilized metal-ion affinity chromatography (IMAC) using a 5 mL HisTrap chelating column (Amersham Biosciences). Prior to loading the filtered extract, the column was charged with Ni^{2+} ions using 0.1 M $NiSO_4$, washed with de-ionized water, and equilibrated with 3 column volumes (CVs) of 20 mM sodium phosphate, 250 mM NaCl, 10 mM imidazole, pH 7.4. After loading the filtered extract, the column was washed with 3 CVs of the previous buffer, washed again with 3 CVs of 20 mM sodium phosphate, 250 mM NaCl, 50 mM imidazole, pH 7.4, and the protein was eluted using 1.5 CVs of 20 mM sodium phosphate, 250 mM NaCl, 350 mM imidazole, pH 7.4. All steps were performed at 2 mL/min (1 cm/min linear velocity). The eluted sample was dialyzed overnight (16 hr) at 4°C into PBS. Purified protein concentration was determined with a UV/vis spectrophotometer (DU 640, Beckman, Fullerton, CA) using UV light at 280nm wavelength. The protein solution was mixed 2:1 with glycerol, alliquoted, and stored at –80°C.

Chitosan preparation.

Chitosan solution was prepared by adding chitosan flakes in de-ionized water, with HCl added dropwise to maintain pH ~ 2, and mixing overnight. The pH was then adjusted to 3.6 by adding 1 M NaOH dropwise, and the chitosan solution was then filtered and stored at 4°C until use.

Chip fabrication.

The microfabrication process for the chips was reported previously (Yi et al. 2004). Briefly, 4″ diameter silicon wafers were coated with 1 μm silicon nitride film, followed by deposition of 50 Å chromium film, and finally, deposition of 2000 Å gold film. The patterns were created by photolithography, and the photoresist removed using acetone. The chips contain two upper gold rectangular patterns (6 mm long × 3 mm wide). The left upper pattern was where the alligator clip was attached. The upper patterns are each linked by 8 mm gold lines to two lower gold rectangular patterns (8 mm long). The left lower patterns are 0.2 mm, 0.5 mm, 1 mm, 2 mm, and 4 mm wide. The right lower patterns are all 1 mm wide. The left lower pattern was where assembly was performed. Before the start of every experiment, each chip was cleaned by incubation in 1.4 M HCl for 30 minutes, followed by incubation in concentrated bleach for 20 minutes.

Pfs-chitosan conjugation and chip assembly.

First, the chip was incubated in 1 % (w/v) BSA – PBS for 2 h, rinsed with de-ionized water, and set aside. The conjugate was prepared by incubating $(His)_6$-Pfs-$(Tyr)_5$ (0.2 mg/mL), tyrosinase (0.1 mg/mL or 166 Units/mL), and chitosan (0.5 % (w/w)) in 50 mM sodium phosphate buffer (final pH of mixture 6.0) for 2 h at 30^{o}C and 250 rpm, followed by incubation in sodium cyanoborohydride (0.2 mg/mL) for 15 min at room temperature and 250 rpm. The conjugate was deposited onto the left gold electrode pattern by dipping the chip into the conjugate until the pattern was submerged and applying negative bias to the pattern (2 min at 2.5 A/m^2). This was done by connecting the cathode and anode (nickel chromium wire) using alligator clips to a DC power supply (Keithley 2400 SourceMeter). After deposition, the chip

was rinsed with de-ionized water. For antibody-binding experiments, the chip was incubated in 5 % non-fat dry milk – PBS for 4 h, rinsed with de-ionized water, and washed with gentle shaking 3 × 5 min in 5 mL TTBS (20 mM Tris-HCl, 500 mM NaCl, 0.05 % (v/v) Tween-20, pH 7.5) followed by antibody incubation. For determining catalytic activity of assembed conjugate, the chip was washed with gentle shaking 3 × 5 min in 5 mL TTBS and 3 × 5 min in 5 mL TBS, and then incubated at 37^{o}C in 1 mL of 1 mM SAH. At reaction time points, samples were taken and immediately extracted with chloroform to stop the reaction, and the extracted samples were stored at – 20^{o}C before injecting on the HPLC.

Pfs activation and assembly onto scaffold of chip.

Chitosan scaffold was deposited onto the left gold electrode pattern by dipping the chip into chitosan solution (0.5 % (w/w), pH 3.7) until the pattern was submerged and applying negative bias to the pattern (2 min at 16 A/m^2). After deposition, the chip was rinsed with de-ionized water and then with PBS. It was incubated in 5 % (w/v) non-fat dry milk – PBS for 4 h, followed by incubation in both tyrosinase (0.1 mg/mL or 166 Units/mL) and $(His)_6$-Pfs-$(Tyr)_5$ (0.1 mg/mL) in PBS for 16 h at 4^{o}C. It was then incubated in sodium cyanoborohydride (0.2 mg/mL) in de-ionized water for 15 min, rinsed with de-ionized water, and washed with gentle shaking 3 × 5 min in 5 mL TTBS. In the antibody-binding experiments, two controls were also performed: (1) chip with assembled scaffold incubated in $(His)_6$-Pfs-$(Tyr)_5$ (0.1 mg/mL) only (no tyrosinase), and (2) chip with assembled scaffold not incubated in $(His)_6$-Pfs-$(Tyr)_5$ or tyrosinase. For all antibody-binding experiments, following TTBS washes the chip was incubated in antibody solution. For determining catalytic activity of assembled

Pfs, following TTBS washes the chip was further washed 3 × 5 min in 5 mL TBS, and then was incubated at 37°C in 1 mL of 1 mM SAH. For determining Michaelis-Menten kinetics, following TTBS washes the chip was further washed 3 × 5 min in 5 mL TBS, and then was incubated at 37°C 225 rpm in 1 mL each of 1 mM, 0.25 mM, and 0.1 mM SAH. At reaction time points, samples were taken and immediately extracted with chloroform to stop the reaction, and the extracted samples were stored at – 20°C before injecting on the HPLC.

Antibody binding to assembled Pfs.

Following TTBS washes, the chip was incubated 1 h in 1:100 mouse anti-poly-histidine in 1 % (w/v) non-fat dry milk – TTBS, and washed 3 × 5 min in 5 mL TTBS. It was then incubated 1 h in 1:100 goat anti-mouse IgG FITC-conjugated in 1 % (w/v) non-fat dry milk – TTBS. Finally, it was washed with gentle shaking 3 × 5 min in 5 mL TTBS and 3 × 5 min in 5 mL TBS (20 mM Tris-HCl, 500 mM NaCl, pH 7.5) before viewing under the fluorescence microscope. ImageJ software (National Institutes of Health) was used to analyze fluorescence intensities of fluorescence micrographs.

HPLC analysis of Pfs reaction samples.

A Waters Spherisorb Silica column (250 × 4.6 mm) with 5 μm beads (80 Å pore) was used in reversed-phase mode with 5 μL sample injection size and a mobile phase of 70:30 acetonitrile:water at 0.5 mL/min. Conversion was calculated from elution data at 210 nm. The HPLC system consisted of two Dynamax model SD-200 pumps (with 10 mL pump heads and mixing valve) and a Dynamax Absorbance

Detector model UV-D II, and data was analyzed using Star 5.5 Chromatography Software (Rainin).

Results

Electrodeposition of enzyme-chitosan conjugate.

We demonstrate patterned enzyme assembly onto a microfabricated chip via electrodeposition of the enzyme-chitosan conjugate onto a selected target electrode pattern, shown schematically in Fig. 1a. For this, we first covalently conjugated Pfs enzyme to chitosan by incubating $(His)_6$-Pfs-$(Tyr)_5$ and tyrosinase in chitosan solution, with chitosan in excess of available Pfs to ensure all available Pfs was conjugated. Tyrosinase activates the tyrosine residues in the C-terminal pentatyrosine pro-tag to covalently link Pfs to the amines of the chitosan in solution. We then electrodeposited the Pfs-chitosan conjugate onto the target (left) gold electrode pattern (8 mm^2) by dipping the chip into the Pfs-conjugate solution until the pattern was submerged and applying negative bias to the pattern for 2 min at a constant current density of 2.5 A/m^2. This chip had been previously incubated in BSA – PBS solution to block non-specific binding of Pfs-chitosan conjugate to the chip surfaces. It should be noted that the same Pfs-chitosan conjugate solution was repeatedly used to assemble Pfs onto multiple chips, and the chips were reused by simply cleaning in dilute hydrochloric acid followed by concentrated bleach.

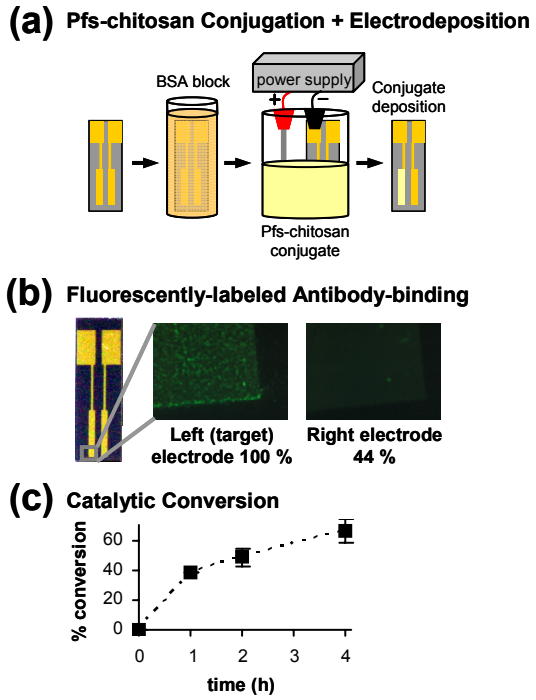

Figure 4. Electrodeposition of Pfs-chitosan conjugate. **(a)** First, Pfs conjugated to chitosan upon tyrosinase-activation of pro-tag. Then, conjugate electrodeposited onto left (target) electrode (8 mm^2) of chip that was previously blocked with BSA. **(b)** Fluorescence micrographs demonstrate binding of fluorescently labeled antibody to assembled Pfs. Percentages indicate relative fluorescence intensities. **(c)** % catalytic conversion by assembled Pfs averaged over 2 different chips.

We first demonstrate that Pfs-chitosan conjugate electrodeposits onto the target electrode pattern. For this, the chip with electrodeposited Pfs-chitosan conjugate was incubated in milk – PBS solution, thoroughly washed, and incubated in mouse anti-poly-histidine (1^o antibody) and then in fluorescencely labeled goat anti-mouse IgG (2^o antibody). Milk was used to block non-specific binding of the antibodies to the conjugate and the chip surfaces. Shown in Fig. 4b are fluorescence micrographs of the target (left) electrode pattern and the right electrode pattern of the same chip with the corresponding fluorescence intensities as determined by ImageJ analysis. The fluorescence micrographs

illustrate: (1) electrodeposition of the Pfs-chitosan conjugate onto the target electrode, (2) negligible binding to the silicon oxide surfaces surrounding the electrodes, and (3) significantly less binding to the other (right) electrode (44 % fluorescence intensity). Overall, these results demonstrate patterned assembly of Pfs onto the chip, as the Pfs-chitosan conjugate predominately assembles onto the target electrode pattern of the chip and does not assemble onto the silicon oxide surfaces. More importantly, we demonstrate that assembled Pfs retains the necessary structure and accessibility for antibody recognition and binding.

Next, we demonstrate catalytic activity of chip-assembled Pfs-chitosan conjugate by measuring its conversion of SAH substrate into products. For this, the chip with electrodeposited Pfs-chitosan conjugate was thoroughly washed and incubated in 1 mM SAH at 37^{o}C. Samples were taken at regular intervals, immediately extracted with chloroform to stop the reaction, and analyzed via HPLC. Shown in Fig. 4c is a plot of % SAH catalytic conversion versus reaction time, where % conversion was calculated as the % decrease in SAH concentration. The plot in Fig. 4c demonstrates that assembled Pfs retained catalytic activity as SAH substrate was converted into enzymatic reaction products. Error bars (standard deviations) were calculated by repeating the experiment twice on different days with different chips and different batches of Pfs and tyrosinase. Importantly, Pfs retained its catalytic activity throughout both the conjugation and electrodeposition steps, which indicates retention of its active site conformation, its 3-dimensional structure, and its accessibility to the substrate.

In summary, Fig. 4 demonstrates a technique for reproducible patterned assembly of active enzyme onto a microfabricated chip. The target enzyme is first covalently

conjugated to chitosan upon activation of the pro-tag, and the conjugate is then electrodeposited onto a patterned electrode. The assembled enzyme remains accessible for antibody recognition and binding, and retains reproducible catalytic activity.

Enzyme conjugation to electrodeposited chitosan scaffold.

Next, we demonstrate patterned enzyme assembly onto a microfabricated chip via covalent conjugation of the enzyme to an already electrodeposited chitosan scaffold pattern, shown schematically in Fig. 5a. For this, we first electrodeposited chitosan scaffold onto the target (left) gold electrode pattern (8 mm^2) by dipping the chip in chitosan solution until the pattern was submerged and applying negative bias to the pattern for 2 min at a constant current density of 16 A/m^2. The chip was then incubated in milk – PBS solution to block non-specific binding of Pfs to chitosan and the chip surfaces. Next, the chip was incubated in a PBS solution containing $(His)_6$-Pfs-$(Tyr)_5$ and tyrosinase. Tyrosinase activates the pro-tag to covalently link Pfs to the amines of the patterned chitosan scaffold. Finally, the chip was thoroughly washed.

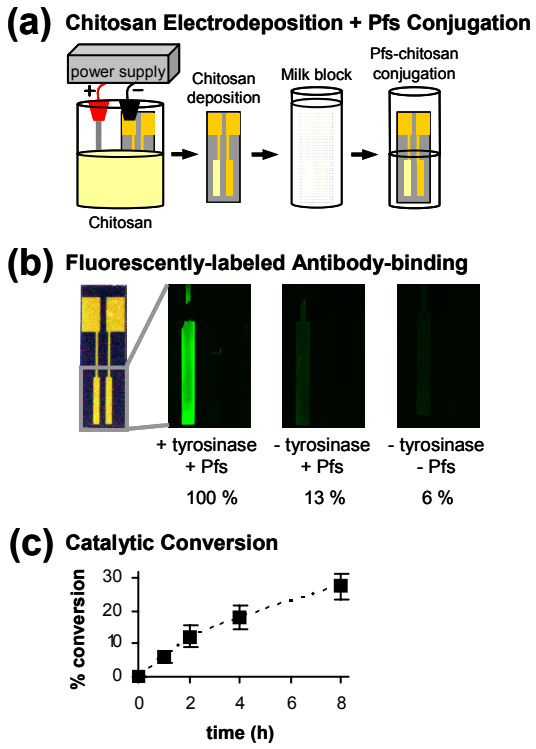

Figure 5. Pfs conjugation to electrodeposited chitosan scaffold. **(a)** First, chitosan scaffold electrodeposited onto left (target) electrode (8 mm^2) of chip. Chip blocked with milk. Then, Pfs conjugated to scaffold upon tyrosinase-activation of pro-tag. **(b)** Fluorescence micrographs demonstrate binding of fluorescently labeled antibody to assembled Pfs. Percentages indicate relative fluorescence intensities. **(c)** % catalytic conversion by assembled Pfs averaged over 6 different chips.

We first demonstrate that tyrosinase-activated Pfs is assembled only onto the patterned scaffold. For this, the chip was incubated in mouse anti-poly-histidine (1^o antibody) and then in fluorescencely labeled goat anti-mouse IgG (2^o antibody). Shown in Fig. 5b are fluorescence micrographs with the corresponding fluorescence intensities as determined by ImageJ analysis. The first micrograph ("+ tyrosinase + Pfs") illustrates that Pfs assembled only onto the patterned scaffold, and that non-specific binding of Pfs to the other chip surfaces was negligible, as there is no discernable fluorescence on the right gold electrode pattern or the silicon oxide. The strong fluorescence intensity illustrates significant antibody binding. The second micrograph ("– tyrosinase + Pfs")

represents a negative control, where the chip with patterned scaffold was incubated in $(His)_6$-Pfs-$(Tyr)_5$ alone (no tyrosinase activation). This chip yielded significantly less fluorescence (13 % fluorescence intensity based on ImageJ analysis), indicating minimal non-specific binding of Pfs to the patterned scaffold, and that tyrosinase activation is required for Pfs assembly. Thus, tyrosinase-activated Pfs assembles covalently onto the scaffold. The third micrograph ("– tyrosinase – Pfs") represents a second control, where the chip with patterned scaffold was not incubated in Pfs or tyrosinase. This chip yielded even less fluorescence (6 % fluorescence intensity based on ImageJ analysis), indicating minimal non-specific binding of the antibodies to the patterned scaffold. Overall, Fig. 5b demonstrates patterned and covalent assembly of Pfs onto the chip, as Pfs assembles only onto the patterned scaffold, and as tyrosinase activation is required for Pfs assembly. Additionally, Fig. 5b demonstrates that assembled Pfs retained the necessary structure and accessibility for antibody recognition and binding.

Next, we demonstrate catalytic activity of assembled Pfs by measuring its conversion of SAH substrate into products. For this, the chip was incubated in 1 mM SAH at 37^{o}C. Samples were taken at regular intervals, immediately extracted with chloroform to stop the reaction, and analyzed via HPLC. Shown in Fig. 5c is a plot of % SAH substrate conversion versus reaction time, where % conversion was calculated as the % decrease in SAH concentration. This plot demonstrates that assembled Pfs retained catalytic activity as SAH substrate was converted into reaction products. Thus, assembled Pfs retained its catalytic activity, indicating retention of its active site conformation, its 3-dimensional structure, and its accessibility to the substrate. Importantly, error bars (standard deviations) were calculated by repeating the experiment

6 times on different days with 6 different chips and using multiple batches of Pfs, tyrosinase, and SAH. The error bars demonstrate the high level of control of our assembly approach, as conversion is reproducible at each reaction time point.

In summary, Fig. 5 demonstrates a technique for reproducible patterned assembly of active enzyme onto a microfabricated chip. The chitosan scaffold is first electrodeposited onto a patterned electrode, and then the target enzyme is covalently conjugated to the patterned scaffold upon activation of the pro-tag. The assembled enzyme remains accessible for antibody recognition and binding, and retains reproducible catalytic activity.

Kinetics of substrate catalytic conversion by assembled enzyme.

Next, we examine the reaction kinetics of SAH substrate conversion by assembled Pfs enzyme by performing initial rate experiments. For this, we first electrodeposited chitosan scaffold onto the target (left) gold electrode pattern (8 mm^2) by dipping the chip in chitosan solution until the pattern was submerged and applying negative bias to the pattern for 2 min at a constant current density of 16 A/m^2. The chip was then incubated in milk – PBS solution to block non-specific binding of Pfs to chitosan and the chip surfaces. Next, Pfs was covalently assembled onto the scaffold by incubating the chip in a PBS solution containing $(His)_6$-Pfs-$(Tyr)_5$ and tyrosinase. After thoroughly washing the chip, it was incubated for 1 h at 37^{o}C with thorough mixing in SAH concentrations of 1 mM, 0.25 mM, and 0.1 mM. Samples were taken at regular intervals, immediately extracted with chloroform to stop the reaction, and analyzed via HPLC.

Shown in Fig. 6 is a plot of initial reaction rate (v_i, in mM/h) versus initial SAH substrate concentration ([SAH], in mM). Error bars (standard deviations) were calculated

by repeating the experiment 3 times on different days with 3 different chips, demonstrating that the rate of catalytic conversion is reproducible for a given substrate concentration. This plot demonstrates that the catalytic conversion of SAH by assembled Pfs follows Michaelis-Menten saturation kinetics. In this model, the reaction rate increases with increasing substrate concentration until reaching a maximum rate, when in effect, the enzyme becomes saturated due to a fixed number of active sites. This model yields the expression, $\nu = V_m \cdot [SAH] / (K_m + [SAH])$, where V_m is the maximum reaction rate, i.e. the rate when the enzyme is saturated, and K_m is the Michaelis-Menten constant. An apparent K_m of 0.12 ± 0.04 mM and an apparent V_m of 0.11 ± 0.02 mM/h were calculated via Lineweaver-Burk method. The dashed line in Fig. 6 is a plot of ν versus [SAH], where ν was calculated from the Michaelis-Menten rate expression using our values of K_m and V_m. As shown, the kinetics model agrees well with our experimental values. Overall, Fig. 6 demonstrates that our assembly approach allows for examination of *in vitro* enzymatic reaction kinetics in a reproducible manner.

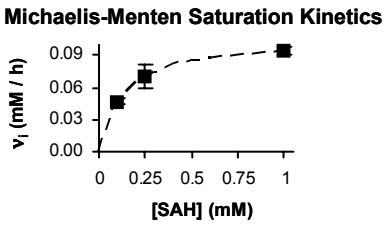

Figure 6. Catalytic conversion by assembled Pfs follows Michaelis-Menten saturation kinetics model (dashed line). Pfs assembled by conjugation to electrodeposited chitosan scaffold.

User-controllable substrate conversion via manipulation of enzyme assembly area.

Finally, we examine the effect of enzyme assembly area on substrate catalytic conversion. For this, we first electrodeposited chitosan scaffolds onto microfabricated chips with increasing areas of the target (left) gold electrode patterns. Shown in Fig. 7a, these chips have target electrode patterns of increasing areas of 1.6 mm^2, 4 mm^2, 8 mm^2, 16 mm^2, and 32 mm^2, respectively. Electrodeposition was performed for each chip by dipping in chitosan solution until the pattern was submerged and applying negative bias to the pattern for 2 min at a constant current density of 16 A/m^2, creating chitosan scaffolds of the same patterned areas as the corresponding electrodes. These chips were then incubated in milk – PBS solution to block non-specific binding of Pfs to chitosan and the chip surfaces. Next, Pfs was covalently assembled onto the scaffolds by incubating the chips in $(His)_6$-Pfs-$(Tyr)_5$ and tyrosinase. Additionally, we examined non-specific assembly of Pfs onto the chip surfaces (gold and silicon oxide) by performing a negative control, where a chip without electrodeposited chitosan scaffold was incubated in milk – PBS, and then incubated in $(His)_6$-Pfs-$(Tyr)_5$ alone (without tyrosinase). After thorough washing, the chips were each incubated in 1 mL of 1 mM SAH at 37^oC. Samples were taken at regular intervals, immediately extracted with chloroform to stop the reaction, and analyzed via HPLC.

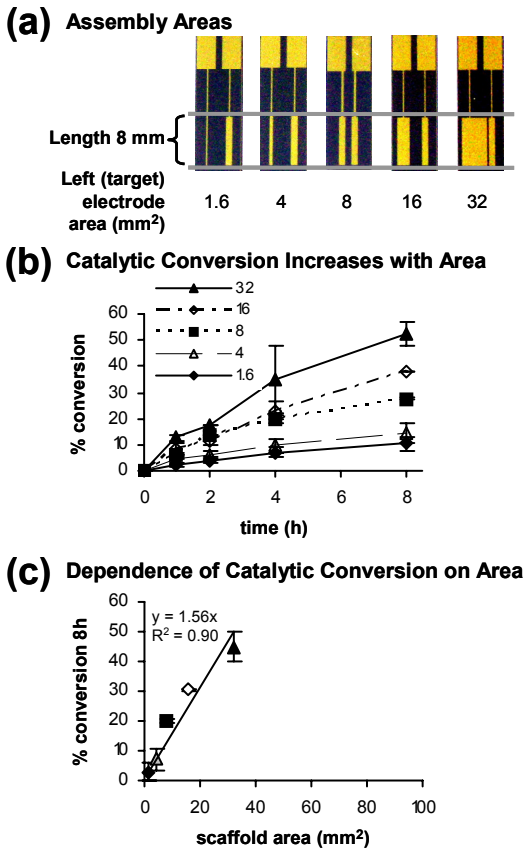

Figure 7. Biocatalysis by assembled Pfs linearly correlates with assembly area. **(a)** Increasing assembly areas. **(b)** % catalytic conversion by assembled Pfs. Legend indicates assembly area (mm^2). **(c)** % catalytic conversion of SAH at 8h, where the [SAH] converted by the non-specifically assembled Pfs has not been included.

Shown in Fig. 7b is a plot of % SAH substrate conversion versus reaction time for each patterned scaffold area, with each point representing the average of 2 separate experiments performed with 2 different chips. Fig. 7b demonstrates that SAH conversion (and presumably the amount of assembled Pfs) increases with scaffold area, and is reproducible for a given area. Thus, catalytic conversion by assembled Pfs is reproducibly correlated to the assembly area. Additionally, we note that 7.5 ± 3.4 % SAH was converted by the non-specifically assembled Pfs at 8 hours reaction time (not shown), demonstrating that there is a baseline level of non-specific Pfs assembly.

Shown in Fig. 7c is a plot of % SAH catalytic conversion at 8 hours reaction time versus scaffold area (in mm^2). For this, the % SAH conversion by the scaffold-assembled Pfs was calculated by subtracting the concentration of SAH converted by the non-specifically assembled Pfs from the total concentration of SAH converted, causing all data points to shift down. As demonstrated through linear regression, the % catalytic conversion increases linearly with scaffold area, however, we note that a doubling of area does not lead to a doubling of conversion. Nonetheless, the end-user can predict the conversion based on the assembly area, allowing for control of conversion through manipulation of the assembly area.

In summary, Fig. 7 demonstrates that the rate of catalytic conversion by assembled enzyme and presumably the amount of assembled enzyme is reproducible for a given assembly area, allowing for control of biocatalysis through user-manipulation of the scaffold patterned area.

Discussion

We report an approach for active enzyme assembly onto microfabricated chip surfaces based on the electrodeposition of chitosan onto selected electrodes of the chips and the covalent conjugation of the target enzyme (in this case, Pfs) to chitosan upon biochemical activation of a C-terminal pro-tag. Using this approach, there are two possible methodologies, as shown in Scheme 5. In the first method (Scheme 5a), the target enzyme is first covalently conjugated to chitosan, and this conjugate is then electrodeposited onto a selected electrode. In the second method (Scheme 5b), chitosan is first electrodeposited onto a selected electrode, and the target enzyme is then

covalently conjugated to the electrodeposited chitosan. These methods are interchangeable in that they both assemble active enzyme in a spatially selective manner. However, there are some differences, as demonstrated by comparison of Fig. 4 (conjugation then electrodeposition) to Fig. 5 (electrodeposition then conjugation).

One difference in the two methods is the level of binding of fluorescently labeled antibody to assembled Pfs, observed by comparing the fluorescence intensities of the micrographs in Fig. 4b and Fig. 5b, which were identically prepared. The micrograph in Fig. 1b displays 21% of the fluorescence intensity of the micrograph in Fig. 2b, indicating less antibody binding. We believe this is due to the accessibility of assembled Pfs for antibody binding. In the first method, the electrodeposited conjugate film contains Pfs imbedded within the film as well as Pfs displayed on the surface of the film, and additionally, this surface-displayed Pfs may not be in any particular orientation with respect to the film surface. Thus, the Pfs assembled by the first method is expected to be less accessible for antibody binding, which is consistent with the weak fluorescence intensity of Fig. 4b. In the second method, the Pfs predominately conjugates to the surface of the electrodeposited chitosan film, as Pfs is presented after chitosan deposition, and as diffusion of Pfs into the film is presumably limited due to steric hindrance effects. Additionally, Pfs preferentially conjugates to chitosan film through its C-terminal pro-tag versus its native tyrosines, indicating that Pfs is preferentially oriented through the pro-tag with respect to the film surface. Thus, the Pfs assembled by the second method is expected to be more accessible for antibody binding, which is consistent with the strong fluorescence intensity of Fig. 5b. Combined, the antibody-binding results of Fig. 4b and Fig. 5b indicate that the second assembly method (electrodeposition then conjugation)

could be more appealing for applications involving protein-protein recognition and protein-protein binding. However, the data clearly demonstrates that both methods assemble enzymes that can recognize and bind antibodies.

Another difference in the two methods is the catalytic conversion of SAH substrate by assembled Pfs, observed by comparing % conversion at 4 h reaction time in Fig. 4c and Fig. 5c. Significantly higher conversion at 4 h is observed when Pfs is assembled by the first method (conjugation then electrodeposition) versus the second method (electrodeposition then conjugation) (66 % versus 18 %). This is somewhat surprising, as the Pfs assembled by the first method is imbedded within the chitosan film (and on the surface of the chitosan film), while the Pfs assembled by the second method is primarily on the surface of the chitosan film and thus more accessible for substrate binding and higher catalytic conversion. The higher catalytic conversion that is observed when Pfs is assembled by the first method could result from a higher amount of assembled Pfs or a higher catalytic activity of assembled Pfs. Methods for precise quantitative analysis of surface assembled enzyme are currently under investigation in our laboratory. Nonetheless, the high conversion observed in Fig. 4c strongly suggests that diffusion of small molecules (e.g. SAH) is possible within the electrodeposited chitosan film. Importantly, the data clearly demonstrates that both methods assemble enzymes that retain catalytic activity.

Our assembly approach allowed for controlled examination of enzymatic catalysis and kinetics. Specifically, we examined the kinetics of SAH catalytic conversion by assembled Pfs, where Pfs was assembled by the second method (conjugation then electrodeposition). We report that this reaction follows Michaelis-Menten saturation

kinetics with an apparent K_m constant of 0.12 ± 0.04 mM. Reported values of the Michaelis-Menten constant K_m have varied widely (Duerre 1962; Ragione et al. 1985). Duerre (Duerre 1962) reports a K_m of 3 mM, while Ragione *et al.* (Ragione et al. 1985)report a K_m of 4.3 μM. This discrepancy in K_m values is attributed by Ragione *et al.* to differences in enzyme purity and in the assay used to determine conversion; we also have used different purification and analytical techniques. Additionally, higher K_m constants for immobilized enzymes compared with free enzymes in solution has been reported (Sung and Bae 2006; Xu et al. 2005). Nonetheless, our calculated K_m is well within the range of reported K_m values.

The two methods of our overall assembly approach both allow for user-controllable patterned assembly of active enzymes onto microfabricated chips, and are appealing for a variety of potential applications. In particular, we envision using the first method (conjugation then electrodeposition) to pattern multiple enzymes onto the same chip, where each enzyme-chitosan conjugate would be sequentially electrodeposited onto its own distinct electrode pattern of a single chip. The electrode patterns (assembly areas) could be different for each enzyme, thus allowing for simultaneous *in vitro* examination and manipulation of multiple-step enzymatic reactions in a controlled manner. The results reported here extend the previously demonstrated ability to sequentially assemble multiple proteins (Yi et al. 2005c) to where it is now possible to assemble catalytically active enzymes through activatable "pro-tags". Finally, we envision using our approach to screen for Pfs inhibitors for the discovery of novel antibiotics.

Conclusions

We report an approach for patterned assembly of active enzymes onto microfabricated chips, based on two strategies: (1) electrodeposition of chitosan onto patterned electrodes, and (2) covalent conjugation of the target enzyme to chitosan upon biochemical activation of a genetically fused pro-tag. Our approach is versatile, in that the procedural order is interchangeable: electrodeposition can be performed first followed by conjugation or conjugation can be performed first followed by electrodeposition. Our results demonstrate patterned assembly of Pfs enzyme fused with a C-terminal pentatyrosine pro-tag. Equally important, they demonstrate that the assembled enzyme retains its biocatalytic activity for small molecule biosynthesis and its accessibility for antibody binding. Moreover, the rate of biocatalysis is reproducible for a particular assembly area, allowing for controlled examination of enzymatic reaction kinetics and user-optimization of biocatalysis in 1-step as well as multi-step enzymatic reactions. We believe this approach is appealing for a broad range of applications in biosensing and metabolic engineering.

Chapter 4: Reproducible Assembly and Catalytic Activity of a Metabolic Pathway Enzyme in Reusable BioMEMS Devices

**This work was done in conjunction with Xiaolong Luo.

Introduction

Microelectricalmechanical systems (MEMS) based on semiconductors convey electrical and optical signals and exhibit huge capability in data manipulation and signal processing. Biological components such as nucleic acid, enzymes and antibodies exhibit molecular recognition capabilities for biosensing functions. The integration of biology with MEMS (bioMEMS), especially with microfluidic systems, offers major advances in our ability to manipulate biomolecular systems (Andersson and van den Berg 2003; Andersson and van den Berg 2006; Atencia and Beebe 2005; Auroux et al. 2002; Beebe et al. 2002; Bilitewski et al. 2003; Dittrich et al. 2006; Hong et al. 2006; Psaltis et al. 2006; Reyes et al. 2002; Shim et al. 2003; Vilkner et al. 2004). The microfluidic environment of bioMEMS devices provides unprecedented advantages for enzyme analysis because of the ability to work with smaller reagent volumes, shorter reaction times, and the possibility of parallel operation (Beebe et al. 2002; Bilitewski et al. 2003; Hong et al. 2006; Shim et al. 2003). Recently, researchers have explored enzyme assembly approaches in microfabricated devices using either entrapment approaches such as packed beads (Bilitewski et al. 2003; Ku et al. 2006; L'Hostis et al. 2000; Urban et al. 2006) or surface immobilization approaches (Bilitewski et al. 2003; Chaki and Vijayamohanan 2002; Deng et al. 2006; Kisailus et al. 2006; Lee et al. 2006; Li et al. 1999; Liu et al. 2006; Malpass et al. 2002; Mao et al. 2002; Niemeyer et al. 2003; Quist

et al. 2005). However, robust and reproducible enzyme assembly within microfluidic devices remains challenging due to the labile nature of these biological molecules that is incompatible with lengthy and dry processing conditions often occurring in the device fabrication.

Additionally, semiconductor-based devices are expensive due to the need of costly photolithographic equipments and the access of clean rooms. Therefore, tremendous research has been directed to fabricate cheap and disposable devices for biological applications by using alternative elastic material such as polydimethylsiloxane (PDMS) (Duffy et al. 1998; Jo et al. 2000; McDonald et al. 2000) and soft lithoghraphic techniques including microcontact printing (Duffy et al. 1998; Jo et al. 2000; McDonald et al. 2000; Quist et al. 2005; Unger et al. 2000). However, this substitution of polymers for semiconductors as the basis for bioMEMS poses new challenges in (a) integrating multiple electrical and optical functions together with microfluidics, and (b) simultaneously facilitating the incorporation of biological species in the bioMEMS.

In this paper, we report a reproducible, chitosan-mediated biofunctionalization strategy for the assembly of catalytically active enzymes within completely packaged and systematically controlled bioMEMS devices. Specifically, we report assembly of the enzyme Pfs (*S*-adenosylhomocysteine nucleosidase), and demonstrate that it retains catalytic activity for small molecule biosynthesis. Pfs catalyzes the irreversible cleavage of *S*-adenosylhomocysteine into adenine and *S*-ribosylhomocysteine (Duerre 1962), and is a member of the autoinducer-2 (AI-2) biosynthesis pathway, a metabolic pathway found in many bacterial species (Federle and Bassler 2003). AI-2 is a small signaling molecule that mediates interspecies bacterial cell-cell communication termed “quorum

sensing" (QS), a process in which the entire population coordinates behavior in response to environmental cues. QS is involved in regulating many of the genes associated with bacterial pathogenesis (Balestrino et al. 2005; Barrios et al. 2006; Ren et al. 2001; Sperandio et al. 2001; Sperandio et al. 2002; Zhu et al. 2002); thus, inhibition or knock-down of enzymes in this pathway represent opportunities for new antimicrobial drugs that could intercept or "rewire" the QS communication network (Rasmussen et al. 2005a; Rasmussen et al. 2005b). Therefore, the Pfs enzyme assembly strategy reported here provides a template towards rebuilding metabolic pathways in microfluidic environments for novel anti-microbial drug discovery.

Our biofunctionalization strategy is different from conventional approaches, which have immobilized enzymes onto packed beads or onto entire surfaces of microchannel walls (Chaki and Vijayamohanan 2002; Deng et al. 2006; Kisailus et al. 2006; Ku et al. 2006; L'Hostis et al. 2000; Lee et al. 2006; Li et al. 1999; Liu et al. 2006; Malpass et al. 2002; Mao et al. 2002; Niemeyer et al. 2003; Quist et al. 2005; Urban et al. 2006) in that we assemble enzymes at a specific address within a microchannel, and the assembly process is guided by localized electrical signals. First, the bioMEMS device in Scheme 6a is prefabricated for multiple uses. Second, Pfs-chitosan conjugate solution is prepared by covalently conjugating Pfs to chitosan in solution upon tyrosinase activation of the pro-tag genetically fused at the enzyme's C-terminus as shown in Scheme 6b. This conjugation step confers the pH-responsive properties of chitosan to the Pfs-chitosan conjugate for one-step assembly onto readily addressable sites within the microfluidic channels. Third, the Pfs-chitosan conjugate is electrodeposited onto an assembly site inside a microfluidic channel by applying negatively biased electrical signal, as shown in

Scheme 6c. With biofunctionalization complete, Scheme 6d shows that the Pfs-mediated enzymatic reaction is performed by introducing the enzyme substrate *S*-adenosylhomocysteine (SAH) into the microchannel, which is then catalytically converted by the assembled Pfs into products *S*-ribosylhomocysteine (SRH) and adenine. After the reaction, Scheme 6e indicates that a mild acid wash removes the assembled Pfs-chitosan conjugate for reuse of the bioMEMS.

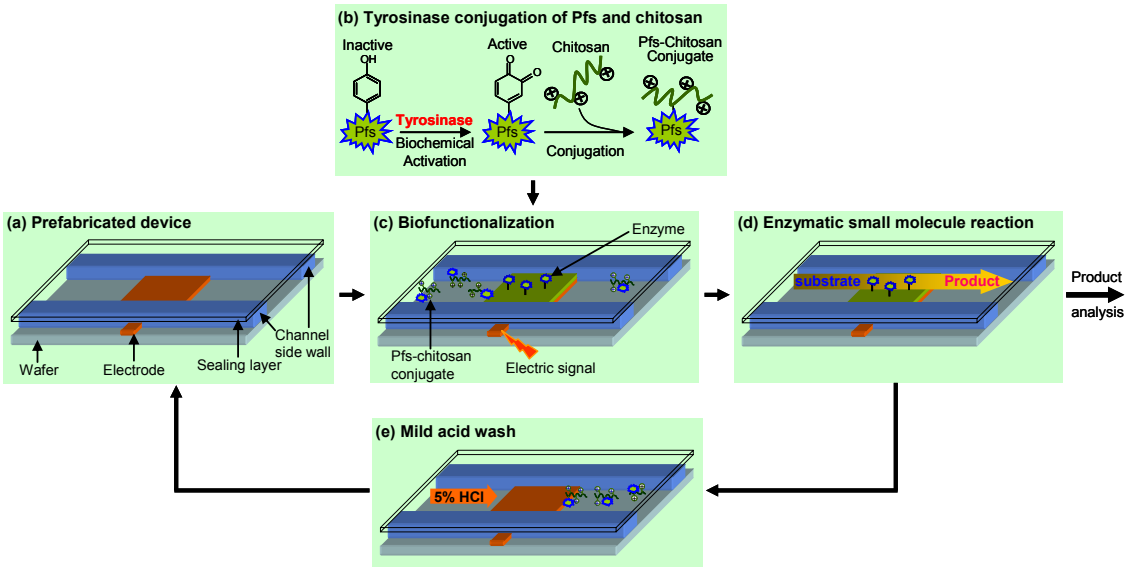

Scheme 6. Schematic flow of reversible enzyme assembly and catalytic activity in reusable bioMEMS device. **(a)** Prefabricated device, **(b)** enzyme-chitosan conjugation, **(c)** electrically programmed assembly of Pfs-chitosan conjugate, **(d)** small-molecule reaction by enzyme catalysis, **(e)** mild acid wash to remove biofunctionalization and reuse bioMEMS device.

Most importantly, the unique feature of this work is that we employ localized electrical signals to guide the assembly of biocatalytically-active enzyme at a specific address within a completely packaged microfluidic channel. This allows device fabrication to be separated from biofunctionalization and enables the prefabricated bioMEMS to be repeatedly biofunctionalized.

Materials and Methods

Materials.

S-adenosylhomocysteine (SAH), bovine serum albumin (BSA), chitosan (minimum 85 % deacetylated chitin; molecular weight 200,000 g/mol) from crab shells, imidazole, isopropyl β-D-thiogalactopyranoside (IPTG), nickel sulfate, phosphate buffered saline (PBS) (2.7 mM KCl, 137 mM NaCl, 1.5 mM KH_2PO_4, 8.1 mM Na_2HPO_4, pH 7.5), sodium cyanoborohydride, and tyrosinase from mushroom were purchased from Sigma (St. Louis, MO). Tyrosinase was reported by the manufacturer to have an activity of 1,530 Units/mg solid. LB (Luria broth) medium was purchased from Becton Dickinson (Cockeysville, MD). Acetonitrile (HPLC grade), ampicillin sodium salt, chloroform, glycerol, sodium phosphate (monobasic), sodium phosphate (dibasic), and water (HPLC grade) were purchased from Fisher Chemical (Fair Lawn, NJ). Hydrochloric acid and sodium chloride were purchased from J. T. Baker (Phillipsburg, NJ). Non-fat dry milk was purchased from BioRad (Hercules, CA). Bleach was purchased from James Austin Co. (Mars, PA). De-ionized water (ddH2O, 18 MΩ·cm, Milli-Q) and PBS (dissolved in de-ionized water) were autoclaved before use.

Plasmid construction.

pTrcHis-Pfs-Tyr plasmid construction was reported elsewhere (Fernandes et al. 2007). Briefly, the plasmid was constructed by PCR amplification of *pfs* from *E. coli* wild type strain W3110. Following digestion, the PCR products were extracted by gel purification and inserted into pTrcHisC (Invitrogen). DNA sequencing was performed to

verify construct integrity. The plasmid was transformed into *E. coli* DH5α (defective *luxS* strain).

Purification of $(His)_6$-Pfs-$(Tyr)_5$.

E. coli DH5α containing pTrcHis-Pfs-Tyr was cultured at 37°C and 250 rpm in LB medium supplemented with ampicillin at 50 μg/mL. When the OD_{600nm} reached 0.5 – 0.6, IPTG was added to induce enzyme production at a final concentration of 1 mM IPTG. After an additional 5 hr, the culture was centrifuged for 10 min at 10,000 g's, and the cell pellet stored at – 20°C. The thawed pellet was resuspended in PBS + 10 mM imidazole, pH 7.5, placed in an ice-water bath, and the cells lysed by sonication (Fisher Scientific Sonic Dismembrator 550). The lysed cells were centrifuged for 10 min 16,000 g's to remove insoluble cell debris, and the supernatant filtered though 0.22 μm PES filter. The enzyme was purified from the filtered soluble cell extract by immobilized metal-ion affinity chromatography (IMAC) using a 5 mL HisTrap chelating column (Amersham Biosciences). Prior to loading the filtered extract, the column was charged with Ni^{2+} ions using 0.1 M $NiSO_4$, washed with de-ionized water, and equilibrated with 3 column volumes (CVs) of 20 mM sodium phosphate, 250 mM NaCl, 10 mM imidazole, pH 7.4. After loading the filtered extract, the column was washed with 3 CVs of the previous buffer, washed again with 3 CVs of 20 mM sodium phosphate, 250 mM NaCl, 50 mM imidazole, pH 7.4, and the protein was eluted using 1.5 CVs of 20 mM sodium phosphate, 250 mM NaCl, 350 mM imidazole, pH 7.4. All steps were performed at 2 mL/min (1 cm/min linear velocity). The eluted sample was dialyzed overnight (16 hr) at 4°C into PBS. Purified protein concentration was determined with a UV/vis spectrophotometer (DU 640, Beckman, Fullerton, CA) using UV light at 280nm

wavelength. The protein solution was mixed 2:1 with glycerol, alliquoted, and stored at – 80^{o}C.

Chitosan and Pfs-chitosan conjugate preparation.

Chitosan solution was prepared by adding chitosan flakes in de-ionized water, with HCl added dropwise to maintain pH ~ 2, and mixing overnight. The pH was then adjusted by adding 1 M NaOH dropwise, and the chitosan solution was then filtered and stored at 4ºC.

The conjugate was prepared by incubating $(His)_6$-Pfs-$(Tyr)_5$ (0.2 mg/mL), tyrosinase (0.1 mg/mL or 166 Units/mL), and chitosan (0.5 % (w/w)) in 50 mM sodium phosphate buffer (final pH of mixture 6.0) for 2 h at room temperature (23 – 24 ^{o}C) and 250 rpm, followed by incubation in sodium cyanoborohydride (0.2 mg/mL) for 30 min at 250 rpm to stabilize Pfs-chitosan binding.

Microfluidic device fabrication and packaging.

The fabrication process of our microfluidic device with packaging was reported previously (Park et al. 2006). Briefly, our microfluidic device (Fig. 8) features six identical microchannels evenly distributed on a 4″ Pyrex wafer with two rectangular gold electrodes underneath each microchannel. A Cr adhesion layer (90 Å) and then a gold layer (2000 Å) were deposited onto a 4″ Pyrex wafer, and rectangular gold electrode patterns (1 mm × 0.5 mm) were created by photolithography. SU8-50 (MicroChem, MA) was patterned on the top of substrate and electrode surface to form structures which serve a dual function, namely (1) sidewalls for a microfluidic channel, and (2) sharp "knife-edge" structures for reliable leak-tight sealing to a PDMS layer above. The microfluidic

channels were thus sealed by a 300-µmthick top sealing PDMS layer spun on a Plexiglas plate, and the SU8-50/PDMS junction was compressed by two package-level Plexiglas plates with six pressure-adjustable compression bolts (1/4″-28) hexagonally spaced on the ring and six force tunable socket screws (4-40) between every two microchannels. The microchannels thus formed were 500µm wide by 150µm high. Fluidic connectors (NanoportTM) and electric Pogo pins (Interconnect Devices, Inc.) were assembled through punched holes on the sealing PDMS and drilled-holes through the top sealing and packaging Plexiglas plates, and then connected to external pressure-driven aqueous transport and electrical signal, correspondingly.

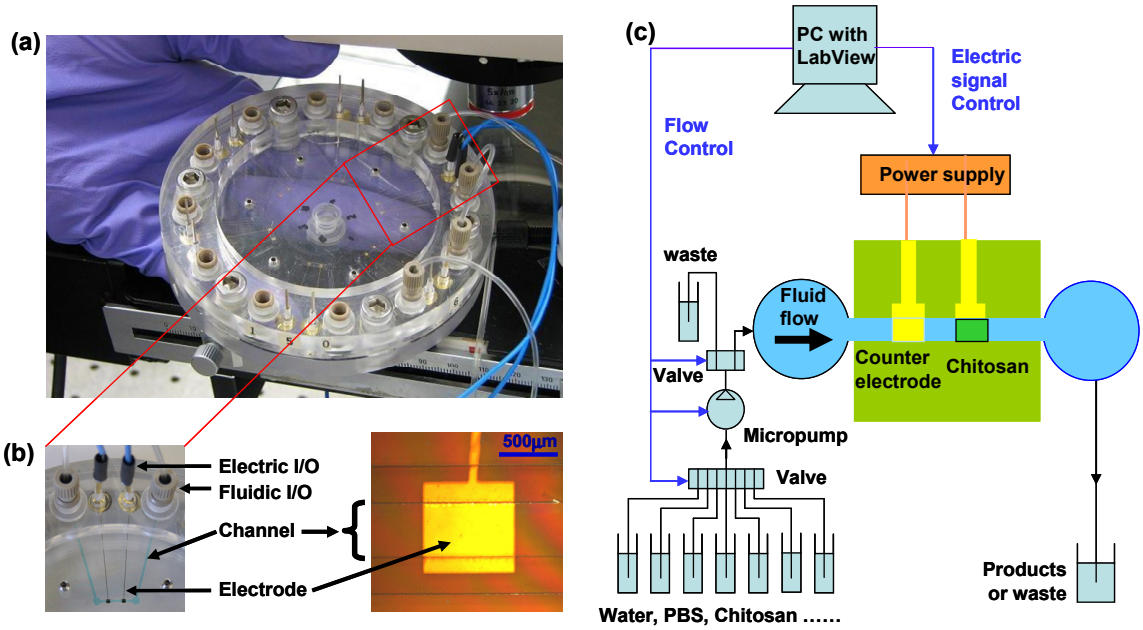

Figure 8. Microfluidic system and experimental setup. **(a)** Completely packaged microfluidic system with electric connectors and fluidic inputs/outputs. There are 6 identical microfluidic channels on a microfluidic wafer which is sealed by a thin PDMS layer and compressed between two Plexiglas plates. **(b)** Color ink running through one microfluidic channel and zoom-in view of one electrode at the bottom of the channel. **(c)** Schematic microlfuidic control system. A PC with LabView program controls the pumping and selection from different fluids and the chitosan electrodeposition process.

Microfluidic system control technology.

A microfluidic control system was built to systematically control the selections from multiple solution sources and the pumping into microfluidic channels, which in the long run aims at systematically controlling a biomolecular factory on microfluidic devices. The control system shown in Fig. 8 mainly consists of a peristaltic micropump (Masterflex1 pump drive, Cole-Palmer Instrument Co) with two cartridges in alternative directions on a 8-roller cartridge pump head (Masterflex pump head, Cole-Palmer Instrument Co) to achieve near puleless combined output flow, a 6-to-1 solenoid valve (Bio-Chem Valve / Omnifit, NJ) with separate tubing (0.19 mm ID, Tygon1) to select solution from multiple sources, a 1-to-2 isolation valve (Bio-Chem Valve / Omnifit, NJ) to direct the pumping either to waste collection (at the beginning of experiment with high flow rate) or to microfluidic chip (when the flow is steady and ready for experiment with low flow rate), and a LabView-based program which sends digital signal to control the selections of solenoid valves and the on/off of pump and analog signal to control the pumping flow rate. The system is capable of controlling the microfluidic flow rate in a range of 2.8 – 280 μL/min. Another LabView program was used to control electrodeposition process and to monitor the voltage of the applied electrical signal, which showed 2 – 3 V during the electrodeposition process. Network simulation (VisSimTM 3.2, Design Science Inc.) shows that at 5 μL/min flow rate, the velocity inside the channel (cross section: 500 μm × 150 μm) is 1.1 mm/s. If the pump is restarted after the channel is filled with static fluid, the response time of the flow in the channel is 30 s.

One-step assembly of Pfs-chitosan conjugate and sequential enzymatic reactions in a microfluidic channel.

As shown in Fig. 9, the experimental microchannel and all the connecting tubing were first rinsed with DI water at 50 μl/min flow rate for 30 min. Then Bovine Serum Albumin (BSA) buffer was pumped into the microchannel at 3μl/min for 2 hours to prevent nonspecific binding. After PBS buffer rinsing at 3μl/min for 30 min, Pfs-chitosan conjugate solution was pumped into the microchannel at 5 μl/min. After the microchannel was completely filled, the pump was stopped and a electrical signal of constant current 3 A/m^2 from was apply to maintain negative bias voltage on the gold (working) electrode for 240 seconds, while a second gold electrode served as the anode (counter). The Pfs-chitosan conjugate solution was then drained from the system, and the electrodeposited Pfs-chitosan conjugate was washed with PBS buffer at 5 μl/min and then at 20 μl/min, each for 15 min. Next, first two cycles of enzymatic reactions were started by pumping substrate SAH solution into the system at a series flow rates of 3 μl/min, 22 μl/min, 3 μl/min, 22 μl/min and then back to 3 μl/min for 2 h at each step. In each step, samples were collected for the second hour every 10 min for 3 min and and stored at – 20^{o}C before injecting on the HPLC.

	Step #	Procedure	Flow rate (µL/min)	Time (min)
Day 1	1	DI water cleaning	50	
	2	BSA	3	120
	3	PBS buffer	3	30
	4	**Pfs-chitosan assembly**	**static**	**4**
	5	PBS buffer	5, 20	30
Day 2	**6**	**Enzymatic reaction (SAH)**	**3, 22**	**600**
	7	HCl wash	22	10
	8	DI water cleaning	50	90
Day 3	**9**	**Enzymatic reaction (SAH)**	**3**	**120**
	10	DI water cleaning	50	60
	11	BSA	5	120
	12	PBS buffer	5	30
	13	**Pfs-chitosan re-assembly**	**static**	**4**
	14	PBS buffer	5, 20	30
Day 4	**15**	**Enzymatic reaction (SAH)**	**3, 22**	**600**
Day 5-7	16	In PBS buffer	static	3 days
Day 8	**17**	**Enzymatic reaction (SAH)**	**3, 22**	**360**
	18	Cleaning	50	

Figure 9. Experimental process to demonstrate enzyme catalytic activity and reproducibility. The background colors of each step correspond to the background colors in Fig. 10.

Analysis of enzymatic reaction products.

A Waters Spherisorb Silica column (250 × 4.6 mm) with 5 µm beads (80 Å pore) was used in reversed-phase mode with 5 µL sample injection size and a mobile phase of 70:30 acetonitrile:water at 0.5 mL/min. Conversion was calculated from elution data at 210 nm. The HPLC system consisted of two Dynamax model SD-200 pumps (with 10 mL pump heads and mixing valve) and a Dynamax Absorbance Detector model UV-D II, and data was analyzed using Star 5.5 Chromatography Software (Rainin).

Results and Discussion

One-step assembly of enzyme-chitosan conjugate and sequential enzymatic reactions.

We demonstrate one-step assembly of Pfs-chitosan conjugate onto readily addressable sites in prefabricated and packaged microfluidic channels, and demonstrate

that the assembled Pfs retains catalytic activity. For this, we first prepared the Pfs-chitosan conjugate by incubating a phosphate buffer solution containing chitosan, the pro-tagged Pfs and tyrosinase (Scheme 6b). Tyrosinase activates the pro-tag to covalently conjugate Pfs to the chitosan in solution. Next, we electrodeposited Pfs-chitosan conjugate onto the patterned assembly site inside a microfluidic channel by filling the microchannel with Pfs-chitosan conjugate solution and then applying a negatively biased electrical signal to the patterned electrode (Scheme 6c). Next, we continually transported through the microchannel a solution containing the substrate SAH, which was catalytically converted into reaction products SRH and adenine by the assembled enzyme Pfs (Scheme 6d). Finally, we performed HPLC analysis of the enzymatic reaction mixtures collected downstream.

To demonstrate the enzyme catalytic activity, its reproducibility after removal and its stability over time, we performed the enzyme assembly and enzymatic reactions in a cycling manner. As shown in Fig. 10a, Pfs-chitosan conjugate from the same batch solution was assembled by negatively-biased electrical signal (day 1), removed by mild acid solution (day 3) and re-assembled (day 3). Correspondingly, SAH substrate solution was introduced after each cycle of enzyme assembly. Finally, the assembled Pfs was left in PBS buffer at room temperature for 4 days and then re-reacted with fresh SAH solution again on day 8. In each cycle of enzymatic reaction, the flow rate was alternately varied between 3 μL/min and 22 μL/min.

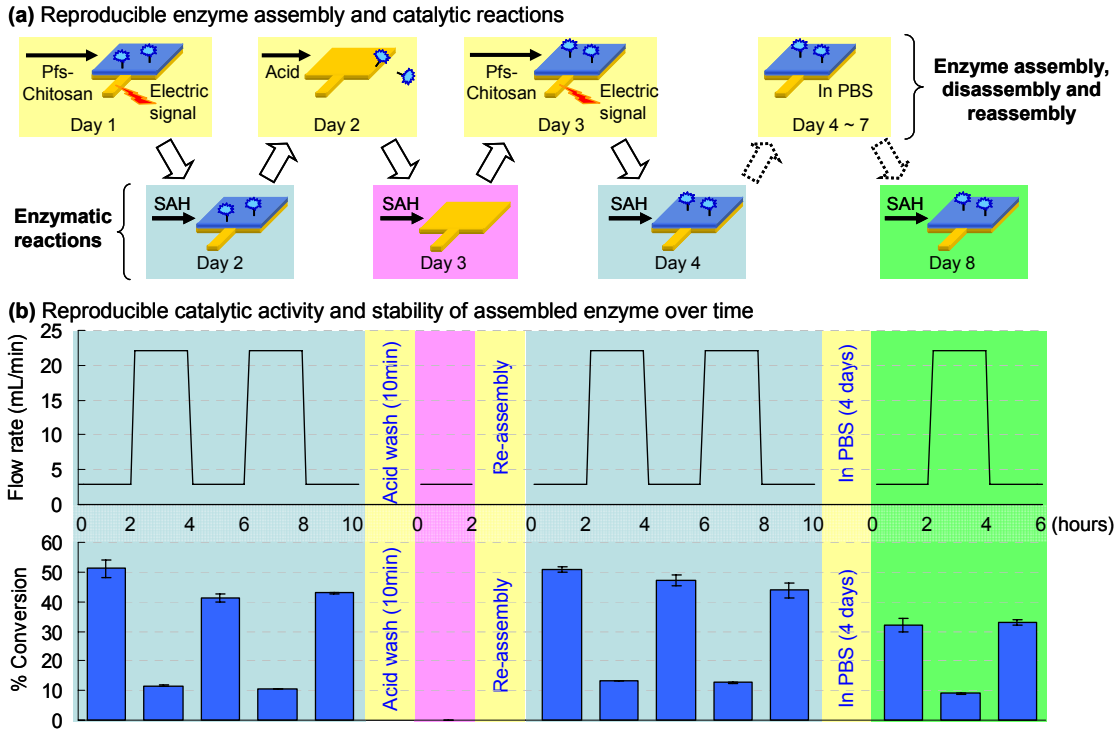

Figure 10. Enzyme catalytic activity, its reproducibility after removal, and its robustness over time. **(a)** Schematic of enzyme assembly, disassembly and reassembly and the corresponding enzymatic reactions. ***(a1)*** Pfs enzyme was assembled in a microchannel (day 1), and enzymatic reaction was performed by introducing substrate SAH in cyclic flow rates between 3 mL/min and 22 mL/min (day 2). Reaction products downstream was collected and analyzed by HPLC. ***(a2)*** Enzyme was then disassembled by acid (day 2) and enzymatic reaction was performed (day 3) to demonstrate complete enzyme disassembly. ***(a3)*** Next, enzyme was re-assembled (day 3) and enzymatic reaction was performed in cyclic flow rates (day 4). ***(a4)*** Finally, enzyme was left in PBS buffer for 4 days (day 4-7) before final cycle of enzymatic reaction was performed (day 8). **(b)** Reproducible catalytic activity after enzyme assembly, disassembly and re-assembly, and stability of assembled enzyme after 4 days. The background colors of each step in **(a)** correspond to the background colors in **(b)** and in Fig. 9.

The HPLC analysis results in Fig. 10b show the following behavior. (1) By varying the flow rate in cyclic manner between 3 μL/min (low flow rate) and 22 μL/min (high flow rate), the SAH conversion correspondingly cycled between 46 ± 4 % for the low flow rate and 12 ± 1 % for the high flow rate. (2) After removal by mild acid solution, there is no conversion. (3) After re-assembly of Pfs enzyme, the SAH conversion recovered back to the cyclic behavior, alternating between 46 ± 4 % and 12 ± 1 %. (4) After leaving the enzyme in the microfluidic environment at room temperature

for 4 days, the conversion substantially retained the original cyclic behavior, alternating between 33 ± 2% and 9 %.

These results show that our model enzyme Pfs was successfully and robustly assembled onto readily addressable sites within prefabricated and packaged microfluidic channels by one-step electrodeposition of the Pfs-chitosan conjugate. Importantly, the assembled enzyme retained its activity in bioMEMS throughout repeated flow cycles. Third, simple acid wash removed the enzyme activity (demonstrated by the 0 % conversion), and also removed the assembled enzyme-chitosan conjugate from the assembly site. The recovery of conversion after the re-deposition of the enzyme-chitosan conjugate demonstrates that we achieved reproducible enzyme assembly. Combined, the removal of the assembled enzyme-chitosan conjugate with dilute acid and the recovery of conversion after re-deposition of the conjugate demonstrate that our assembly approach enables reproducible biofunctionalization of reusable bioMEMS. Finally, the retention of conversion after storing the enzyme in the microfluidic system at room temperature for 4 days shows that the assembled enzyme was stable enough to retain substantial activity for an extended period of time.

We further examined Pfs stability by comparing catalytic activities over 4 days of the electrodeposited Pfs-chitosan conjugate (device-assembled Pfs) to Pfs-chitosan conjugate solution and free and unconjugated Pfs solution. For this, we reacted the Pfs solutions with SAH on day 1, left the solutions in PBS buffer at room temperature for 4 days, and then re-reacted the same Pfs solutions with fresh SAH on day 5. We found that the catalytic activity of the deposited conjugate is better retained with time: 70 % retained for the deposited conjugate (at 3 μL/min flow rate), 74 % retained for the deposited

conjugate (at 22 μL/min flow rate), only 13 % retained for the conjugate solution (not shown), and only 6 % retained for the free and unconjugated enzyme solution (not shown). Thus, enzymes assembled into microchannels (or other devices) using our assembly approach are more stable and resistant to environmental changes for better retention of catalytic activities with time. This compares favorably to the stabilities of free enzymes in bulk solution, and is consistent to what has been observed in literature (Cao 2005).

Combined, these results show the catalytic activity and stability of the assembled enzymes and the reproducibility of our electrochemical enzyme assembly process. These results also show the unique advantages such as retaining 3-dimensional structure, temporal programmability within completely packaged and systematically controlled microfluidic devices.

Negative control to examine non-specific binding and dead volume.

We next examined what portion, if any, of the SAH conversion in Fig. 10b was a result of Pfs bound non-specifically to the microchannel surfaces and/or of Pfs retained in the dead volume of the microfluidic system. For this, we performed the following negative control experiment. First, Pfs solution was introduced into the microchannel without the activating enzyme tyrosinase and without chitosan, so that there was no covalent binding. Next, we continually transported through the microchannel SAH substrate solution (Fig. 11a) and performed HPLC analysis of the reaction mixtures collected downstream of the channel. The HPLC analysis results in Fig. 11b shows that there was 7 – 18 % of SAH conversion into SRH and adenine with various flow rates. This conversion results from any Pfs binding non-specifically to the channel surfaces

(floor, ceiling, walls) and/or from any Pfs remaining in the system dead volume. These issues are common in biofunctionalized microfluidic systems due to the structural characteristics of enzymes and other proteins, the high surface area to volume ratio of the system, and the minimal mixing due to the laminar flow characteristics of the system (Beebe et al. 2002; Holden et al. 2004; Ku et al. 2006; Mao et al. 2002).

However, the 12 – 46 % conversion for the Pfs assembled onto the electrode site (Fig. 9b) is significantly above the 7 – 18 % conversion measured here in the control (Fig. 10b), demonstrating that the majority of catalytic reactions occur at the electrode site. This is particularly striking because (1) the electrode site comprises only 0.2 % of the total surface area within the bioMEMS available for non-specific binding of the enzyme, and (2) the fluid volume above the electrode site comprises only 0.3 % of the total fluid volume in the bioMEMS available for trapping any free unattached enzyme. New device and packaging designs are under investigation to minimize non-specific binding and dead volume effects.

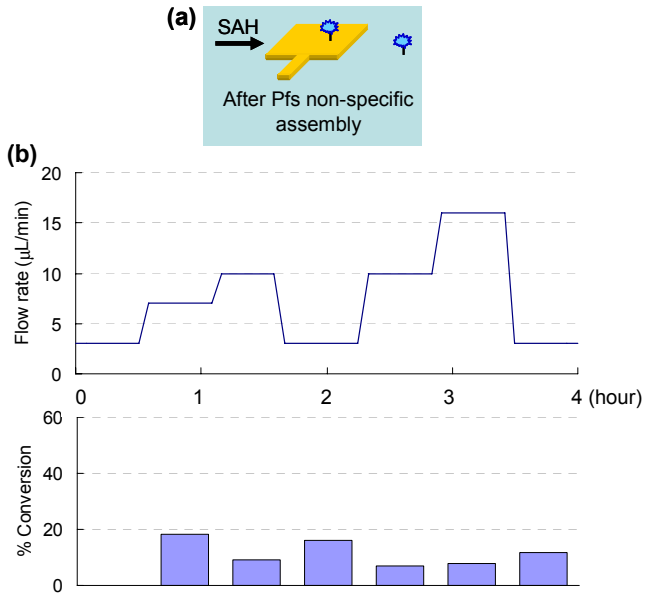

Figure 11. Negative control. **(a)** Pfs was introduced into microfluidic channel without the activating enzyme tyrosinase and without chitosan. (b) 7 – 18 % of SAH was converted by Pfs non-specifically bound to the microchannel surfaces and/or by Pfs retained in the dead volume of the microfluidic system. The majority of catalytic reactions occur at the electrode site which comprises only 0.2 % of the total surface area within the bioMEMS.

Transient response of bioMEMS.

Using our current bioMEMS packaging system, we observed a time delay between changing the flow rate over the reaction site (assembled with Pfs enzyme) and measuring the corresponding change in SAH concentration at the sample collection point downstream. To further examine the transient system response, we performed numerical modeling of the bioMEMS by simulating the mixing purely due to mass diffusion and the laminar transport (Reynolds number = 0.1). The simulation result in Fig. 12 shows that in the low flow rate case (3 µL/min) it takes 10 minutes for a concentration change at the reaction site to travel downsteam and arrive at the sample collection site, and it takes 25 minutes for the concentration response at the sample collection site to reach 95 % of the concentration change at the reaction site. This is mainly due to dead volume (~20 µL) in

the packaging between the microchannel and the external tubing. This transient response of the bioMEMS justifies why we collected the samples for HPLC analysis only at the 2nd hour in each flow rate step after the concentration completely stabilized, as shown in Fig. 10b. The response time of the current system design also partially explains the conversions in the control experiment as any enzyme in the dead volume contributes to the enzymatic conversion. The minimization or elimination of dead volume is also under investigation and will be the focus of subsequent studies.

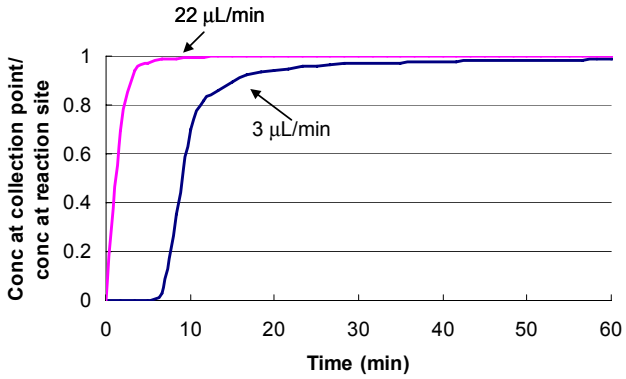

Figure 12. Simulation of the transient concentration response at the sample collection point versus the concentration change at the reaction site.

Discussion.

Background.

Recently, the aminopolysaccharide chitosan, a key enabling material for biofabrication, has recently been intensively exploited for post-fabrication biofunctionalization on patterned inorganic surfaces (Fernandes et al. 2004; Koev et al. 2007; Park et al. 2006; Wu et al. 2002; Wu et al. 2003; Yi et al. 2005a; Yi et al. 2005b; Yi et al. 2004; Yi et al. 2005c). Briefly, chitosan's pH responsive property enables electrical signal-guided assembly of chitosan onto user-selected conductive inorganic

surfaces from aqueous solution, and chitosan's abundant primary amine groups are exploited for assembly of biomolecules onto the chitosan scaffold. We demonstrated in situ protein assembly onto a chitosan scaffold in a microfluidic device by chemically activating the amine groups of chitosan with glutaraldehyde (Park et al. 2006). We also demonstrated *in situ* biochemical activation and protein assembly onto a chitosan scaffold in a microfluidic device (Lewandowski et al. in press). In both reports, the assembled green fluorescence protein (GFP) retained fluorescence and hence its 3-dimensional structure. Additionally, we reported that the model protein GFP preferentially assembles onto the chitosan scaffold through the C-terminal pentatyrosine pro-tag upon biochemical activation, demonstrating orientational control of protein assembly (Lewandowski et al. 2006).

Enzyme assembly and activity in bioMEMS.

Here we report an enzyme assembly strategy based on electrodeposition of the enzyme-chitosan conjugate onto readily addressable electrode sites into a microchannel of a pre-fabricated and packaged microfluidic device. Specifically, we report assembly of Pfs enzyme, a member of the AI-2 biosynthesis pathway, which catalyzes the cleavage of SAH into SRH and adenine. The significance of this result is that enzymes can be programmably assembled within a bioMEMS while maintaining their catalytic activity over time. This provides the underpinnings for a viable bioMEMS technology platform to support metabolic engineering research and development for applications from elucidating biochemical reaction kinetics to discovering new drugs.

Our enzyme assembly strategy described here offers several unique advantages over conventional techniques such as microcontact printing (Quist et al. 2005) and self

assembly layers (Chaki and Vijayamohanan 2002). First, the enzymes conjugated to chitosan were covalently bonded, and the assembly of the enzyme-chitosan conjugate onto the patterned electrode in the microchannel can be programmed conveniently by electrical signals. Second, the enzyme assembly was performed in mild aqueous conditions inside prefabricated and completely packaged microfluidic devices, thus avoiding direct contact and complex facilities. Third, we achieve temporal programmability since we are able to assemble the enzymes just prior to using the enzyme for small molecule biocatalysis. This is advantageous for biological components that have limited shelf life.

Quantification.

While the purpose here was to demonstrate the assembly and activity of enzymes within the bioMEMS, quantification of the activity and comparison to alternatives is an important and natural question. Such quantification is challenging and is the subject of ongoing research. In the meantime, it is possible to identify or estimate several semi-quantitative results of note.

Fig. 11b shows that some parasitic or background reaction occurs, presumably due to non-specific enzyme binding to the channel surfaces and/or due to free unbound enzyme or enzyme-chitosan conjugate suspensions. Fig. 10b and Fig. 11b further demonstrate that such conversion is significantly less (39 % = 18 % / 46 %) than the conversion by the enzyme assembled at the specific electrode site. This factor, however, grossly underestimates the efficiency of the localized electrode and enzyme upon it in providing a catalytically active device. The electrode, with only 0.5 mm^2 area, represents only 0.2 % of the total microenvironment surface (221 mm^2), and the volume above the

electrode site (0.075 μL) represents only 0.3 % of the total microenvironment volume (23.9 μL). Therefore, the enzyme-activated electrode is > 2 orders of magnitude more efficient in executing the catalytic reaction than other areas of the microfluidic environment.

In a meaningful sense, these quantitative results are already encouraging. An overriding concern with microfluidic technologies and applications is that the vastly enhanced surface/volume ratio over conventional chemical reactors may dramatically alter pathways and kinetics, rendering microfluidic environments not viable. For localized reaction sites in a bioMEMS, the concern takes two somewhat different but equally important forms: (1) will nonspecific binding at the large area of channel surfaces dominate over the small area of the active electrode? and (2) will parasitic reaction with the enzyme in the aqueous phase of the entire channel volume dominate over that at the electrode? Results here show that the assembled enzyme on the small electrode can control the catalytic conversion of small molecules in the bioMEMS.

Optimization.

There is ample opportunity to optimize conversion rates in our bioMEMS environments (Lewandowski et al. in press). One means is through process parameters such as flow rates, process time, concentrations, surface passivation, and pH. Another is through device design, such as channel dimensions and geometry, reduction of dead volumes such as reservoirs, and new network designs that minimize cross-talk between enzyme assembly and subsequent catalytic conversion. With present conversion rates at 46 %, there is room to improve the efficiency of enzyme conversion at the electrode and

reduce the parasitic conversion pathways (due to enzyme non-specific binding to channel surfaces and/or free unbound enzyme in aqueous volumes).

Conclusions and Applications

This work demonstrates a chitosan-mediated biofunctionalization strategy for the assembly of catalytically active enzymes within completely packaged and systematically controlled bioMEMS devices. The HPLC analysis of downstream reaction mixtures shows that the assembled enzymes are catalytically active, robust, and stable with time, and that our strategy is reproducible, allowing for multiple uses of bioMEMS devices. While further quantification is needed, the enzyme assembled at the specific electrode site is much more efficient overall in substrate catalytic conversion than are the parasitic channels associated with non-specific binding of the enzyme at the other channel surfaces or with free unbound enzyme in the aqueous volume.

In any case, we report here for the first time the generation of catalytically active enzyme at localized sites which can be programmed within the bioMEMS both spatially and temporally. The demonstration of enzyme catalytic activity represents a key step in progress toward a bioMEMS technology to support metabolic engineering research and development, where multi-step biochemical reactions are common, and separation of these steps is highly desirable for understanding reaction details, and modifying pathways and kinetics for various applications (e.g. drug discovery).

This novel strategy of enzyme assembly was achieved through two unique techniques: (1) the covalent conjugaton of the target enzyme to chitosan in solution upon biochemical activation of a pro-tag and (2) the electrodeposition of the resulting enzyme-

chitosan conjugate. Because the assembly of biological elements is signal-guided through electrodeposition process, the active biology (enzyme-chitosan conjugate) can be introduced into prefabricated bioMEMS devices upon demand. We anticipate that the methodology can be extended to multiple sites and with different enzymes to accommodate multi-step metabolic pathways, as would be valuable for replicating specific bacterial pathways, and seeking new antimicrobial drugs that modify or suppress those pathways.

Chapter 5: Assembly of Metabolic Pathway Enzymes onto Patterned Microfabricated Chips

Introduction

The assembly of metabolic pathways and other multi-step enzymatic reactions onto device surfaces presents an advantageous technique for their high-throughput examination and manipulation while minimizing reagent volume. Research has mainly focused on microchip arrays (Arenkov et al. 2000; Curey et al. 2002; Song et al. 2007), which generally necessitate expensive instrumentation, and microfluidic devices, where enzyme patterning remains challenging (Holden et al. 2004; Ku et al. 2006; Lee et al. 2003b; Mao et al. 2002; Wang et al. 2001). The assembly approach described here enables multi-enzyme patterning onto microchips and into microchannels without the need for expensive instrumentation.

Our unique approach for patterned assembly has been previously described (Chen et al. 2003a; Yi et al. 2005c). This approach is based on two strategies: (1) electrodeposition of a chitosan scaffold onto an electrode surface of the microfabricated device, and (2) covalent conjugation of the target enzyme to the scaffold upon biochemical activation of a genetically fused pro-tag. Briefly, the aminopolysaccharide chitosan electrodeposits as a stable thin film due to its pH-responsive properties conferred by its amine groups (Luo et al. 2004; Pang and Zhitomirsky 2005; Wu et al. 2002; Wu et al. 2003). Second, tyrosinase activates accessible tyrosine residues of the C-terminal pentatyrosine pro-tag into reactive *o*-quinones, which then covalently link to chitosan's

nucleophilic amine groups to form the protein-chitosan conjugate (Chen et al. 2002a; Chen et al. 2003a; Freddi et al. 2006).

We report patterned assembly of Pfs (*S*-adenosylhomocysteine nucleosidase) and LuxS (*S*-ribosylhomocysteinase) enzymes (each fused with the pro-tag) onto microfabricated chips. This represents the first time that LuxS has been assembled onto a device surface. As shown previously in Scheme 1, Pfs and LuxS are members of the autoinducer-2 (AI-2) biosynthesis pathway found in many (≥ 55) various bacterial species (Gram-positive and Gram-negative) (Federle and Bassler 2003). In this pathway, Pfs catalyzes the irreversible cleavage of SAH into adenine and *S*-ribosylhomocysteine (SRH) (Duerre 1962). SRH is then converted by LuxS into homocysteine and 4,5-dihydroxy-2,3-pentanedione (DPD) (Miller and Duerre 1968; Zhao et al. 2003), which is unstable and presumably spontaneously cyclizes and complexes with borate to form AI-2, a furanosyl borate diester (Chen et al. 2002b). More recently, however, Miller *et al.* (Miller et al. 2004) determined that AI-2 is in equilibrium with DPD and other furanone rings not containing boron, which may mean that AI-2 is actually a mixture of compounds. Nonetheless, the products of the LuxS reaction, regardless of species, strongly induce light production in the AI-2-specific reporter strain of the bioluminescent marine bacterium *Vibrio harveyi* (Federle and Bassler 2003; Surette and Bassler 1998). Due to the variety of possible structures, AI-2 is quantified via a bioassay developed by Surette and Bassler (Surette and Bassler 1998), which uses this *V. harveyi* reporter strain.

AI-2 is a "universal" chemical signaling molecule that mediates interspecies bacterial cell-cell communication termed type II quorum sensing (QS) (Miller and Bassler 2001), whereby the population as a whole, upon reaching a quorum of cells,

regulates phenotype via altering the expression of a variety of genes. Type II QS has become a target for novel "anti-pathogenic drug" (Bjarnsholt and Givskov 2007; Hentzer et al. 2003; Rasmussen and Givskov 2006) design due to its involvement in the pathogenesis of the bacterial population through regulation of cellular processes such as motility (Sperandio et al. 2001; Sperandio et al. 2002), possibly leading to increased colonization of the host, biofilm formation and architecture (Balestrino et al. 2005; Barrios et al. 2006; Ren et al. 2001), and other virulence factors (Sperandio et al. 2001; Zhu et al. 2002), including toxin production. Such anti-pathogenic drugs could function by inhibiting AI-2 biosynthesis through inhibition of Pfs and/or LuxS catalytic activities. Importantly for such novel drug design, Pfs and LuxS are not found in mammalian cells. For this, several researchers have designed inhibitors of Pfs (Cornell et al. 1996; Singh et al. 2005; Singh et al. 2006) or LuxS (Alfaro et al. 2004; Shen et al. 2006) as possible drugs, and such research is ongoing. Thus, a microchip with assembled Pfs and LuxS could be used to screen for such novel drugs.

We report patterned assembly of Pfs and LuxS enzymes onto a single microfabricated chip. For this, we investigated two possible assembly methodologies based on our previous work (Lewandowski et al. in review; Lewandowski et al. in press): (1) electrodeposition of chitosan followed by covalent conjugation of the enzyme to chitosan or (2) covalent conjugation of the enzyme to chitosan followed by electrodeposition of the enzyme-chitosan conjugate. To assemble catalytically active LuxS, the first method (electrodeposition followed by conjugation) must be utilized. We demonstrate in initial studies using this method that Pfs and LuxS could be assembled onto a single chip, demonstrating for the first time using our approach the assembly of

multiple enzymes representing a metabolic pathway. We believe that our approach allows for user-controlled examination of multi-step enzymatic reactions, in particular those of metabolic pathways, and we envision many potential biomedical and metabolic engineering applications.

Materials and Methods

Materials.

S-adenosylhomocysteine (SAH), chitosan (minimum 85 % deacetylated chitin; molecular weight 200,000 g/mol) from crab shells, goat anti-mouse IgG (whole molecule) conjugated to fluorescein isothiocyanate (FITC), imidazole, isopropyl β-D-thiogalactopyranoside (IPTG), monoclonal mouse anti-poly-histidine, nickel sulfate, phosphate buffered saline (PBS) (2.7 mM KCl, 137 mM NaCl, 1.5 mM KH_2PO_4, 8.1 mM Na_2HPO_4, pH 7.5), sodium cyanoborohydride, tyrosinase from mushroom, and zinc acetate were purchased from Sigma (St. Louis, MO). Tyrosinase was reported by the manufacturer to have an activity of 1,530 Units/mg solid. LB (Luria broth) medium was purchased from Becton Dickinson (Cockeysville, MD). Acetone, ampicillin sodium salt, chloroform, glycerol, sodium phosphate (monobasic), sodium phosphate (dibasic), and Tris base (trishydroxymethylaminomethane) were purchased from Fisher Chemical (Fair Lawn, NJ). Hydrochloric acid and sodium chloride were purchased from J. T. Baker (Phillipsburg, NJ). Non-fat dry milk and Tween 20 were purchased from BioRad (Hercules, CA). Goat anti-mouse IgG (H+L) conjugated to Alexa Fluor® 594 was purchased from Invitrogen (Carlsbad, CA). Bleach was purchased from James Austin

Co. (Mars, PA). De-ionized water (ddH2O, 18 MΩ·cm, Milli-Q) and PBS (dissolved in de-ionized water) were autoclaved before use.

Plasmid construction.

Construction of pTrcHis-Pfs-Tyr and pTrcHis-LuxS-Tyr plasmids was reported previously (Fernandes et al. 2007). Briefly, the plasmids were constructed by PCR amplification of *pfs* (in the case of pTrcHis-Pfs-Tyr) and *luxS* (in the case of pTrcHis-LuxS-Tyr) from *E. coli* wild type strain W3110. Following digestion, the PCR products were extracted by gel purification and inserted into pTrcHisC (Invitrogen). DNA sequencing was performed to verify construct integrity. The pTrcHis-Pfs-Tyr plasmid was transformed into *E. coli* DH5α (defective *luxS* strain), and the pTrcHis-LuxS-Tyr plasmid was transformed into *E. coli* NC13 (*pfs* null-mutant strain).

Production and purification of $(His)_6$-Pfs-$(Tyr)_5$ and $(His)_6$-LuxS-$(Tyr)_5$.

The production and purification of $(His)_6$-Pfs-$(Tyr)_5$ was previously described (Lewandowski et al. in review). This procedure was also used for $(His)_6$-LuxS-$(Tyr)_5$. Briefly, *E. coli* DH5α and NC13 strains containing pTrcHis-Pfs-Tyr and pTrcHis-LuxS-Tyr, respectively, were cultured in LB medium supplemented with ampicillin, with IPTG was added to induce enzyme production. Additionally, zinc acetate was added at induction during NC13 culture, as this stabilizes the LuxS metalloenzyme by substituting Fe^{2+} with Zn^{2+} in the active site (Zhu et al. 2003). Ultimately, the enzymes were purified via immobilized metal-ion affinity chromatography (IMAC) using a 5 mL HiTrap Chelating HP column charged with Ni^{2+} ions (Amersham Biosciences), and dialyzed into PBS. Purified protein concentration was determined with a UV/vis spectrophotometer

(DU 640, Beckman, Fullerton, CA) using UV light at 280nm wavelength. The protein solution was mixed 2:1 with glycerol, alliquoted, and stored at – 80^{o}C until use.

Chitosan preparation.

Chitosan solution was prepared by adding chitosan flakes in de-ionized water, with HCl added dropwise to maintain pH ~ 2, and mixing overnight. The pH was then adjusted to 3.6 by adding 1 M NaOH dropwise, and the chitosan solution was then filtered and stored at 4^{o}C until use.

Chip fabrication.

The microfabrication process for the chips was reported previously. Briefly, 4″ diameter silicon wafers were coated with 1 μm silicon nitride film, followed by deposition of 50 Å chromium film, and finally, deposition of 2000 Å gold film. The patterns were created by photolithography, and the photoresist removed using acetone. The chips contain two upper gold rectangular patterns (6 mm long × 3 mm wide) each linked by 8 mm gold lines to two lower gold rectangular patterns (8 mm long × 1 mm wide), where enzyme assembly took place. Before the start of every experiment, each chip was cleaned by incubation in 5 M HCl for 20 minutes, followed by incubation in concentrated bleach for 20 minutes, with thorough rinsing with de-ionized water after each step, and finally were incubated in PBS until use.

Chitosan electrodeposition followed by enzyme conjugation.

Chitosan scaffold was deposited onto the gold electrode pattern by dipping the chip into chitosan solution (0.5 % (w/w), pH 3.6) until the pattern was submerged and applying negative bias to the pattern (2 min at 16 A/m^2). After deposition, the chip was

rinsed with de-ionized water, and incubated in 5 % (w/v) non-fat dry milk – PBS for 2 h. For the experiments with LuxS alone, the chip was then incubated in LuxS (0.1 mg/mL) and tyrosinase (0.1 mg/mL or 166 Units/mL) in PBS for 16 h at 4^{o}C, followed by incubation in sodium cyanoborohydride (0.2 mg/mL) for 15 min at room temperature, and washed with gentle shaking 3 × 5 min in 5 mL PBS. Finally, the chip was incubated at 37^{o}C in 1 mL of 1 mM SRH, produced by incubating a chip with assembled Pfs at 37^{o}C in 1 mL of 1 mM SAH (in 10 mM Tris-HCl pH 7.8), and allowing the reaction to go to completion. At reaction time points, samples were taken and immediately extracted with chloroform to stop the reaction, and the extracted samples were stored at – 20^{o}C before analysis.

Enzyme-chitosan conjugation followed by electrodeposition.

First, two chips were incubated in 5 % (w/v) milk – PBS for 2 h, rinsed with de-ionized water, and set aside. The conjugates were prepared by incubating Pfs or LuxS (0.5 mg/mL), tyrosinase (0.1 mg/mL or 166 Units/mL), and chitosan (0.5 % (w/w)) in sodium phosphate buffer (final concentration 5.5 – 5.9 mM PO_4^{3-}) (mixture final pH 5.5 – 6.0) for 2 h at room temperature and 250 rpm, followed by incubation in sodium cyanoborohydride (0.2 mg/mL) for 15 min at room temperature and 250 rpm. Each conjugate was deposited onto the gold electrode pattern by dipping the chip into the conjugate until the pattern was submerged and applying negative bias to the pattern (2 min at 2.5 A/m^2). This was done by connecting the cathode and anode (nickel chromium wire) using alligator clips to a DC power supply (Keithley 2400 SourceMeter). After deposition, the chip was gently rinsed with de-ionized water. For biocatalysis, the chips with assembled conjugates were washed with gentle shaking 3 × 5 min in 5 mL PBS, and

then incubated at 37°C in 1 mL of 1 mM SAH (in 10 mM Tris-HCl pH 7.8). At reaction time points, samples were taken and immediately extracted with chloroform to stop the reactions, and the extracted samples were stored at – 20°C before analysis. For antibody-binding experiments, the chip was washed with gentle shaking 3 × 5 min in 5 mL TTBS (20 mM Tris-HCl, 500 mM NaCl, 0.05 % (v/v) Tween-20, pH 7.5) after electrodeposition of each enzyme-chitosan conjugate before incubating in the antibody solutions.

Antibody binding.

Following TTBS washes, the chip was incubated 1.5 h with gentle shaking in mouse anti-poly-histidine (0.1 mg/mL) in 1 % (w/v) non-fat dry milk – TTBS, and washed 3 × 5 min in 5 mL TTBS with gentle shaking. It was then incubated 1 h with gentle shaking in goat anti-mouse IgG (0.1 mg/mL) in 1 % (w/v) non-fat dry milk – TTBS. For assembled Pfs, Alexafluor 594-conjugated 2° antibody was used, and for assembled LuxS, FITC-conjugated 2° antibody was used. Finally, the chip was washed with gentle shaking 3 × 5 min in 5 mL TTBS and 3 × 5 min in 5 mL TBS (20 mM Tris-HCl, 500 mM NaCl, pH 7.5) before viewing under the fluorescence microscope.

LuxS stability studies.

LuxS-chitosan conjugate solution was prepared by incubating LuxS (0.5 mg/mL), tyrosinase (0.1 mg/mL or 166 Units/mL), and chitosan (0.5 % (w/w)) in sodium phosphate buffer (5.8 mM PO_4^{3-}) at a final pH ~ 6 for 2 h at room temperature and 250 rpm, followed by incubation in sodium cyanoborohydride (0.2 mg/mL) for 15 min at room temperature and 250 rpm. Free unconjugated LuxS solution was prepared by incubating LuxS (0.5 mg/mL) in sodium phosphate buffer (5.8 mM PO_4^{3-}) at a final pH ~

6 for 2 h room temperature. To 75 µL of each solution, 300 µL of various buffers were added, and the solutions/suspensions incubated 2 min at room temperature. The following buffers were added: 6 mM sodium phosphate pH 6.2, 6 mM sodium phosphate pH 7.6, 6 mM Tris-HCl pH 7.6, 6 mM glycine-NaOH pH 10.6, and 12 mM KCl-NaOH pH 12.1. To the 375 µL solutions/suspensions, 125 µL of 0.25 mM SAH (in 10 mM Tris-HCl pH 7.8) was added, and the solutions/suspensions incubated 10 min at room temperature. The final pH conditions were: 6.7, 7.5, 7.5, 9.2, and 11.5, respectively compared with the buffers added above. The reaction mixtures were extracted with chloroform to stop the reaction. Additionally, the conjugate reaction mixtures were centrifuged 5 min at 14,000 g's to remove any precipitated chitosan. Finally, the extracted/centrifuged samples were stored at – 20^{o}C before analysis.

AI-2 activity bioassay.

The LuxS reaction mixtures were tested for AI-2 using the AI-2 activity bioassay developed by Surette and Bassler (Surette and Bassler 1998), which uses the *V. harveyi* reporter strain BB170. Briefly, 20 µL of each reaction mixture was mixed with 180 µL of BB170 culture, prepared by 1:5000 dilution in AB medium of an overnight culture (grown 16 h 30^{o}C 250 rpm in AB medium). The internal bioassay negative control was 20 µL of AB medium. The 200 µL bioassay samples were then grown at 30^{o}C 250 rpm. Bioluminescence of each sample was normalized against that of the bioassay negative control. At least 3 bioassay samples of each reaction mixture were separately prepared to confirm reproducibility.

HPLC analysis of Pfs reaction samples.

A Waters Spherisorb Silica column (250 × 4.6 mm) with 5 μm beads (80 Å pore) was used in reversed-phase mode with 5 μL sample injection size and a mobile phase of 70:30 acetonitrile:water at 0.5 mL/min. Conversion was calculated from elution data at 210 nm. The HPLC system consisted of two Dynamax model SD-200 pumps (with 10 mL pump heads and mixing valve) and a Dynamax Absorbance Detector model UV-D II, and data was analyzed using Star 5.5 Chromatography Software (Rainin).

Results and Discussion

Single enzyme assembly: conjugation to electrodeposited chitosan scaffold.

We assemble LuxS enzyme onto a patterned chitosan scaffold of a microfabricated chip, and demonstrate that it retains biocatalytic activity for the biosynthesis of AI-2, shown schematically in Fig. 13a. For this, we first electrodeposited chitosan scaffold onto an 8 mm^2 gold electrode pattern of a chip. Next, the chip was incubated in 5 % milk – PBS to block non-specific binding. It was then incubated in a PBS solution containing $(His)_6$-LuxS-$(Tyr)_5$ and tyrosinase, which activates the $(Tyr)_5$ pro-tag to covalently link LuxS to the amines of the patterned chitosan scaffold. Finally, after thorough PBS washing, the chip was incubated in 1 mM SRH at 37^oC for 2 hours. The reaction mixture was extracted with chloroform to stop the reaction, and analyzed via the AI-2 activity bioassay developed by Surette and Bassler (Surette and Bassler 1998). AI-2 activities are normalized against the internal bioassay negative control.

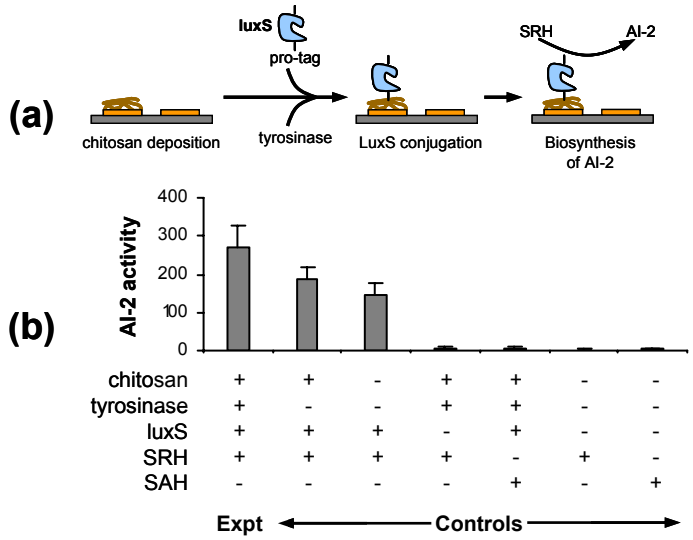

Figure 13. Chips with assembled LuxS enzyme synthesize AI-2 from SRH substrate. **(a)** LuxS was assembled via chitosan electrodeposition followed by LuxS-chitosan conjugation. **(b)** AI-2 activites of the 2h reaction time points of the experimental reaction mixture and of multiple experimental negative controls, measured via *Vibrio harveyi* bioassay. AI-2 activities were normalized against the bioassay negative control. Error bars (standard deviations) were averaged over multiple experiments and bioassay measurements.

Shown in Fig. 13b is a plot of normalized AI-2 activities, with error bars (standard deviations) calculated from several bioassay measurements of several samples. The first bar (271 ± 55) represents the reaction of SRH with the experimental chip ("+chitosan +tyrosinase +luxS +SRH –SAH"), and demonstrates that this chip produced AI-2 activity. To demonstrate that this AI-2 activity was in fact produced by covalently assembled LuxS, several negative controls were performed. The second bar (185 ± 34) represents a negative control ("+chitosan –tyrosinase +luxS +SRH –SAH"), where a chip with patterned chitosan scaffold was incubated in LuxS alone (without tyrosinase activation). This chip yielded less AI-2 activity, indicating that less LuxS assembled non-specifically onto the patterned scaffold than assembled covalently through tyrosinase activation. The third bar (148 ± 29) represents a negative control ("–chitosan –tyrosinase +luxS +SRH –SAH"), where a chip alone (without patterned chitosan scaffold) was

incubated in LuxS alone (without tyrosinase activation). This chip yielded even less AI-2 activity, indicating that even less LuxS assembled non-specifically onto the chip surfaces (gold and silicon oxide). The fourth bar (6 ± 6) represents a negative control ("+chitosan +tyrosinase –luxS +SRH –SAH"), where a chip with patterned chitosan scaffold was incubated in tyrosinase alone (without LuxS). This chip yielded negligible AI-2 activity, demonstrating that a chip must contain assembled LuxS for production of AI-2 activity. The fifth bar (6 ± 7) represents a negative control, where SAH (rather than SRH) was reacted with the experimental chip ("+chitosan +tyrosinase +luxS –SRH +SAH"). As shown previously in Scheme 1, SRH is produced through Pfs-catalyzed hydrolysis of SAH. As expected, the reaction of SAH with assembled LuxS produced negligible AI-2 activity, and demonstrates that assembled LuxS must react with its specific substrate SRH for any significant production of AI-2 activity. Finally, the sixth (2 ± 2) and seventh (4 ± 4) bars represent unreacted SRH and SAH solutions, respectively. These final negative controls demonstrate that the bioassay detected AI-2 activities produced by assembled LuxS, and not any extraneous AI-2 in the substrate solutions or the cell culture media used in the bioassay.

The results of the first, second, and third bars of Fig. 13b demonstrate that more LuxS assembled covalently onto the electrodeposited chitosan through tyrosinase activation than assembled non-specifically onto the chitosan or the chip surfaces; however, the amount of assembled LuxS cannot be quantified from results of the AI-2 activity bioassay. This bioassay is based on bioluminescence of the marine bacterium *V. harveyi*, a quorum sensing response to a threshold level of AI-2. Thus, AI-2 activity does not correlate linearly with AI-2 concentration (De Keersmaecker et al. 2005; Rajamani et

al. 2007; Turovskiy and Chikindas 2006; Vilchez et al. 2007). We are currently investigating alternative assays to accurately measure catalytic conversion of SRH by assembled LuxS.

In summary, Fig. 13 demonstrates the assembly of a metabolic pathway enzyme onto microfabricated chips via conjugation to electrodeposited chitosan scaffold. The assembled enzyme retains reproducible biocatalytic activity for the biosynthesis of a small molecule that is the end product of a metabolic pathway.

Assembly of multiple enzymes representing a metabolic pathway via conjugation to electrodeposited chitosan scaffold.

We next performed initial studies examining the assembly of both Pfs and LuxS enzymes onto patterned chitosan of a single microfabricated chip, and demonstrate the biosynthesis of AI-2 by the assembled quorum sensing pathway, as shown in Fig. 14a. For this, we first electrodeposited chitosan scaffold onto the left gold electrode (8 mm^2) of a chip. After incubating this chip in 5 % milk – PBS to block non-specific binding, it was then incubated in a solution containing tyrosinase, Pfs, and LuxS. Finally, after thorough washing, the chip was incubated in 1 mM SAH at 37^oC for 8 hours. The reaction mixture was extracted with chloroform to stop the reaction, and analyzed via the AI-2 activity bioassay. AI-2 activities are normalized against the internal bioassay negative control.

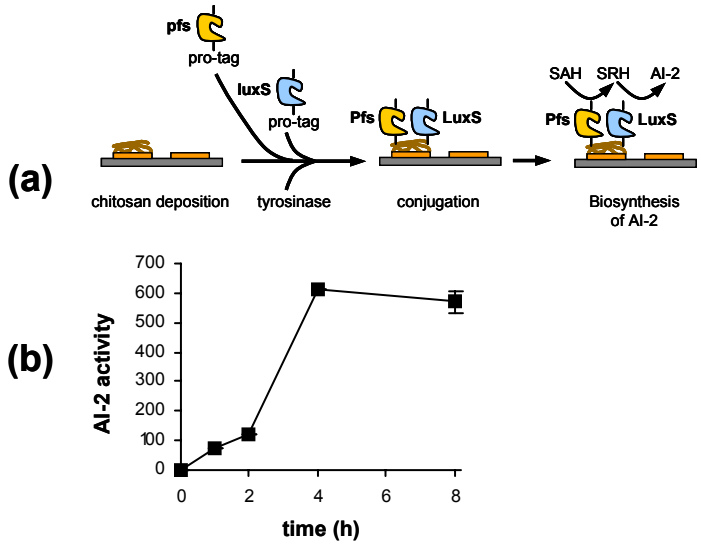

Figure 14. Initial studies examining the assembly of Pfs and LuxS enzymes via **(a)** chitosan electrodeposition followed by enzyme-chitosan conjugation. **(b)** AI-2 activites of the reaction solutions were measured via *Vibrio harveyi* bioassay and normalized against the bioassay negative control. The error bar (standard deviation) was averaged over multiple bioassay measurements.

Shown in Fig. 14b is a plot of normalized AI-2 activities versus reaction time, with the error bar (standard deviation) at the 8 h time point calculated from several bioassay measurements. This plot demonstrates that the assembled Pfs and LuxS enzymes produced reproducible AI-2 activity from the initial substrate SAH. The AI-2 activity increases with reaction time, indicating an increase in AI-2 yield with reaction time, with a final AI-2 activity of 571 ± 37 measured at 8 h. Additionally, AI-2 activities of 1 ± 0.2 and 1 ± 0.1 for unreacted SRH and SAH solutions, respectively, were measured (not shown). We note that there appears to be a slight decline in AI-2 activity from 4 to 8 h reaction time produced by the chip where Pfs and LuxS were assembled onto the same electrode. We believe this is due to error resulting from sampling and/or the bioassay, and presume that the reaction is complete at 4 h reaction time. Finally, and most importantly, we note that these are initial results demonstrating for the first time the patterned assembly of both Pfs and LuxS onto a single device. Additionally and more

importantly, these results represent the first time using our approach that we have assembled multiple enzymes representing a metabolic pathway onto a single device surface. In future work, we will examine multiple enzyme patterning through optimization of chip design and fluorescent labeling of enzymes.

In summary, Fig. 14 demonstrates the assembly of multiple enzymes representing a metabolic pathway onto microfabricated chips via conjugation to electrodeposited chitosan scaffold. The assembled enzymes both retain catalytic activities for the biosynthesis of the pathway end-product from the initial pathway substrate.

Patterned assembly of multiple enzymes representing a metabolic pathway via sequential electrodeposition of enzyme-chitosan conjugates.

Finally, we sequentially assemble Pfs and LuxS enzymes onto separate electrode patterns of a single microfabricated chip via sequential electrodeposition of enzyme-chitosan conjugates, as shown in Scheme 8. For this, we prepared Pfs-chitosan conjugate solution and LuxS-chitosan conjugate solution by incubating chitosan, tyrosinase, and $(His)_6$-Pfs-$(Tyr)_5$ or $(His)_6$-LuxS-$(Tyr)_5$, respectively. Chitosan was in excess to ensure that all of the available Pfs and LuxS were conjugated to chitosan. We then sequentially electrodeposited the Pfs-chitosan and the LuxS-chitosan conjugates onto the left and right gold electrode patterns (8 mm^2), respectively, of a single chip. This chip had been previously incubated in 5 % milk – PBS solution to block non-specific binding.

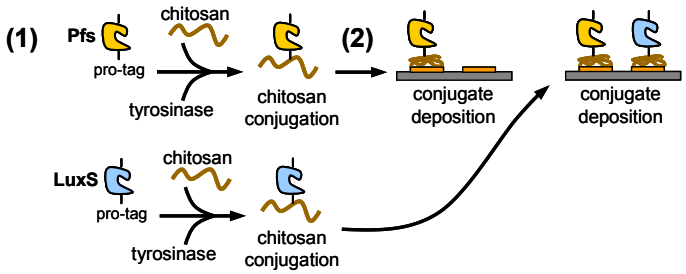

Scheme 7. Sequential patterned assembly of Pfs and LuxS enzymes via enzyme-chitosan conjugation followed by electrodeposition. (1) Pfs and LuxS were conjugated to chitosan solution. (2) Electrodeposition of Pfs-chitosan conjugate followed by electrodeposition of LuxS-chitosan conjugate.

We first examined the localization of the deposited enzyme-chitosan conjugates onto their respective target electrodes, and the abilities of the deposited conjugates to bind antibodies. For this, we first electrodeposited Pfs-chitosan conjugate onto the chip, which was then incubated in mouse anti-poly-histidine (1^{o} antibody), and in red fluorescently labeled goat anti-mouse IgG (Pfs 2^{o} antibody), with thorough washing after each step. Next, we electrodeposited LuxS-chitosan conjugate onto the chip, which was incubated in the same 1^{o} antibody, and then in green fluorescently labeled goat anti-mouse IgG (LuxS 2^{o} antibody), with thorough washing after each step. Shown in Fig. 15a is an original fluorescence micrograph of this chip, which has not been edited in Adobe Photoshop. The fluorescence micrograph illustrates the electrodeposition of each enzyme-chitosan conjugate is localized onto its respective target electrode, with negligible fluorescence of the surrounding silicon oxide surface. Thus, these results demonstrate patterned assembly of Pfs and LuxS enzymes through sequential electrodeposition of Pfs- and LuxS-chitosan conjugates onto selected patterned electrodes. More importantly, these results demonstrate that the patterned Pfs and LuxS retain the necessary structures and accessibilities for antibody binding.

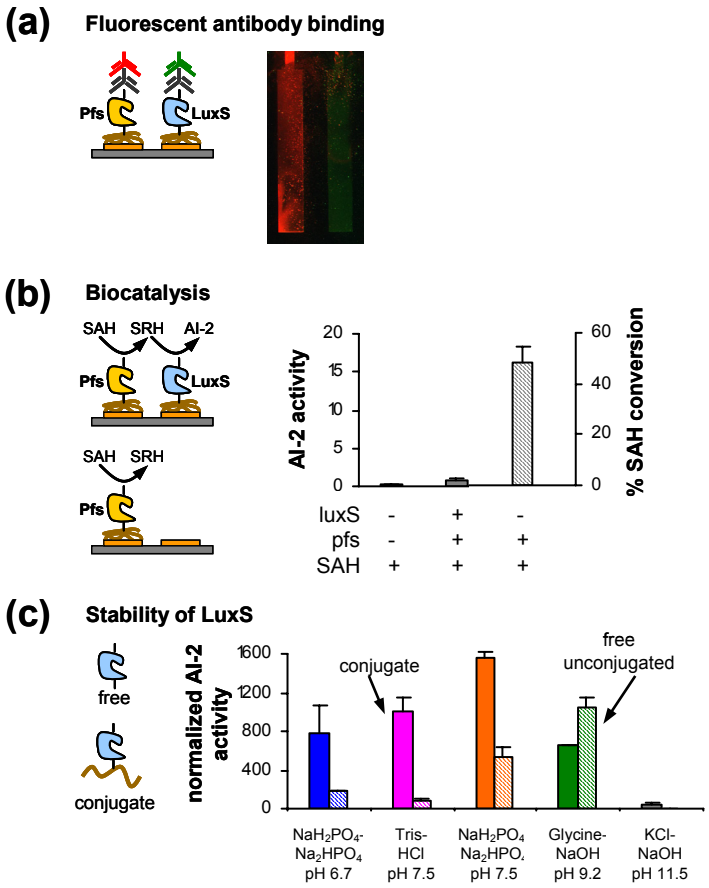

Figure 15. Sequential patterned assembly of Pfs and LuxS enzymes via enzyme-chitosan conjugation followed by electrodeposition. **(a)** Fluorescent antibody binding to assembled enzymes: Pfs assembly followed by binding of red fluorescently labeled 2° antibody, and LuxS assembly followed by binding of green fluorescently labeled 2° antibody. Shown is a fluorescent micrograph of this chip. **(b)** Biocatalysis by assembled enzymes. Shown are AI-2 activities of the Pfs-LuxS reaction solution at 2h and of unreacted SAH (solid bars), and % SAH conversion by assembled Pfs at 2h (striped bar; measured via HPLC). **(c)** Dependence of LuxS stability on pH and buffer. Shown is a plot of the AI-2 activities of free, unconjugated LuxS (lined bars) and LuxS-chitosan conjugate (solid bars) at different pH and buffer conditions. In **(b)** and **(c)**, AI-2 activities were measured via *Vibrio harveyi* bioassay and normalized against the bioassay negative control. Error bars (standard deviations) were averaged over multiple bioassay measurements.

We next examined the catalytic activities of the electrodeposited Pfs- and LuxS-chitosan conjugates. For this, two chips were prepared: onto one chip both Pfs and LuxS were assembled, and onto the second chip only Pfs was assembled. The chips were then incubated in 1 mM SAH at 37°C for 2 hours, and the reaction mixtures were extracted with chloroform to stop the reactions. The reaction mixture from the chip with assembled Pfs and LuxS was analyzed via the AI-2 activity bioassay, and the reaction

mixture from the chip with assembled Pfs was analyzed via HPLC. Shown in Fig. 15b is a plot of normalized AI-2 activities (normalized against the internal bioassay negative control; solid bars) of unreacted SAH ("–luxS –pfs +SAH", 0.3) and the Pfs-LuxS reaction solution ("+luxS +pfs +SAH", 0.8 ± 0.2), with error bars (standard deviations) calculated from multiple bioassay measurements. Also shown in Fig. 15b is a plot of the % SAH catalytic conversion (striped bar) of the Pfs reaction solution ("–luxS +pfs +SAH", 48 ± 6 %), with the error bar (standard deviation) calculated from two experiments. These results demonstrate that a chip with assembled Pfs and LuxS produced negligible AI-2 activity from the initial pathway substrate SAH. Thus, this method for sequential assembly of Pfs and LuxS (through sequential electrodeposition of Pfs- and LuxS-chitosan conjugates) is not a viable option for significant AI-2 biosynthesis. However, these results also demonstrate that a chip with assembled Pfs significantly catalyzed the conversion of SAH, and thus, catalytically active Pfs could be assembled using this method. Therefore, we conclude that the lack of AI-2 production is due to the loss of LuxS catalytic activity.

The loss of LuxS catalytic activity may be a result of this method's pH-dependence for enzyme assembly. In this method, the enzyme is first covalently conjugated to soluble chitosan, which transfers its pH-responsive properties to the enzyme upon conjugation, and then this enzyme-chitosan conjugate is electrodeposited. Chitosan conjugation occurred at pH 5.7 (below chitosan's pKa of 6.3) to maintain chitosan solubility, which may have destabilized LuxS, as this pH is close to its isoelectric point of 5.3 (measured via isoelectric focusing gel electrophoresis; not shown).

Next, electrodeposition occurred for 2 minutes at pH 11 – 12, which also may have destabilized LuxS.

We further examined the affects of pH and buffer on LuxS stability by performing additional experiments. For this, we incubated LuxS-chitosan conjugate suspension and free, unconjugated LuxS solution (both initially at pH ~ 6) for 2 minutes at room temperature in various pH and buffer conditions. We then added SRH (final SRH concentration 0.25 mM; final LuxS concentration 75 μg/mL) and reacted for 10 minutes at room temperature. The reaction mixtures were extracted with chloroform to stop the reactions, the conjugate reaction mixtures were centrifuged to remove precipitated chitosan, and the extracted/centrifuged samples were analyzed via the AI-2 activity bioassay. AI-2 activities are normalized against the internal bioassay negative control. Shown in Fig. 15c is a plot of normalized AI-2 activities of the LuxS conjugate and free unconjugated LuxS at different final pH conditions, with error bars (standard deviations) calculated from several bioassay measurements. The plot in Fig. 15c demonstrates that pH and buffer significantly affect AI-2 production by LuxS *in vitro*. Importantly, more AI-2 activity is produced by the LuxS conjugate than produced by free LuxS at all conditions except pH 9.2, indicating that chitosan conjugation stabilizes the LuxS for increased catalytic activity. Also importantly, minimal AI-2 activity is produced by either the LuxS conjugate (34 ± 25) or the free LuxS (4 ± 2) at pH 11.5, indicating loss of LuxS catalytic activity at high pH due to high pH-sensitivity. Combined, these results demonstrate that the loss of LuxS catalytic activity during chip assembly occurs during electrodeposition (not during chitosan conjugation), presumably due to the high pH of electrodeposition. It may be possible to retain some LuxS activity through reduction of

electrodeposition time or current density (μAmps/mm^2). This will be the subject of further experimentation.

In summary, Fig. 15 demonstrates sequential patterned assembly of multiple enzymes representing a metabolic pathway onto microfabricated chips through sequential electrodeposition of enzyme-chitosan conjugates. The assembled enzymes retain the necessary structures and accessibilities for antibody binding, but are not able to produce the pathway end-product from the initial pathway substrate, presumably due to the high pH of electrodeposition. Thus, while antibody-protein binding studies are possible with this method, biocatalysis with assembled enzymes may not be possible, owing to the particular challenges of assembling catalytically active enzymes (i.e. retention of active site conformation and accessibility). Optimization of this method is currently underway to minimize any instability caused by the assembly process.

Conclusions

We report for the first time the patterned assembly of the bacterial quorum sensing pathway enzyme LuxS onto microfabricated chips. More importantly, we report the patterned assembly of both enzymes of the pathway, Pfs and LuxS, onto a single microfabricated chip, and demonstrate the biosynthesis of AI-2, a small molecule that is the end-product of this pathway, using the assembled enzymes. For this, we investigated two possible methodologies for patterned enzyme assembly: (1) electrodeposition of chitosan followed by covalent conjugation of the enzyme to chitosan, and (2) covalent conjugation of the enzyme to chitosan followed by electrodeposition of the enzyme-chitosan conjugate. Results indicate that the second method (conjugation than

electrodeposition) may not be suitable for assembly of catalytically active enzymes that are high pH-sensitive.

Nonetheless, using our overall approach, we have demonstrated the patterned assembly of multiple enzymes representing a metabolic pathway onto a microfabricated chip, and demonstrate that the assembled enzymes retain catalytic activities for biosynthesis of the pathway end-product. We believe our approach is appealing for a variety of potential biomedical and metabolic engineering applications, where multi-step enzymatic reactions could be examined and manipulated. Specifically, Pfs and LuxS enzymes could be assembled using our approach to create a screening device to discover novel "anti-pathogenic" drugs that would inhibit Pfs and/or LuxS catalytic activities.

Chapter 6: Conclusions and Future Work

Conclusions

Bio-micro-chips, or biofunctionalized microfabricated devices, are advantageous for a variety of drug screening and medical diagnostics applications as they allow for rapid and automated analyses with minimal consumption of expensive reagents. I have biofunctionalized flat microchips and 3-dimensional microfluidic devices using our unique protein assembly approach. This approach is based on electrodeposition of the aminopolysaccharide chitosan onto a selected electrode pattern of the device, and the covalent conjugation of the target protein to chitosan upon biochemical activation of a C-terminal pentatyrosine "pro-tag."

This approach has several unique advantages over conventional protein assembly approaches. First, the entire assembly process occurs under mild experimental conditions ideal for maintaining protein bioactivity: in aqueous solution and through biochemical activation. Second, the devices are pre-fabricated, allowing for device reusability as chitosan can be removed with dilute acid solution and re-deposited, and allowing the devices to be biofunctionalized on-demand. This is additionally advantageous as proteins are labile with a limited shelf-life. Third, assembly is "spatially selective", occurring only on selected electrode patterns, allowing for user-control of assembly through manipulation of the assembly area. Finally, the target protein covalently and robustly conjugates to chitosan upon selective activation of a C-terminal pro-tag, and thus, our approach confers orientational control, as the protein links to chitosan primarily through

the C-terminal pro-tag versus the native tyrosine residues. For these advantages, our approach is appealing for a variety of potential biosensing and bioMEMS applications.

I have examined assembly of enzymes from bacterial metabolic pathway. Through binding of fluorescently labeled antibodies to the assembled enzymes, I have demonstrated that the enzymes primarily assemble onto a user-selected electrode pattern of the device, and thus, are patterned onto the device. More importantly, the assembled enzymes retain the necessary structures and accessibilities to recognize and bind antibodies from solution. Additionally, the assembled enzymes retain reproducible catalytic activities for a given patterned assembly area, allowing for user-control of substrate catalytic conversion through manipulation of the assembly area. This also allows for examination of enzyme reaction kinetics. Finally, enzyme assembly was also demonstrated in 3-dimensional microfluidic devices, which are advantageous over batch reactor systems due to their rapid response time. The assembled enzymes in the microfluidic device retain reproducible catalytic activities for a given substrate flow rate, and are stable over extended time at room temperature.

I have specifically examined assembly of Pfs and LuxS enzymes, members of the autoinducer-2 (AI-2) biosynthesis pathway found in many bacterial species. AI-2 is a small chemical signaling molecule that mediates type II, or interspecies, quorum sensing, through which an entire bacterial population coordinates behavior in response to changing environmental cues. Quorum sensing has become a target for novel "anti-pathogenic" drug design as it is known to be involved in regulating the pathogenesis of the bacterial population. By assembling Pfs and LuxS enzymes onto a device, AI-2 biosynthesis inhibitors could be screened to discover such anti-pathogenic drugs.

Significantly, this represents the first time that Pfs and LuxS enzymes have been device-assembled. More significantly, I have demonstrated patterned assembly of both Pfs and LuxS onto a single device, representing assembly of an entire metabolic pathway onto a single device. Thus, *in vitro* examination and manipulation of metabolic pathways is possible with our approach, which has potential metabolic engineering applications.

In summary, I have demonstrated patterned assembly of catalytically active enzymes onto flat microfabricated chips and into 3-dimensional fully packaged microfluidic devices. Importantly, I have shown that the substrate catalytic conversions by assembled enzymes can be user-manipulated by simple modulation of assembly areas and/or substrate flow rates over the assembled enzymes. More importantly, I have demonstrated that assembly of multiple enzymes representing metabolic pathways is possible. I envision many potential biosensing, bioMEMS, drug screening, and metabolic engineering applications.

Future Work

The overall goal of our entire research project is the creation of a bio-micro-chip with assembled Pfs and LuxS to screen for inhibitors of AI-2 biosynthesis. I have accomplished the first critical step by demonstrating that chip-assembled Pfs and LuxS reproducibly produce AI-2. The next critical goal is to assemble Pfs and LuxS into a 3-dimensional microfluidic device and produce AI-2. A subsequent future goal is to screen inhibitors of Pfs and/or LuxS by measuring a decrease in AI-2 biosynthesis. Finally, I envision assembling each enzyme onto separate patterns of a single device, and manipulating the overall AI-2 biosynthesis through user-modulation of each pattern.

References

Alfaro JF, Zhang T, Wynn DP, Karschner EL, Zhou ZS. 2004. Synthesis of LuxS inhibitors targeting bacterial cell-cell communication. Organic Letters 6(18):3043-3046.

Andersson H, van den Berg A. 2003. Microfluidic devices for cellomics: a review. Sensors and Actuators B-Chemical 92(3):315-325.

Andersson H, van den Berg A. 2006. Where are the biologists? A series of mini-reviews covering new trends in fundamental and applied research, and potential applications of miniaturised technologies. Lab on a Chip 6(4):467-470.

Angenendt P, Lehrach H, Kreutzberger J, Glokler J. 2005. Subnanoliter enzymatic assays on microarrays. Proteomics 5(2):420-425.

Arenkov P, Kukhtin A, Gemmell A, Voloshchuk S, Chupeeva V, Mirzabekov A. 2000. Protein microchips: Use for immunoassay and enzymatic reactions. Analytical Biochemistry 278(2):123-131.

Atencia J, Beebe DJ. 2005. Controlled microfluidic interfaces. Nature 437(7059):648-655.

Auroux PA, Iossifidis D, Reyes DR, Manz A. 2002. Micro total analysis systems. 2. Analytical standard operations and applications. Analytical Chemistry 74(12):2637-2652.

Balestrino D, Haagensen JAJ, Rich C, Forestier C. 2005. Characterization of type 2 quorum sensing in Klebsiella pneumoniae and relationship with biofilm formation. Journal of Bacteriology 187(8):2870-2880.

Barrios AFG, Zuo RJ, Hashimoto Y, Yang L, Bentley WE, Wood TK. 2006. Autoinducer 2 controls biofilm formation in Escherichia coli through a novel motility quorum-sensing regulator (MqsR, B3022). Journal of Bacteriology 188(1):305-316.

Bassler BL. 1999. How bacteria talk to each other: regulation of gene expression by quorum sensing. Curr Opin Microbiol 2(6):582-7.

Bassler BL, Greenberg EP, Stevens AM. 1997. Cross-species induction of luminescence in the quorum-sensing bacterium Vibrio harveyi. J Bacteriol 179(12):4043-5.

Bassler BL, Wright M, Silverman MR. 1994. Multiple signalling systems controlling expression of luminescence in Vibrio harveyi: sequence and function of genes encoding a second sensory pathway. Mol Microbiol 13(2):273-86.

Beebe DJ, Mensing GA, Walker GM. 2002. Physics and applications of microfluidics in biology. Annual Review of Biomedical Engineering 4:261-286.

Bilitewski U, Genrich M, Kadow S, Mersal G. 2003. Biochemical analysis with microfluidic systems. Analytical and Bioanalytical Chemistry 377(3):556-569.

Bjarnsholt T, Givskov M. 2007. The role of quorum sensing in the pathogenicity of the cunning aggressor Pseudomonas aeruginosa. Analytical and Bioanalytical Chemistry 387(2):409-414.

Borchardt RT. 1980. S-Adenosyl-L-Methionine-Dependent Macromolecule Methyltransferases - Potential Targets for the Design of Chemotherapeutic-Agents. Journal of Medicinal Chemistry 23(4):347-357.

Breiman RF, Butler JC, Tenover FC, Elliott JA, Facklam RR. 1994. Emergence of Drug-Resistant Pneumococcal Infections in the United-States. Jama-Journal of the American Medical Association 271(23):1831-1835.
Cadieux N, Bradbeer C, Reeger-Schneider E, Koster W, Mohanty AK, Wiener MC, Kadner RJ. 2002. Identification of the periplasmic cobalamin-binding protein BtuF of Escherichia coli. Journal of Bacteriology 184(3):706-717.
Caelen I, Gao H, Sigrist H. 2002. Protein density gradients on surfaces. Langmuir 18(7):2463-2467.
Cao LQ. 2005. Immobilised enzymes: science or art? Current Opinion in Chemical Biology 9(2):217-226.
Chaki NK, Vijayamohanan K. 2002. Self-assembled monolayers as a tunable platform for biosensor applications. Biosensors & Bioelectronics 17(1-2):1-12.
Chang Y, Ahn YS, Hahn HT, Chen Y. 2007. Sub-micrometer patterning of proteins by electric lithography. Langmuir 23(8):4112-4114.
Chen TH, Embree HD, Wu LQ, Payne GF. 2002a. In vitro protein-polysaccharide conjugation: Tyrosinase-catalyzed conjugation of gelatin and chitosan. Biopolymers 64(6):292-302.
Chen TH, Small DA, Wu LQ, Rubloff GW, Ghodssi R, Vazquez-Duhalt R, Bentley WE, Payne GF. 2003a. Nature-inspired creation of protein-polysaccharide conjugate and its subsequent assembly onto a patterned surface. Langmuir 19(22):9382-9386.
Chen X, Jia JB, Dong SJ. 2003b. Organically modified sol-gel/chitosan composite based glucose biosensor. Electroanalysis 15(7):608-612.
Chen X, Schauder S, Potier N, Van Dorsselaer A, Pelczer I, Bassler BL, Hughson FM. 2002b. Structural identification of a bacterial quorum-sensing signal containing boron. Nature 415(6871):545-549.
Choi CJ, Cunningham BT. 2007. A 96-well microplate incorporating a replica molded microfluidic network integrated with photonic crystal biosensors for high throughput kinetic biomolecular interaction analysis. Lab Chip 7(5):550-6.
Choi JW, Oh KW, Thomas JH, Heineman WR, Halsall HB, Nevin JH, Helmicki AJ, Henderson HT, Ahn CH. 2002. An integrated microfluidic biochemical detection system for protein analysis with magnetic bead-based sampling capabilities. Lab on a Chip 2(1):27-30.
Clayton J. 2005. Go with the microflow. Nature Methods 2(8):621-627.
Cornell KA, Swarts WE, Barry RD, Riscoe MK. 1996. Characterization of recombinant Escherichia coli 5'-methylthioadenosine/S-adenosylhomocysteine nucleosidase: Analysis of enzymatic activity and substrate specificity. Biochemical and Biophysical Research Communications 228(3):724-732.
Cosnier S, Molins C, Mousty C, Galland B, Lepellec A. 2006. A simple strategy based on photobiotin irradiation for the photoelectrochernical immobilization of proteins on electrode surfaces. Materials Science & Engineering C-Biomimetic and Supramolecular Systems 26(2-3):436-441.
Curey TE, Salazar MA, Oliveira P, Javier J, Dennis PJ, Rao P, Shear JB. 2002. Enzyme-based sensor arrays for rapid characterization of complex disaccharide solutions. Analytical Biochemistry 303(1):42-48.

Davies D. 2003. Understanding biofilm resistance to antibacterial agents. Nature Reviews Drug Discovery 2(2):114-122.
de Boer AR, Bruyneel B, Krabbe JG, Lingeman H, Niessen WMA, Irth H. 2005. A microfluidic-based enzymatic assay for bioactivity screening combined with capillary liquid chromatography and mass spectrometry. Lab on a Chip 5(11):1286-1292.
De Keersmaecker SCJ, Varszegi C, van Boxel N, Habel LW, Metzger K, Daniels R, Marchal K, De Vos D, Vanderleyden J. 2005. Chemical synthesis of (S)-4,5-dihydroxy-2,3-pentanedione, a bacterial signal molecule precursor, and validation of its activity in Salmonella typhimurium. Journal of Biological Chemistry 280(20):19563-19568.
Delahaba G, Cantoni GL. 1959. Enzymatic Synthesis of S-Adenosyl-L-Homocysteine from Adenosine and Homocysteine. Journal of Biological Chemistry 234(3):603-608.
Deng JL, Guo CX, Lu WS, Liu T, Jiang L. 2006. Polydiacetylene vesicle - A device based on molecular assembly for biological molecular recognition. Progress in Chemistry 18(11):1397-1408.
Diao JP, Ren DC, Engstrom JR, Lee KH. 2005. A surface modification strategy on silicon nitride for developing biosensors. Analytical Biochemistry 343(2):322-328.
Dittrich PS, Manz A. 2006. Lab-on-a-chip: microfluidics in drug discovery. Nat Rev Drug Discov 5(3):210-8.
Dittrich PS, Tachikawa K, Manz A. 2006. Micro total analysis systems. Latest advancements and trends. Analytical Chemistry 78(12):3887-3907.
Dove A. 2003. Screening for content--the evolution of high throughput. Nat Biotechnol 21(8):859-64.
Duerre JA. 1962. Hydrolytic Nucleosidase Acting on S-Adenosylhomocysteine and on 5'-Methylthioadenosine. Journal of Biological Chemistry 237(12):3737-&.
Duffy DC, McDonald JC, Schueller OJA, Whitesides GM. 1998. Rapid prototyping of microfluidic systems in poly(dimethylsiloxane). Analytical Chemistry 70(23):4974-4984.
Dupuy AM, Lehmann S, Cristol JP. 2005. Protein biochip systems for the clinical laboratory. Clin Chem Lab Med 43(12):1291-302.
Ehrlich GD, Stoodley P, Kathju S, Zhao Y, McLeod BR, Balaban N, Hu FZ, Sotereanos NG, Costerton JW, Stewart PS and others. 2005. Engineering approaches for the detection and control of orthopaedic biofilm infections. Clin Orthop Relat Res(437):59-66.
Federle MJ, Bassler BL. 2003. Interspecies communication in bacteria. Journal of Clinical Investigation 112(9):1291-1299.
Fernandes R, Tsao CY, Hashimoto Y, Wang L, Wood TK, Payne GF, Bentley WE. 2007. Magnetic nanofactories: Localized synthesis and delivery of quorum-sensing signaling molecule autoinducer-2 to bacterial cell surfaces. Metabolic Engineering 9(2):228-239.
Fernandes R, Yi HM, Wu LQ, Rubloff GW, Ghodssi R, Bentley WE, Payne GF. 2004. Thermo-biolithography: A technique for patterning nucleic acids and proteins. Langmuir 20(3):906-913.

Fodor SPA, Read JL, Pirrung MC, Stryer L, Lu AT, Solas D. 1991. Light-Directed, Spatially Addressable Parallel Chemical Synthesis. Science 251(4995):767-773.
Freddi G, Anghileri A, Sampaio S, Buchert J, Monti P, Taddei P. 2006. Tyrosinase-catalyzed modification of Bombyx mori silk fibroin: Grafting of chitosan under heterogeneous reaction conditions. Journal of Biotechnology 125(2):281-294.
Fuqua C, Greenberg EP. 1998. Cell-to-cell communication in Escherichia coli and Salmonella typhimurium: they may be talking, but who's listening? Proc Natl Acad Sci U S A 95(12):6571-2.
Garcia E, Hasenbank MS, Finlayson B, Yager P. 2007. High-throughput screening of enzyme inhibition using an inhibitor gradient generated in a microchannel. Lab on a Chip 7(2):249-255.
Gold HS, Moellering RC. 1996. Drug therapy - Antimicrobial-drug resistance. New England Journal of Medicine 335(19):1445-1453.
Grayson ACR, Shawgo RS, Johnson AM, Flynn NT, Li YW, Cima MJ, Langer R. 2004. A BioMEMS review: MEMS technology for physiologically integrated devices. Proceedings of the Ieee 92(1):6-21.
Hadd AG, Raymond DE, Halliwell JW, Jacobson SC, Ramsey JM. 1997. Microchip device for performing enzyme assays. Analytical Chemistry 69(17):3407-3412.
Hentzer M, Wu H, Andersen JB, Riedel K, Rasmussen TB, Bagge N, Kumar N, Schembri MA, Song ZJ, Kristoffersen P and others. 2003. Attenuation of Pseudomonas aeruginosa virulence by quorum sensing inhibitors. Embo Journal 22(15):3803-3815.
Holden MA, Jung SY, Cremer PS. 2004. Patterning enzymes inside microfluidic channels via photoattachment chemistry. Analytical Chemistry 76(7):1838-1843.
Hong JW, Chen Y, Anderson WF, Quake SR. 2006. Molecular biology on a microfluidic chip. Journal of Physics-Condensed Matter 18(18):S691-S701.
Hyun J, Zhu YJ, Liebmann-Vinson A, Beebe TP, Chilkoti A. 2001. Microstamping on an activated polymer surface: Patterning biotin and streptavidin onto common polymeric biomaterials. Langmuir 17(20):6358-6367.
Jo BH, Van Lerberghe LM, Motsegood KM, Beebe DJ. 2000. Three-dimensional micro-channel fabrication in polydimethylsiloxane (PDMS) elastomer. Journal of Microelectromechanical Systems 9(1):76-81.
Jung GY, Stephanopoulos G. 2004. A functional protein chip for pathway optimization and in vitro metabolic engineering. Science 304(5669):428-431.
Kane RS, Takayama S, Ostuni E, Ingber DE, Whitesides GM. 1999. Patterning proteins and cells using soft lithography. Biomaterials 20(23-24):2363-2376.
Kartalov EP, Zhong JF, Scherer A, Quake SR, Taylor CR, Anderson WF. 2006. High-throughput multi-antigen microfluidic fluorescence immunoassays. Biotechniques 40(1):85-90.
Kim YD, Park CB, Clark DS. 2001. Stable sol-gel microstructured and microfluidic networks for protein patterning. Biotechnology and Bioengineering 73(5):331-337.
Kisailus D, Truong Q, Amemiya Y, Weaver JC, Morse DE. 2006. Self-assembled bifunctional surface mimics an enzymatic and templating protein for the synthesis of a metal oxide semiconductor. Proceedings of the National Academy of Sciences of the United States of America 103(15):5652-5657.

Koev ST, Powers MA, Yi H, Wu LQ, Bentley WE, Rubloff GW, Payne GF, Ghodssi R. 2007. Mechano-transduction of DNA hybridization and dopamine oxidation through electrodeposited chitosan network. Lab on a Chip 7(1):103-111.

Ku BS, Cha JH, Srinivasan A, Kwon SJ, Jeong JC, Sherman DH, Dordick JS. 2006. Chip-based polyketide biosynthesis and functionalization. Biotechnology Progress 22(4):1102-1107.

L'Hostis E, Michel PE, Fiaccabrino GC, Strike DJ, de Rooij NF, Koudelka-Hep M. 2000. Microreactor and electrochemical detectors fabricated using Si and EPON SU-8. Sensors and Actuators B-Chemical 64(1-3):156-162.

Lee CS, Lee SH, Kim YG, Choi CH, Kim YK, Kim BG. 2006. Biochemical reactions on a microfluidic chip based on a precise fluidic handling method at the nanoliter scale. Biotechnology and Bioprocess Engineering 11(2):146-153.

Lee CS, Lee SH, Park SS, Kim YK, Kim BG. 2003a. Protein patterning on silicon-based surface using background hydrophobic thin film. Biosensors & Bioelectronics 18(4):437-444.

Lee MY, Park CB, Dordick JS, Clark DS. 2005. Metabolizing enzyme toxicology assay chip (MetaChip) for high-throughput microscale toxicity analyses. Proceedings of the National Academy of Sciences of the United States of America 102(4):983-987.

Lee MY, Srinivasan A, Ku B, Dordick JS. 2003b. Multienzyme catalysis in microfluidic biochips. Biotechnology and Bioengineering 83(1):20-28.

Lewandowski AT, Small DA, Chen TH, Payne GF, Bentley WE. 2006. Tyrosine-based "activatable pro-tag": Enzyme-catalyzed protein capture and release. Biotechnology and Bioengineering 93(6):1207-1215.

Lewandowski AT, Yi H, Payne GF, Ghodssi R, Rubloff GW, Bentley WE. in review. Assembly of active Pfs enzyme onto patterned areas of microfabricated chips. Biotechnology Progress.

Lewandowski AT, Yi HM, Luo XL, Payne GF, Ghodssi R, Rubloff GW, Bentley WE. in press. Protein assembly onto patterned microfabricated devices through enzymatic activation of fusion pro-tag. Biotechnology and Bioengineering.

Li C, Lee KH. 2004. Affinity depletion of albumin from human cerebrospinal fluid using Cibacron-blue-3G-A-derivatized photopatterned copolymer in a microfluidic device. Analytical Biochemistry 333(2):381-388.

Li YG, Zhou YX, Feng JL, Jiang ZH, Ma LR. 1999. Immobilization of enzyme on screen-printed electrode by exposure to glutaraldehyde vapour for the construction of amperometric acetylcholinesterase electrodes. Analytica Chimica Acta 382(3):277-282.

Liu Y, Zhong W, Meng S, Kong JL, Lu HJ, Yang PY, Girault HH, Liu BH. 2006. Assembly-controlled biocompatible interface on a microchip: Strategy to highly efficient proteolysis. Chemistry-a European Journal 12(25):6585-6591.

Luo XL, Xu JJ, Du Y, Chen HY. 2004. A glucose biosensor based on chitosan-glucose oxidase-gold nanoparticles biocomposite formed by one-step electrodeposition. Analytical Biochemistry 334(2):284-289.

Luo XL, Xu JJ, Wang JL, Chen HY. 2005a. Electrochemically deposited nanocomposite of chitosan and carbon nanotubes for biosensor application. Chemical Communications(16):2169-2171.

Luo XL, Xu JJ, Zhang Q, Yang GJ, Chen HY. 2005b. Electrochemically deposited chitosan hydrogel for horseradish peroxidase immobilization through gold nanoparticles self-assembly. Biosensors & Bioelectronics 21(1):190-196.
Malpass CA, Millsap KW, Sidhu H, Gower LB. 2002. Immobilization of an oxalate-degrading enzyme on silicone elastomer. Journal of Biomedical Materials Research 63(6):822-829.
Mao HB, Yang TL, Cremer PS. 2002. Design and characterization of immobilized enzymes in microfluidic systems. Analytical Chemistry 74(2):379-385.
Mayer M, Yang J, Gitlin I, Gracias DH, Whitesides GM. 2004. Micropatterned agarose gels for stamping arrays of proteins and gradients of proteins. Proteomics 4(8):2366-2376.
McDonald JC, Duffy DC, Anderson JR, Chiu DT, Wu HK, Schueller OJA, Whitesides GM. 2000. Fabrication of microfluidic systems in poly(dimethylsiloxane). Electrophoresis 21(1):27-40.
Miao Y, Tan SN. 2001. Amperometric hydrogen peroxide biosensor with silica sol-gel/chitosan film as immobilization matrix. Analytica Chimica Acta 437(1):87-93.
Miller CH, Duerre JA. 1968. S-Ribosylhomocysteine Cleavage Enzyme from Escherichia Coli. Journal of Biological Chemistry 243(1):92-&.
Miller MB, Bassler BL. 2001. Quorum sensing in bacteria. Annual Review of Microbiology 55:165-199.
Miller ST, Xavier KB, Campagna SR, Taga ME, Semmelhack MF, Bassler BL, Hughson FM. 2004. Salmonella typhimurium recognizes a chemically distinct form of the bacterial quorum-sensing signal AI-2. Molecular Cell 15(5):677-687.
Neu HC. 1992. The Crisis in Antibiotic-Resistance. Science 257(5073):1064-1073.
Niemeyer CM, Wacker R, Adler M. 2003. Combination of DNA-directed immobilization and immuno-PCR: very sensitive antigen detection by means of self-assembled DNA-protein conjugates. Nucleic Acids Research 31(16).
Norde W. 1986. Adsorption of Proteins from Solution at the Solid-Liquid Interface. Advances in Colloid and Interface Science 25(4):267-340.
Pajula RL, Raina A. 1979. Methylthioadenosine, a Potent Inhibitor of Spermine Synthase from Bovine Brain. Febs Letters 99(2):343-345.
Pang X, Zhitomirsky I. 2005. Electrodeposition of composite hydroxyapatite-chitosan films. Materials Chemistry and Physics 94(2-3):245-251.
Park JJ, Luo XL, Yi HM, Valentine TM, Payne GF, Bentley WE, Ghodssi R, Rubloff GW. 2006. Chitosan-mediated in situ biomolecule assembly in completely packaged microfluidic devices. Lab on a Chip 6(10):1315-1321.
Pessela BCC, Dellamora-Ortiz G, Betancor L, Fuentes M, Guisan JM, Fernandez-Lafuente R. 2007. Modulation of the catalytic properties of multimeric beta-galactosidase from E-coli by using different immobilization protocols. Enzyme and Microbial Technology 40(2):310-315.
Petrou PS, Chatzichristidi M, Douvas AA, Argitis P, Misiakos K, Kakabakos SE. 2007. A biomolecule friendly photolithographic process for fabrication of protein microarrays on polymeric films coated on silicon chips. Biosensors & Bioelectronics 22(9-10):1994-2002.
Pihl J, Karlsson M, Chiu DT. 2005a. Microfluidic technologies in drug discovery. Drug Discovery Today 10(20):1377-1383.

Pihl J, Sinclair J, Sahlin E, Karlsson M, Petterson F, Olofsson J, Orwar O. 2005b. Microfluidic gradient-generating device for pharmacological profiling. Analytical Chemistry 77(13):3897-3903.
Psaltis D, Quake SR, Yang CH. 2006. Developing optofluidic technology through the fusion of microfluidics and optics. Nature 442(7101):381-386.
Quist AP, Pavlovic E, Oscarsson S. 2005. Recent advances in microcontact printing. Analytical and Bioanalytical Chemistry 381(3):591-600.
Ragione ED, Porcelli M, Cartenifarina M, Zappia V. 1985. Escherichia-Coli S-Adenosylhomocysteine/5'-Methylthioadenosine Nucleosidase - Purification, Substrate-Specificity and Mechanism of Action. Biochemical Journal 232(2):335-341.
Raina A, Tuomi K, Pajula RL. 1982. Inhibition of the Synthesis of Polyamines and Macromolecules by 5'-Methylthioadenosine and 5'-Alkylthiotubercidins in Bhk-21-Cells. Biochemical Journal 204(3):697-703.
Rajamani S, Zhu JG, Pei DH, Sayre R. 2007. A LuxP-FRET-based reporter for the detection and quantification of AI-2 bacterial quorum-sensing signal compounds. Biochemistry 46(13):3990-3997.
Rasmussen TB, Bjarnsholt T, Skindersoe ME, Hentzer M, Kristoffersen P, Kote M, Nielsen J, Eberl L, Givskov M. 2005a. Screening for quorum-sensing inhibitors (QSI) by use of a novel genetic system, the QSI selector. Journal of Bacteriology 187(5):1799-1814.
Rasmussen TB, Givskov M. 2006. Quorum-sensing inhibitors as anti-pathogenic drugs. International Journal of Medical Microbiology 296(2-3):149-161.
Rasmussen TB, Skindersoe ME, Bjarnsholt T, Phipps RK, Christensen KB, Jensen PO, Andersen JB, Koch B, Larsen TO, Hentzer M and others. 2005b. Identity and effects of quorum-sensing inhibitors produced by Penicillium species. Microbiology-Sgm 151:1325-1340.
Ren D, Bedzyk LA, Ye RW, Thomas SM, Wood TK. 2004. Differential gene expression shows natural brominated furanones interfere with the autoinducer-2 bacterial signaling system of Escherichia coli. Biotechnol Bioeng 88(5):630-42.
Ren D, Sims JJ, Wood TK. 2001. Inhibition of biofilm formation and swarming of Escherichia coli by (5Z)-4-bromo-5-(bromomethylene)-3-butyl-2(5H)-furanone. Environ Microbiol 3(11):731-6.
Reyes DR, Iossifidis D, Auroux PA, Manz A. 2002. Micro total analysis systems. 1. Introduction, theory, and technology. Analytical Chemistry 74(12):2623-2636.
Riscoe MK, Tower PA, Ferro AJ. 1984. Mechanism of Action of 5'-Methylthioadenosine in S49 Cells. Biochemical Pharmacology 33(22):3639-3643.
Rozkiewicz DI, Kraan Y, Werten MWT, de Wolf FA, Subramaniam V, Ravoo BJ, Reinhoudt DN. 2006. Covalent microcontact printing of proteins for cell patterning. Chemistry-a European Journal 12(24):6290-6297.
Rusling JF, Hvastkovs EG, Schenkman JB. 2007. Toxicity screening using biosensors that measure DNA damage. Curr Opin Drug Discov Devel 10(1):67-73.
Sampaio S, Taddei P, Monti P, Buchert J, Freddi G. 2005. Enzymatic grafting of chitosan onto Bombyx mori silk fibroin: kinetic and IR vibrational studies. Journal of Biotechnology 116(1):21-33.

Sebra RP, Masters KS, Cheung CY, Bowman CN, Anseth KS. 2006. Detection of antigens in biologically complex fluids with photografted whole antibodies. Analytical Chemistry 78(9):3144-3151.
Shanazarova IM, Valuev LI, Valuev IL, Valueva TA, Obydennova IV. 2007. Immobilization of ovomucoid on chitosan. Applied Biochemistry and Microbiology 43(2):150-152.
Shen G, Rajan R, Zhu JG, Bell CE, Pei DH. 2006. Design and synthesis of substrate and intermediate analogue inhibitors of S-ribosylhomocysteinase. Journal of Medicinal Chemistry 49(10):3003-3011.
Shim J, Bersano-Begey TF, Zhu XY, Tkaczyk AH, Linderman JJ, Takayama S. 2003. Micro- and nanotechnologies for studying cellular function. Current Topics in Medicinal Chemistry 3(6):687-703.
Singh V, Evans GB, Lenz DH, Mason JM, Clinch K, Mee S, Painter GF, Tyler PC, Furneaux RH, Lee JE and others. 2005. Femtomolar transition state analogue inhibitors of 5 '-methylthioadenosine/S-adenosylhomocysteine nucleosidase from Escherichia coli. Journal of Biological Chemistry 280(18):18265-18273.
Singh V, Shi WX, Almo SC, Evans GB, Furneaux RH, Tyler PC, Painter GF, Lenz DH, Mee S, Zheng RJ and others. 2006. Structure and inhibition of a quorum sensing target from Streptococcus pneumoniae. Biochemistry 45(43):12929-12941.
Song MJ, Yun DH, Min NK, Hong SI. 2007. Electrochemical biosensor array for liver diagnosis using silanization technique on nanoporous silicon electrode. Journal of Bioscience and Bioengineering 103(1):32-37.
Sperandio V, Torres AG, Giron JA, Kaper JB. 2001. Quorum sensing is a global regulatory mechanism in enterohemorrhagic Escherichia coli O157: H7. Journal of Bacteriology 183(17):5187-5197.
Sperandio V, Torres AG, Kaper JB. 2002. Quorum sensing Escherichia coli regulators B and C (QseBC): a novel two-component regulatory system involved in the regulation of flagella and motility by quorum sensing in E-coli. Molecular Microbiology 43(3):809-821.
Stroeher UH, Paton AW, Ogunniyi AD, Paton JC. 2003. Mutation of luxS of Streptococcus pneumoniae affects virulence in a mouse model. Infection and Immunity 71(6):3206-3212.
Su XL, Li YB. 2004. A self-assembled monolayer-based piezoelectric immunosensor for rapid detection of Escherichia coli O157: H7. Biosensors & Bioelectronics 19(6):563-574.
Suh KY, Seong J, Khademhosseini A, Laibinis PE, Langer R. 2004. A simple soft lithographic route to fabrication of poly(ethylene glycol) microstructures for protein and cell patterning. Biomaterials 25(3):557-563.
Sung WJ, Bae YH. 2006. Glucose oxidase, lactate oxidase, and galactose oxidase enzyme electrode based on polypyrrole with polyanion/PEG/enzyme conjugate dopant. Sensors and Actuators B-Chemical 114(1):164-169.
Surette MG, Bassler BL. 1998. Quorum sensing in Escherichia coli and Salmonella typhimurium. Proceedings of the National Academy of Sciences of the United States of America 95(12):7046-7050.

Surette MG, Miller MB, Bassler BL. 1999. Quorum sensing in Escherichia coli, Salmonella typhimurium, and Vibrio harveyi: a new family of genes responsible for autoinducer production. Proc Natl Acad Sci U S A 96(4):1639-44.
Tachibana S, Suzuki M, Asano Y. 2006. Application of an enzyme chip to the micro quantification of L-phenylalanine. Analytical Biochemistry 359(1):72-78.
Tangkuaram T, Ponchio C, Kangkasomboon T, Katikawong P, Veerasai W. 2007. Design and development of a highly stable hydrogen peroxide biosensor on screen printed carbon electrode based on horseradish peroxidase bound with gold nanoparticles in the matrix of chitosan. Biosensors & Bioelectronics 22(9-10):2071-2078.
Tender LM, Worley RL, Fan HY, Lopez GP. 1996. Electrochemical patterning of self-assembled monolayers onto microscopic arrays of gold electrodes fabricated by laser ablation. Langmuir 12(23):5515-5518.
Turovskiy Y, Chikindas ML. 2006. Autoinducer-2 bioassay is a qualitative, not quantitative method influenced by glucose. Journal of Microbiological Methods 66(3):497-503.
Unger MA, Chou HP, Thorsen T, Scherer A, Quake SR. 2000. Monolithic microfabricated valves and pumps by multilayer soft lithography. Science 288(5463):113-116.
Urban PL, Goodall DM, Bruce NC. 2006. Enzymatic microreactors in chemical analysis and kinetic studies. Biotechnology Advances 24(1):42-57.
Veiseh M, Zareie MH, Zhang MQ. 2002. Highly selective protein patterning on gold-silicon substrates for biosensor applications. Langmuir 18(17):6671-6678.
Vilchez R, Lemme A, Thiel V, Schulz S, Sztajer H, Wagner-Dobler I. 2007. Analysing traces of autoinducer-2 requires standardization of the Vibrio harveyi bioassay. Analytical and Bioanalytical Chemistry 387(2):489-496.
Vilkner T, Janasek D, Manz A. 2004. Micro total analysis systems. Recent developments. Analytical Chemistry 76(12):3373-3385.
Walsh C. 2000. Molecular mechanisms that confer antibacterial drug resistance. Nature 406(6797):775-781.
Wang FC, Yuan R, Chai YQ. 2006. Direct electrochemical immunoassay based on a silica nanoparticles/sol-gel composite architecture for encapsulation of immunoconjugate. Applied Microbiology and Biotechnology 72(4):671-675.
Wang G, Xu JJ, Chen HY, Lu ZH. 2003. Amperometric hydrogen peroxide biosensor with sol-gel/chitosan network-like film as immobilization matrix. Biosensors & Bioelectronics 18(4):335-343.
Wang J, Chatrathi MP, Tian BM. 2001. Microseparation chips for performing multienzymatic dehydrogenase/oxidase assays: Simultaneous electrochemical measurement of ethanol and glucose. Analytical Chemistry 73(6):1296-1300.
Wang J, Chen L, Mulchandani A, Mulchandani P, Chen W. 1999. Remote biosensor for in-situ monitoring of organophosphate nerve agents. Electroanalysis 11(12):866-869.
Wessa T, Rapp M, Sigrist H. 1999. Immunosensing of photoimmobilized proteins on surface acoustic wave sensors. Colloids and Surfaces B-Biointerfaces 15(2):139-146.

Wilde LM, Farace G, Roberts CJ, Davies MC, Sanders GHW, Tendler SJB, Williams PM. 2001. Molecular patterning on carbon based surfaces through photobiotin activation. Analyst 126(2):195-198.
Wilhelm T, Wittstock G. 2002. Generation of periodic enzyme patterns by soft lithography and activity imaging by scanning electrochemical microscopy. Langmuir 18(24):9485-9493.
Williams RA, Blanch HW. 1994. Covalent Immobilization of Protein Monolayers for Biosensor Applications. Biosensors & Bioelectronics 9(2):159-167.
Wu LQ, Gadre AP, Yi HM, Kastantin MJ, Rubloff GW, Bentley WE, Payne GF, Ghodssi R. 2002. Voltage-dependent assembly of the polysaccharide chitosan onto an electrode surface. Langmuir 18(22):8620-8625.
Wu LQ, Payne GF. 2004. Biofabrication: using biological materials and biocatalysts to construct nanostructured assemblies. Trends in Biotechnology 22(11):593-599.
Wu LQ, Yi HM, Li S, Rubloff GW, Bentley WE, Ghodssi R, Payne GF. 2003. Spatially selective deposition of a reactive polysaccharide layer onto a patterned template. Langmuir 19(3):519-524.
Xia YN, Whitesides GM. 1998. Soft lithography. Annual Review of Materials Science 28:153-184.
Xu F, Zhen GL, Yu F, Kuennemann E, Textor M, Knoll W. 2005. Combined affinity and catalytic biosensor: In situ enzymatic activity monitoring of surface-bound enzymes. Journal of the American Chemical Society 127(38):13084-13085.
Yamada K, Aoki T, Ikeda N, Hirata M. 2007. Application of enzymatically gelled chitosan solutions to water-resistant adhesives. Journal of Applied Polymer Science 104(3):1818-1827.
Yang MH, Yang YH, Yang Y, Shen GL, Yu RQ. 2004. Bienzymatic amperometric biosensor for choline based on mediator thionine in situ electropolymerized within a carbon paste electrode. Analytical Biochemistry 334(1):127-134.
Yi HM, Nisar S, Lee SY, Powers MA, Bentley WE, Payne GF, Ghodssi R, Rubloff GW, Harris MT, Culver JN. 2005a. Patterned assembly of genetically modified viral nanotemplates via nucleic acid hybridization. Nano Letters 5(10):1931-1936.
Yi HM, Wu LQ, Bentley WE, Ghodssi R, Rubloff GW, Culver JN, Payne GF. 2005b. Biofabrication with chitosan. Biomacromolecules 6(6):2881-2894.
Yi HM, Wu LQ, Ghodssi R, Rubloff GW, Payne GF, Bentley WE. 2004. A robust technique for assembly of nucleic acid hybridization chips based on electrochemically templated chitosan. Analytical Chemistry 76(2):365-372.
Yi HM, Wu LQ, Ghodssi R, Rubloff GW, Payne GF, Bentley WE. 2005c. Signal-directed sequential assembly of biomolecules on patterned surfaces. Langmuir 21(6):2104-2107.
Zhang CX, Liu HP, Tang ZM, He NY, Lu ZH. 2003. Cell detection based on protein array using modified glass slides. Electrophoresis 24(18):3279-3283.
Zhao G, Wan W, Mansouri S, Alfaro JF, Bassler BL, Cornell KA, Zhou ZHS. 2003. Chemical synthesis of S-ribosyl-L-homocysteine and activity assay as a LuxS substrate. Bioorganic & Medicinal Chemistry Letters 13(22):3897-3900.
Zhen GL, Eggli V, Voros J, Zammaretti P, Textor M, Glockshuber R, Kuennemann E. 2004. Immobilization of the enzyme beta-lactamase on biotin-derivatized poly(L-lysine)-g-poly(ethylene glycol)-coated sensor chips: A study on oriented

attachment and surface activity by enzyme kinetics and in situ optical sensing. Langmuir 20(24):10464-10473.
Zhu J, Miller MB, Vance RE, Dziejman M, Bassler BL, Mekalanos JJ. 2002. Quorum-sensing regulators control virulence gene expression in Vibrio cholerae. Proceedings of the National Academy of Sciences of the United States of America 99(5):3129-3134.
Zhu JG, Dizin E, Hu XB, Wavreille AS, Park J, Pei DH. 2003. S-ribosylhomocysteinase (LuxS) is a mononuclear iron protein. Biochemistry 42(16):4717-4726.